UNCLASSIFIED

CENTRAL RESEARCH LIBRARY
DOCUMENT COLLECTION

MARTIN MARIETTA ENERGY SYSTEMS LIBRARIES
3 4456 0059401 5

ORNL-1852
Progress
Cy 7

SOLID STATE DIVISION

SEMIANNUAL PROGRESS REPORT

FOR PERIOD ENDING FEBRUARY 28, 1955

CENTRAL RESEARCH LIBRARY
DOCUMENT COLLECTION

LIBRARY LOAN COPY

DO NOT TRANSFER TO ANOTHER PERSON

If you wish someone else to see this document, send in name with document and the library will arrange a loan.

OAK RIDGE NATIONAL LABORATORY
OPERATED BY
CARBIDE AND CARBON CHEMICALS COMPANY
A DIVISION OF UNION CARBIDE AND CARBON CORPORATION

POST OFFICE BOX P
OAK RIDGE, TENNESSEE

UNCLASSIFIED

ORNL-1852

COPY NO. 92

Contract No. W-7405-eng-26

SOLID STATE DIVISION

SEMIANNUAL PROGRESS REPORT

For Period Ending February 28, 1955

D. S. Billington, Director

J. H. Crawford, Jr., Assistant Director

Edited by
J. T. Howe

DATE ISSUED

MAY 16 1955

MARTIN MARIETTA ENERGY SYSTEMS LIBRARIES

3 4456 0059401 5

OAK RIDGE NATIONAL LABORATORY
Operated by
CARBIDE AND CARBON CHEMICALS COMPANY
A Division of Union Carbide and Carbon Corporation
Post Office Box P
Oak Ridge, Tennessee

Reports previously issued in this series are:

ORNL-1025	Period Ending January 31, 1951
ORNL-1095	Period Ending April 30, 1951
ORNL-1128	Period Ending July 31, 1951
ORNL-1214	Period Ending October 31, 1951
ORNL-1261	Period Ending January 31, 1952
ORNL-1301	Period Ending May 10, 1952
ORNL-1359	Period Ending August 10, 1952
ORNL-1429	Period Ending November 10, 1952
ORNL-1506	Period Ending February 10, 1953
ORNL-1606	Period Ending August 31, 1953
ORNL-1677	Period Ending February 28, 1954
ORNL-1762	Period Ending August 30, 1954
ORNL-1851	Period Ending February 28, 1955

INTERNAL DISTRIBUTION

1. C. D. Baumann
2. R. G. Berggren
3. J. O. Betterton, Jr.
4. D. S. Billington
5. D. Binder
6. T. H. Blewitt
7. C. D. Bopp
8. B. S. Borie
9. G. E. Boyd
10. E. J. Boyle
11. H. Brooks (consultant)
12. W. E. Browning
13. W. E. Brundage
14. D. W. Cardwell
15. C. E. Center
16. R. A. Charpie
17. J. W. Cleland
18. G. H. Clewett
19. A. F. Cohen
20. D. D. Cowen
21. J. H. Crawford, Jr.
22. F. L. Culler
23. J. E. Cunningham
24. S. E. Dismuke
25. L. B. Emlet (K-25)
26. M. J. Feldman
27. J. H. Frye, Jr.
28. J. L. Gabbard
29. R. J. Gray
30. W. O. Harms
31. C. S. Harrill
32. A. Hollaender
33. D. K. Holmes
34. A. S. Householder
35. J. T. Howe
36. L. K. Jetter
37. R. W. Johnson
38. R. J. Jones
39. W. H. Jordan
40. G. W. Keilholtz
41. C. P. Keim
42. M. T. Kelley
43. R. H. Kernohan
44. E. M. King
45. H. V. Klaus
46. G. E. Klein
47. C. E. Larson
48. T. A. Lincoln
49. S. C. Lind
50. R. S. Livingston
51. H. G. MacPherson (consultant)
52. W. D. Manly
53. A. J. Miller
54. E. C. Miller
55. J. G. Morgan
56. K. Z. Morgan
57. E. J. Murphy
58. J. P. Murray (Y-12)
59. R. B. Oliver
60. W. W. Parkinson
61. P. M. Reyling
62. M. T. Robinson
63. H. C. Schweinler
64. F. Seitz (consultant)
65. E. D. Shipley
66. O. Sisman
67. M. J. Skinner
68. G. P. Smith
69. A. H. Snell
70. R. L. Sproull (consultant)
71. E. E. Stansbury
72. D. K. Stevens
73. W. J. Sturm
74. C. D. Susano
75. J. A. Swartout
76. E. H. Taylor
77. J. B. Trice
78. F. C. VonderLage
79. J. M. Warde
80. C. C. Webster
81. M. S. Wechsler
82. R. A. Weeks
83. A. M. Weinberg
84. E. P. Wigner (consultant)
85. G. C. Williams
86. W. R. Willis
87. J. C. Wilson
88. C. E. Winters
89. M. C. Wittels
90. Biology Library

91-93. Central Research Library
94. Health Physics Library
95-99. Laboratory Records Department
100. Laboratory Records, ORNL R.C.

101. ORNL Document Reference Library, Y-12
102. Reactor Experimental Engineering Library

EXTERNAL DISTRIBUTION

103. R. F. Bacher, California Institute of Technology
104. W. W. Shaver, Corning Glass Works, Corning, New York
105. Division of Research and Medicine, AEC, ORO
106-415. Given distribution as shown in TID-4500 under Physics category

DISTRIBUTION PAGE TO BE REMOVED IF REPORT IS GIVEN PUBLIC DISTRIBUTION

CONTENTS

PUBLICATIONS vii

SUMMARY 1

SOLID STATE REACTIONS 6

- Energy Levels in Fast-Neutron Irradiated p-Type Germanium 6
- Effect of Bombardment on Hole Mobility in p-Type Germanium 13
- Photoconductivity and Minority-Carrier Traps in Bombarded n-Type Germanium 15
- Annealing of Irradiated Germanium 16
- Determination of Energy Levels in Germanium by Transmutation Doping 17
- Radiation Effects in Gallium Antimonide 20
- Magnetic Susceptibility of Indium Antimonide 24
- Low-Temperature Apparatus for Magnetic-Susceptibility Measurements 26
- Radiation Effects in Ionic Crystals 27
- Optical Spectra of Irradiated Quartz and Silica 28
- Fast-Neutron Effects in Some Refractory Single Crystals 29
- X-Ray Scattering from Covalent Single Crystals 30

ENGINEERING PROPERTIES 33

- Radiation Effects on Thermal Conductivity of Ceramics 33
- X-Ray Examination of Ceramic Samples 35
- A Correlation of the Radiation Stability of Plastics with the Young's Modulus 35

CRYSTAL PHYSICS 41

- Low-Temperature In-Pile Cryostat 41
- The Critical Shear Stress in Alpha Brass as a Function of Zinc Concentration and Temperature 41

SPECIAL PROJECTS 44

- Elastic Effects in Neutron-Irradiated LiF 44
- Two-Stage Annealing Process in Neutron-Irradiated LiF 45
- A Study of Lattice Defects in Gold-Cadmium Alloy 46
- Effect of Neutron Radiation on the Precipitation Hardening Reaction 48
- Reactor-Induced Resistivity Changes in Copper-Base Solid Solutions 50
- Lattice Parameters of Some Copper Alloys 53
- Paramagnetic Resonances in Irradiated Materials 53
- Operation of the Shielded X-Ray Diffractometer 59

PUBLICATIONS

M. J. Feldman, "Advantages of Ultrasonic Cleaning," *Nucleonics* **12**(11), 65 (1954).

D. Binder and W. J. Sturm, "Equivalence of X-Ray Lattice Parameter and Density Changes in Neutron-Irradiated LiF," *Phys. Rev.* **96**, 1519 (1954).

S. E. Dismuke, "Robot-Run Tools Machine Hot Materials at Oak Ridge," *Am. Machinist* **98**, 161 (1954).

S. E. Dismuke, "Operating Busy Hot Cells," *Nucleonics* **12**(11), 89 (1954).

J. W. Cleland and J. H. Crawford, Jr., "Neutron Irradiation of Indium Antimonide," *Phys. Rev.* **95**, 1177 (1954).

M. S. Wechsler, "The Effect of Quench on the Structure of Au-Cd," *Bull. Am. Phys. Soc.* **29**(7), 30 (1954).

D. S. Billington, book review of "Physical Properties of Solid Materials" (by C. Zwikker, Interscience, 1954), *Nucleonics* **13**(2), 82 (1955).

SOLID STATE DIVISION SEMIANNUAL PROGRESS REPORT

INTRODUCTION AND SUMMARY

This semiannual progress report and future progress reports will be published as two documents to permit a wider distribution of the unclassified material. The report numbers are assigned in sequence so that the two reports will fall together when filed by report number.

SOLID STATE REACTIONS

Energy Levels in Fast-Neutron Irradiated *p*-Type Germanium (AEC Activity 5411). An analysis of the behavior of *p*-type germanium bombarded with fast neutrons at room temperature gave excellent agreement with the model proposed by James and Lark-Horovitz at the beginning of the irradiation but diverged from the predicted behavior as bombardment proceeded. The data indicate that there is a difference in annealing rates of the two types of defects (interstitials and vacancies). This would alter the distribution of energy levels by changing the relative concentration of energy levels that arise from each type.

After bombardment, the results for samples with high initial hole concentrations are in qualitative agreement with the model, but for low initial hole concentrations there is a serious lack of agreement. A lower-than-expected acceptor ionization energy apparently results from some process that occurs during bombardment or during the room-temperature aging period. Trapping of minority carriers and differential annealing of interstitials and vacancies are probable processes.

The temperature dependence of hole concentration after successive bombardments at about 40°C indicates that there is a broad distribution of acceptor ionization energies with a discrete level (or closely grouped set of levels) superimposed on the broad distribution at about 0.10 ev above the band edge. For an *n*-type specimen converted to *p*-type by bombardment, the corresponding energy level was found at 0.08 ev and is tentatively identified with the deep trap.

Effect of Bombardment on Hole Mobility in *p*-Type Germanium (AEC Activity 5411). Studies of the effect of radiation on hole mobility of *p*-type germanium indicate that the nature of the scattering mechanism of bombardment-introduced defects is uncertain. Although certain features of the temperature and concentration dependence of the scattering probability are not consistent with charge-center scattering, the magnitude of the scattering probability is approximately that which would be expected if approximately nine singly ionized defects were introduced for each ionized acceptor at 77°K. The reason for the large disparity in the behavior of electron mobility to that observed for holes in bombarded germanium is unknown. More extensive experimental information is necessary before the phenomenon can be understood.

Photoconductivity and Minority-Carrier Traps in Bombarded *n*-Type Germanium (AEC Activity 5411). The peculiar oscillatory behavior of conductivity as a function of temperature that occurred during warming of *n*-type germanium after irradiation at low temperature was re-examined as a result of observation at Bell Laboratories. These observations indicate that low-temperature electron bombardment of both *n*- and *p*-type germanium introduces minority-carrier traps which give rise to appreciable photoconductivity at low temperature.

During slow warmup the conductivity shows two decided peaks at 134 and 165°K. The conductivity then falls to a minimum value at about 195°K, after which temperature, further heating causes a rapid increase with no more peaks. The oscillatory behavior is interpreted as the successive escape of trapped holes (and their subsequent recombination with excess electrons) from two discrete trapping levels of different energy. No peaks were observed on recooling and on later heating, and it is concluded that the traps responsible for the oscillatory behavior were annealed. The cooling curve also showed a decrease in conductivity at the low-temperature end; this would be expected if the hole traps had annealed, since an important source of photoconductivity would have been removed. These results are consistent with the findings on electron-bombarded germanium.

Annealing of Irradiated Germanium (AEC Activity 5411). It is known that radiation-produced effects may be annealed out of germanium by treatment at a temperature sufficiently above the irradiation temperature. It has also been found that the effects introduced at room temperature after irradiation are sometimes opposite to those normally to be expected by annealing treatments.

An n-type germanium specimen was irradiated at 35°C until its room-temperature conductivity was decreased by a factor of about 8. The Hall coefficient and conductivity were measured as a function of temperature over the range from liquid-nitrogen to room temperature. Isothermal anneals produced a decrease in conductivity at 0 and 23.3°C, an increase at 40 and 60°C, and a decrease at 80 and 100°C. At least two and probably three kinetic processes are indicated. A tentative explanation is that removal of the interstitial atoms decreases the concentration of shallow electron traps and, in effect, replaces them by deeper traps situated below the middle of the forbidden band to cause a further decrease in concentration; recombination of interstitials and vacancies would thus remove two electron traps.

Determination of Energy Levels in Germanium by Transmutation Doping (AEC Activity 5411). Nuclear doping has been investigated as an agent for determining the energy levels in semiconductors. Nuclear doping of germanium transmutes Ge^{71} with an 11.4-day half life to Ga^{71}, which is an acceptor impurity, and transmutes Ge^{75} with an 82-min half life to As^{75}, which is a donor impurity. Measurements of conductivity and Hall coefficient at proper time intervals permit the Fermi level to be followed across the forbidden band.

Experimental evidence indicates that the capture gamma rays from the various germanium isotopes are not sufficiently energetic to displace the atoms that capture a thermal neutron from their normal lattice positions. The decaying radiation of the germanium, the sample holder, and the lead wires has been found to produce, at the end of the decay period, an electron concentration several orders of magnitude larger than that expected, probably by saturating the minority carrier traps and producing an excess electron concentration. The high concentration of excess carriers would mask the presence of discrete energy levels at liquid-nitrogen temperature, but at dry-ice temperature the photosensitivity is such that the excess electron concentration is negligible and the discrete levels should be detectable.

Radiation Effects in Gallium Antimonide (AEC Activity 5411). Hall coefficient and resistivity of both n- and p-type GaSb were measured before and after irradiation in the ORNL Graphite Reactor. Some of the samples were wrapped in two thin foils, one of indium and one of cadmium, to prevent transmutation of the gallium and antimony. Conductivity (recorded continuously during exposure) of both n- and p-type samples, shielded and unshielded, decreased monotonically during irradiation. The removal rate of current carriers was approximately the same for all samples of high carrier concentration. This indicates the introduction of approximately equal numbers of acceptors and donors whose center of gravity is apparently near the middle of the forbidden-energy band.

High-temperature, long-time anneals remove some of the radiation-produced acceptors, but indications are that a large number of additional current carriers are introduced. Differential annealing of radiation-produced defects must occur.

The removal rate of current electrons from n-type material is not dependent on initial carrier concentration. This indicates that the donor atoms, which are presumably interstitials, ionize and lose electrons to the lower-lying acceptor states, which are presumably lattice vacancies. These donors can act as electron traps in n-type material.

The rate of removal of holes in p-type material decreases rapidly for lower initial hole concentrations; these low-lying filled acceptors can act as hole traps.

Since an interstitial in GaSb can be either a gallium or an antimony atom and a vacancy can be either type of vacant lattice site, it is possible for four simple defects to exist; multiple ionization may also complicate the situation. A detailed model of the energy-level spectrum associated with irradiation-produced defects in GaSb is therefore not yet complete.

Magnetic Susceptibility of Indium Antimonide (AEC Activity 5411). Magnetic-susceptibility data on p-type InSb have been extended to 636°K, and data on n-type have been taken from 293 to 634°K. Diamagnetism for both types increases with temperature and was attributed to intrinsic carriers. The susceptibility, which should be the same for n- and p-type GaSb at the higher temperatures, differed by 1.2% at about 630°K. This difference is attributed to thermal expansion of the molybdenum suspension fiber. The suspension expansion may also explain the discrepancy between the measured 0.095 ev for the half-value forbidden-energy gap as compared with the reported value of 0.115 ev.

Low-Temperature Apparatus for Magnetic-Susceptibility Measurements (AEC Activity 5411). An apparatus has been built to permit magnetic-susceptibility measurements to be made at temperatures down to 1°K. It will replace the present liquid-nitrogen cryostat, which has a lower limit of about 90°K.

Radiation Effects in Ionic Crystals (AEC Activity 5411). Annealing of alkali halide crystals produces changes in conductivity. Potassium chloride crystals were heated to temperature and were allowed to cool immediately; the temperature of each excursion was raised by 50 to 100°C intervals until a maximum of 400°C was reached. A pronounced decrease in activation energy at about 240°C, which was not expected, was observed; this is different from the one that contributes to the conductivity at the lower temperatures; NaCl, KBr, and LiF behaved similarly.

In KCl and V_3 band at 2150 Å of the optical spectra is apparently associated with holes trapped at positive ion vacancies which influence the ionic conductivity. A study of the effects of reactor and Co^{60} radiation on the V centers of KCl will be continued in more detail.

Optical Spectra of Irradiated Quartz and Silica (AEC Activity 5411). Optical absorption curves were made on a sample of very pure silica after it had been subjected to various bombardments. No absorption bands occurred in the visible spectrum, and only one occurred in the ultraviolet spectrum at 2150 Å. The optical density is approximately proportional to the length of bombardment.

Fast-Neutron Effects in Some Refractory Single Crystals (AEC Activity 4540). Fast-neutron irradiation of silica structures easily displaces oxygen atoms, and the damage does not anneal at room temperature. The study has been extended to other materials whose structures are dominated by oxygen atoms and in which binding is partially covalent.

Bombardment of zircon up to 3.6×10^{20} neutrons/cm^2 at 100°C induced an apparent bending or warping of large mosaic blocks in the crystal lattice, but long-range order was retained. The (200) and (101) warped 6.2 and 4.6 deg. Expansion and distortion in both crystal lattices of garnet and topaz are similar and of the same order of magnitude. There is a pronounced structure dependence for displacements.

Bombardment-produced displacements and lattice expansions in beryl, chrysoberyl, and phenacite indicate that oxygen atoms are readily displaced and frozen in at room temperature. The expansion effects are structure dependent, and the oxygen-beryllium bonds apparently re-form at relatively low temperatures. Beryl has a less stable structure than chrysoberyl or phenacite.

X-Ray Scattering from Covalent Single Crystals (AEC Activity 4540). As a result of theoretical calculations an extensive x-ray diffraction investigation is being conducted in search of forbidden reflections in diamond, germanium, silicon, and other semiconductors. Several of these reflections have been observed to date.

ENGINEERING PROPERTIES

Radiation Effects on the Thermal Conductivity of Ceramics (AEC Activity 4540). The thermal conductivity has been measured in the temperature range from 35 to 45°C for a group of irradiated ceramic specimens. The small, thin specimens were sandwiched between mercury baths, heat was applied to the upper bath, and the temperature gradient across the specimen was measured.

Comparison of conductivities with x-ray diffraction studies showed that materials which disorder rapidly also decrease rapidly in thermal conductivity and that quite often a thermal conductivity change could be detected before a change could be found by x-ray methods.

X-Ray Examination of Ceramic Samples (AEC Activity 4540). The shielded x-ray diffractometer was used to obtain diffractometer patterns of a group of ceramics that had been exposed to 1×10^{20} and 2×10^{20} neutrons/cm^2. Optimum accuracy was not obtained because the specimens were polycrystalline, had high activity counts, and contained more impurities than are normally found in single crystals.

A Correlation of the Radiation Stability of Plastics with the Young's Modulus (AEC Activity 4540). High-energy radiation produces crosslinking and chain cleavage in organic polymers. The rates of crosslinking and cleavage are governed by the chemical structure and by the strength of the van der Waals forces. The radiation-induced changes in mechanical properties are controlled by the rates of crosslinking and cleavage. The commercial plastics previously tested are grouped according to the values of their preirradiation Young's moduli.

A theory has been postulated to account for the differences in radiation effects on the mechanical

properties of different materials. It is thought that the rate of crosslinking may be diffusion controlled, since there is evidence that during crosslinking hydrogen evolves from the sample and that there is a volume decrease. The rate of diffusion is low for the more rigid materials with strong van der Waals forces. Since increased rigidity due to crosslinking, however, does not change the van der Waals forces very much, the rate of reaction is independent of the degree of crosslinking.

The rate of chain cleavage appears to be predominantly controlled by the chemical structure of the material and is affected by rigidity only for very rigid materials.

CRYSTAL PHYSICS

Low-Temperature In-Pile Cryostat (AEC Activity 5411). Studies of copper bombarded at ~160°C indicate that some neutron-induced defects are mobile below this temperature. The laboratory has acquired a helium refrigerator with sufficient capacity to maintain the temperature of a sample below 20°K in hole 12 of the ORNL Graphite Reactor. Delivery of the machine is expected in April. The cryostat sample chamber has a diameter of $1\frac{1}{4}$ in. and a usable length of about 18 in.

The Critical Shear Stress in Alpha Brass as a Function of Zinc Concentration and Temperature (AEC Activity 5411). Preirradiation measurements were made of the critical shear stress of alpha brass with a variety of zinc compositions up to 30 at. % zinc at 4.2, 78, 195, and 297°K. Since the concentration dependence of the critical shear stress at room temperature is well known, the ratio of critical shear stress at each temperature to that at 297°K was used, rather than the measured stresses, as a standard for comparison. The ratios at each of the lower temperatures show a sharp increase from unity for 0% zinc to a plateau at about 7% zinc and then begin another increase at about 20% zinc. Below about 4% zinc, the critical shear stress at 4.2°K is actually lower than that at 78°K.

SPECIAL PROJECTS

Elastic Effects in Neutron-Irradiated LiF (AEC Activity 4540). X-ray and density changes for irradiated LiF single crystals were interpreted by correcting the original data for the elastic behavior of the crystal and were found to be equivalent within experimental error. This proves that the lattice displacements lead to Frenkel defects (equal numbers of vacancies and interstitial atoms). Thin LiF crystals were irradiated to avoid attenuation effects.

Two-Stage Annealing Process in Neutron-Irradiated LiF (AEC Activity 4540). An LiF crystal was used to determine the effects of radiation on the x-ray line broadening of the 200 and 400 reflections of copper K_β and the 200 reflection of chromium K_β at Bragg angles of 20, 44, and 31 deg. The initial broadening caused by radiation followed a tan θ law and is known as "strain broadening."

When the crystal was subjected to step anneals between 300 and 400°C, the line breadths showed no change or else changed toward their pre-exposure values. This initial stage of annealing occurs mostly within the mosaic blocks.

The anneal at 400°C decreased the radiation-produced lattice-parameter expansion by a factor of 8 or more; this reduction was apparently sufficient for the mosaic boundaries to influence the ease with which the interstitial atoms filled vacancies, and a new type of x-ray line broadening was observed. The line breadth increased for anneals at higher temperatures and decreased toward the preirradiation value.

A Study of Lattice Defects in Gold-Cadmium Alloys (AEC Activity 5411). If gold-cadmium alloys of about 50 at. % composition are quenched from 450°C, imperfections are introduced into the crystal structure; these imperfections cause an increase of more than 10% in electrical resistivity. The cause of the increase and the mechanism by which it anneals are under study. After a quench from 450 to 40°C, resistivity was measured upon isothermal annealing at a series of temperatures in the range 60 to 85°C. The defects frozen in by the quench were found to have an activation energy for movement of about 0.6 ev.

X-ray studies indicate that the alloy is ordered at temperatures up to 600°C, and therefore the increase in resistivity could not be due to the quenching in of nonequilibrium disorder. There is no evidence of the formation of a new phase, nor do quenching stresses, resulting from differential cooling between the surface and the inside of the specimen, contribute to the increased resistance.

Effect of Neutron Radiation on the Precipitation Hardening Reaction (AEC Activity 4540). Neutron irradiation of copper-beryllium alloys produced changes very similar to low-temperature precipitation hardening of the alloy, and an irradiation of

the alloy at liquid-nitrogen temperature confirmed the hypothesis that the changes were diffusion controlled.

To answer the question of whether radiation alone causes an increase in beryllium precipitation, a study was made of nickel-beryllium alloys. Nickel-beryllium was chosen because it is ferromagnetic and its Curie temperature is a function of the amount of beryllium in solid solution. Thus measurements of Curie temperature before and after irradiation and comparison with the measurements made on the control specimen will indicate whether radiation has increased the precipitation rate.

Radiation of specimens for 2×10^{18} neutrons/cm^2 at 40°C produced no change in Curie temperature. The same samples were then irradiated for 1.5×10^{18} neutrons/cm^2 at 275°C (about 200°C below the normal precipitation temperature). The Curie temperature of the control specimens corresponded to about 13.1 at. % dissolved beryllium, and that of the irradiated samples corresponded to about 12 at. % dissolved beryllium.

Reactor-Induced Resistivity Changes in Copper-Base Solid Solutions (AEC Activity 4540). Several years ago radiation was observed to decrease rather than increase the electrical resistivity of a number of stable copper solid-solution alloys, whereas an increase would be expected to result from disruption of the lattice or from transmutation. More careful measurements are being made to confirm this observation.

The resistance of 23 high-purity copper-alloy specimens was measured at three temperatures after they had been thoroughly cleaned and annealed. These specimens were then irradiated for about 2×10^{18} neutrons/cm^2 at about 40 or 50°C. The absorption cross sections of the elements were small enough for transmutation effects on resistivity to be undetectable.

All samples but the Cu-Mn alloys exhibited changes in resistivity of about the same order of magnitude for the three temperatures. It is therefore probable that the change occurs in the residual resistivity rather than in the temperature-dependent part of the resistivity for all but the Cu-Mn alloy. No satisfactory explanation has been found for the decrease in resistivity which some of the alloys exhibited.

Lattice Parameters of Some Copper Alloys (AEC Activity 4540). Polycrystalline copper-alloy samples that had been used in studies of the effect of radiation on electrical resistivity were used for x-ray diffraction studies. At low percentages of solute the lattice parameters vary nearly linearly with atomic composition and deviate only slightly from Vegard's law. Irradiated alloys studied exhibited no lattice-parameter changes after exposure.

Paramagnetic Resonances in Irradiated Materials (AEC Activity 4540). An electronic apparatus has been designed and built to measure paramagnetic resonance of piezo quartz, glass, vitreous silica, and other materials.

It has been shown that irradiation induces paramagnetic centers in quartz. The paramagnetic resonances were measured for two of the irradiated crystals on which magnetic-susceptibility measurements had been made and for a sample of diphenyl-picryl-hydrazyl. The molecular weight of the hydrazyl is 400, and there is one paramagnetic electron per molecule; on this basis the numbers of paramagnetic electrons in the two quartz crystals were calculated. The calculations indicate that there is an increase in the paramagnetic-electron concentration with increased bombardment; magnetic-susceptibility measurements show a decrease in concentration with increased bombardment. Many sources of error exist in the resonance apparatus and methods, and considerable work remains before the reliability of concentration measurements obtained by this method can be established.

Operation of the Shielded X-Ray Diffractometer (AEC Activity 4540). X-ray diffraction studies are now being conducted on specimens emitting activity of as much as 11 r/hr at 1 cm. Diffraction patterns can be obtained on either solid or powdered metal samples.

SOLID STATE REACTIONS

ENERGY LEVELS IN FAST-NEUTRON IRRADIATED p-TYPE GERMANIUM

J. W. Cleland J. H. Crawford, Jr.
J. C. Pigg

In a previous report[1] it was shown that the behavior of n-type germanium bombarded with fast neutrons at room temperature is qualitatively consistent with predictions of the energy-level model of James and Lark-Horovitz.[2] The analysis revealed that the data could be quantitatively explained by assuming that each interstitial-vacancy pair introduced by bombardment has associated with it two vacant localized states, one located 0.20 ev below the conduction band and the second below the middle of the forbidden-energy band. A similar analysis has been carried out on p-type germanium. Specimens irradiated in both the room-temperature range and at –78°C have been studied. Although the results at –78°C have been discussed previously,[3] the present analysis is based on more extensive data and, in addition, is more complete and more definitive.

It was shown in a previous report[3] that both the magnitude and the sign of the initial rate of change of hole concentration

$$\left[\frac{dp}{d(nvt_f)}\right]_{t=0}$$

are dependent on the initial hole concentration p_0 and the temperature of exposure T_e. This result is consistent with the proposed model of energy levels associated with Frenkel defects, since both occupied and vacant localized states above the top of the valence band are predicted by this model. Consequently, the situation is characterized by two competing processes: production of holes by the vacant states (acceptors) and trapping of holes by the occupied states (deep-lying donors). Under conditions of thermal equilibrium, the effect of Frenkel-defect introduction depends on the position of the initial Fermi level ζ_0 relative to the limiting value ζ^*, which is determined solely by the positions of the defect energy levels and the temperature. According to the model, two occupied levels and one vacant level are expected. If it is assumed that all the chemical acceptors are completely ionized, the law of electrical neutrality requires that

$$p = p_0 + N_1^- - N_2^+ - N_3^+ \quad , \tag{1}$$

where N_1^- is the concentration of ionized acceptors and N_2^+ and N_3^+ are the concentration of holes in the deep and shallow hole traps, respectively. If it is assumed that these levels are discrete, the law of mass action gives

$$\begin{aligned} N_1^- &= \frac{NK_1}{p + K_1} \\ N_2^+ &= \frac{Np}{p + K_2} \\ N_3^+ &= \frac{Np}{p + K_3} \quad , \end{aligned} \tag{2}$$

where

$$N = N_1 = N_2 = N_3 \quad ,$$

N is the defect concentration, and

$$K_i = \gamma_i C(T) e^{-\epsilon_i/kT} \quad , \tag{3}$$

where

$$C(T) = \left(\frac{2\pi m_h kT}{h^2}\right)^{3/2} \quad ,$$

ϵ_i is the energy of the level measured from the top of the valence band, and γ_i takes a value of either unity or 4, depending on whether the state occupied by the hole has a residual electronic spin or not.[4] Substitution of Eqs. 2 in Eq. 1 yields

$$p = p_0 + N\left[\frac{K_1}{p + K_1} - \frac{p}{p + K_2} - \frac{p}{p + K_3}\right] \quad , \tag{4}$$

[1] J. W. Cleland and J. H. Crawford, Jr., *Solid State Semiann. Prog. Rep. Aug. 30, 1954*, ORNL-1762, p 71–75.

[2] H. M. James and K. Lark-Horovitz, *Z. physik. Chem.* 198, 107 (1951).

[3] J. H. Crawford, Jr., and J. W. Cleland, *Solid State Quar. Prog. Rep. May 10, 1952*, ORNL-1301, p 39–45.

[4] N. F. Mott and R. W. Gurney, *Electronic Processes in Ionic Crystals*, 2d ed., p 157–158, Oxford University Press, London, 1948. (The necessity of using this statistical factor was pointed out to the authors by H. M. James.)

a quartic equation in p. If

$$(5) \qquad p_0 = p^* = 2\,C(T)e^{-\zeta^*/kT} \quad ,$$

where p^* is the limiting hole concentration for the temperature in question, p will remain invariant with defect introduction. Under these conditions Eq. 5 reduces to the cubic equation:

$$(6) \qquad p^{*3} + \frac{1}{2}(K_1 + K_2 + K_3)p^{*2} - \frac{1}{2}K_1K_2K_3 = 0 \quad .$$

Only the positive root of Eq. 6 is significant, and, to a good approximation, it is given by

$$(7) \qquad p^* = \left(\frac{K_1K_2K_3}{K_1 + K_2 + K_3}\right)^{1/2} \quad .$$

With the use of Eqs. 3 and 5, Eq. 7 becomes

$$(8) \qquad \zeta^* = \frac{\epsilon_1 + \epsilon_2 + \epsilon_3}{2} - \frac{1}{2}kT\left[\frac{4\left(\gamma_1 e^{-\epsilon_1/kT}\gamma_2 e^{-\epsilon_2/kT}\gamma_3 e^{-\epsilon_3/kT}\right)}{\gamma_1\gamma_2\gamma_3}\right] \quad .$$

If ϵ_3 is significantly smaller than ϵ_2 and hence ϵ_1, Eq. 8 may be approximated by

$$(9) \qquad \zeta^* \cong \frac{\epsilon_1 + \epsilon_2}{2} - \frac{1}{2}kT \ln \frac{4}{\gamma_1\gamma_2} \quad ,$$

which is identical to the expression obtained for a single trapping level and a single acceptor. The temperature dependence of ζ^* clearly enters through the logarithmic term of Eq. 9, which, in this approximation, is

$$(10) \qquad \frac{d\zeta^*}{dT} = -\frac{1}{2}k \ln \frac{4}{\gamma_1\gamma_2} \quad .$$

From the nature of the levels below the middle of the band as suggested by the theory,[2] it can be shown, whatever the identification of levels in question with those available, that $\gamma_1\gamma_2 = 4$. Hence $d\zeta^*/dT \cong 0$.

The value of ζ^* indicates only the mid-point between the acceptor and the deepest hole traps. It is possible in principle to determine ϵ_1 and ϵ_2 from initial rates of change of p during bombardment as a function of p_0, provided that the relation between N and integrated flux is known. The derivative of Eq. 4 with respect to N, the number of defects, evaluated at $N = 0$ and $p = p_0$, gives for the initial rate of change

$$(11) \qquad \left(\frac{dp}{dN}\right)_{N=0} = \frac{K_1}{p_0 + K_1} - \frac{p_0}{p_0 + K_2} - \frac{p_0}{p_0 + K_3} \quad .$$

Hence, there are apparently three adjustable parameters, which would seem to indicate that the curve fitting with Eq. 11 may not be a sensitive test of the theory. In actual fact, however, the condition imposed by either Eq. 8 or Eq. 9 reduces the number of parameters to 2. Furthermore, the contribution of the last term of Eq. 11 is negligible until ζ_0 lies within about $2kT$ of ϵ_3.

In order to test the theory rigorously it is necessary to use the values of ϵ_1, ϵ_2, and ϵ_3 obtained by using Eq. 11 to reproduce a representative conductivity vs bombardment curve according to Eq. 4. The latter test is possible only if (1) the effect of bombardment on mobility is negligible compared with the effect on hole concentration, (2) there is no differential annealing of different types of defects during exposure, and (3) appreciable photoconductivity is absent. In the following section these relations will be applied to the behavior of conductivity measured during bombardment at ambient (30 to 60°C) and dry-ice temperature.

The conductivity, σ, of a large number of single-crystal p-type samples with a wide range of hole concentrations has been measured during bombardment in the reactor at ambient temperature. Under the assumption that the initial change of mobility is negligible compared with the effect on hole concentration, the initial change in hole concentration per incident fast neutron $[dp/d(nvt_f)]_{t=0}$ was calculated from σ vs nvt curves by using the

initial conductivity σ_0 and uncorrected values[5] of p_0 obtained from Hall coefficient measurements. Values of p_0, $[dp/d(nvt_f)]_{t=0}$, and the exposure temperature for these specimens are listed in Table 1. Although there is scatter in the data, it is apparent that $[dp/d(nvt_f)]_{t=0}$ changes from positive to negative with increasing p_0 at $p^* = (6.5 \pm 1.5) \times 10^{16}$ cm^{-3}. The value of ζ^* at this temperature (~50°C) may be obtained from Eq. 5 provided that m_h is known. Studies of cyclotron resonance[6,7] indicate that $m_h \cong 0.3\, m_0$. With this value of m_h, $\zeta^* = 0.120 \pm 0.006$ ev at 323°K. Besides ambient exposures, a number of specimens have been irradiated at dry-ice temperature. At −78°C, $p^* = (1.5 \pm 0.2) \times 10^{15}$ cm^{-3}, which gives $\zeta^* = 0.123 \pm 0.003$ ev. Hence it appears that ζ^* is temperature independent within experimental error. This would indicate that the approximation that leads to Eq. 9 is a good one.

Attempts have been made to evaluate ϵ_1, ϵ_2, ϵ_3 by using Eq. 11 to fit the $[dp/d(nvt_f)]_{t=0}$ vs p_0 curve for the −78°C exposures. It has been shown[8] that ~3.2 electrons are removed per incident fast neutron in moderate to high conductivity n-type material. Since two electron traps are expected per Frenkel defect,[9] this result indicates that C, the number of defects per incident neutron, is approximately 1.6. The results of the analysis are shown in Fig. 1. The points are experimental, and the solid curve was calculated from Eq. 11 by using $\epsilon_1 = 0.180$ ev, $\epsilon_2 = 0.066$ ev, and $\epsilon_3 \cong 0$ and by assuming that $\gamma_1 = 4$ and $\gamma_2 = 1$. When expected experimental uncertainties are considered, a reasonable fit to

[5] Here, hole concentrations were calculated from the customary relation

$$p = \frac{7.37 \times 10^{18}}{R}.$$

No attempt was made to correct the values for impurity scattering, since recent work of F. J. Morin [*Phys. Rev.* **93**, 62 (1954)] has shown that the ratio of Hall to drift mobility, μ_H/μ_d, for holes not only does not have the proper magnitude but is markedly temperature dependent. Willardson, Harman, and Beer (submitted to *Phys. Rev.*) have shown that this discrepancy is due to the complex nature of the valence band in germanium. Consequently, values of p given in this paper may be in error by as much as a factor of 2.

[6] G. Dresselhaus, A. F. Kip, and C. Kittel, *Phys. Rev.* **92**, 827 (1953).

[7] R. N. Dexter, H. J. Zeiger, B. Lax, and E. S. Rosenblum, *Phys. Rev.* **95**, 597 (1954).

[8] J. W. Cleland *et al.*, *Phys. Rev.* **83**, 312 (1951).

[9] H. M. James and K. Lark-Horovitz, *Z. physik. Chem.* **198**, 107 (1951).

TABLE 1. INITIAL RATE OF CHANGE OF HOLE CONCENTRATION DURING REACTOR AMBIENT-TEMPERATURE BOMBARDMENT

Sample No.	p_0, Initial Hole Concentration (cm^{-3})	T_e, Exposure Temperature (°C)	$[dp/d(nvt_f)]_{t=0}$, Initial Rate of Change of Hole Concentration
1	4.2×10^{14}	20	0.70
2	1.7×10^{15}	30	0.77
3	3.5×10^{16}	53	0.08
4	4.0×10^{16}	55	0.20
5	5.7×10^{16}	62	0.037
6	7.2×10^{16}	49	−0.058
7	8.1×10^{16}	50	−0.10
8	1.5×10^{17}	62	−0.05
9	5.3×10^{17}	45	0.80
10	7.0×10^{17}	32	−0.50
11	1.3×10^{19}	48	−2.2
12	1.5×10^{19}	48	−2.9

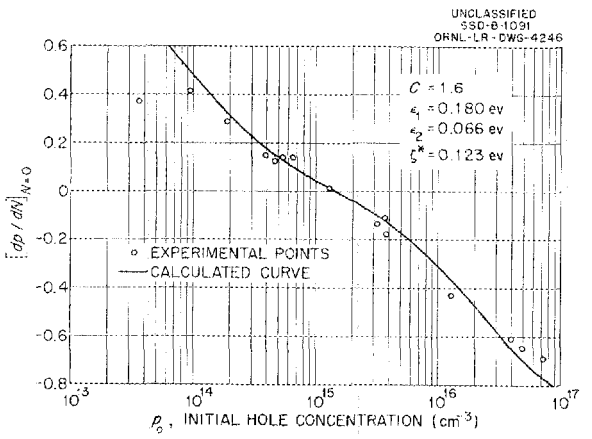

Fig. 1. Initial Rate of Hole Removal vs Initial Hole Concentration at –78°C for p-Type Germanium.

the data was obtained. Interchange of the values of γ_1 and γ_2 did not permit a good correlation even for a wide range of choice of energy parameters. These results strongly indicate that, provided the model is valid, ϵ_3 is quite small and therefore that only one hole trap need be considered at this temperature, as well as at higher temperatures. Furthermore, the required choice of values for γ_1 and γ_2 indicates that the acceptor can be identified with the doubly ionized interstitial atom.

The energy parameters obtained above were used in Eq. 4 to calculate σ vs nvt_f curves obtained at –78°C on the assumption that the mobility was unaffected by exposure. Although reasonable correspondence was obtained early in the exposure, as the bombardment proceeded, the calculated and observed curves began to diverge. It is interesting to note that the calculated curve predicts a lower value of σ after appreciable exposure than is actually observed for p_0 either greater or less than p^*. A decrease in mobility during exposure would cause this discrepancy to be reversed. The greater observed values of σ may be due to either of two processes or to both of them: (1) trapped minority carriers which produce an excess concentration of majority carriers, thus enhancing σ, and (2) a difference in the annealing rate of the two types of defects which would alter the relative concentration of energy levels arising from each type and, thereby, the distribution of energy levels. If the second process is responsible, the alteration of the distribution must occur in such a direction to cause p^* apparently to increase as bombardment progresses. Evidence for both these processes will be discussed in more detail.

The results of the foregoing analysis of the initial behavior of conductivity during bombardment reveal that the model proposed by James and Lark-Horovitz is consistent with observation. When applied to the behavior on prolonged bombardment, qualitative agreement is still obtained, but the data indicate that additional processes appear which require explanation. In this connection it should be pointed out that similar studies carried out with 10-Mev deuterons[10] at a much higher rate of defect introduction showed some interesting differences. The value of ζ^* obtained by fitting a σ vs bombardment curve at –78°C was 0.089 ev, a considerably smaller value than the one obtained above from initial behavior. In addition, specimens with p_0 only slightly greater than the value of p^* obtained with fast neutrons showed first a decrease in σ followed by an increase after additional deuteron bombardment. Although it is possible that the different results may be due to differences in the effect of fast neutrons and charged particles, it is interesting to note that these deviations are in the direction expected if process 2 were operating.

In general, the hole concentration before exposure is only slightly temperature dependent. Since, according to the model in question, ζ^* is essentially temperature independent and p^* is given by Eq. 5, p^* is expected to correspond to p_0 at some temperature T^* in an easily attainable temperature range (77 to 300°K) over a wide range of p_0 values (10^{13} to 10^{17} cm^{-3}). Consequently, an increase in p above T^* and a decrease in p below T^* should result from bombardment. As bombardment proceeds, the log R vs $1/T$ curve is expected to rotate about the point $1/T^*$ and to approach a limiting slope of ζ^*/k for large exposures.

Log R vs $1/T$ curves have been obtained after various exposures on a number of p-type specimens. Because of the induced radioactivity in the specimen and holder, it was usually necessary to wait appreciable periods (one to three days) before handling was safe. Since room-temperature

[10] H. Y. Fan, J. H. Forster, and K. Lark-Horovitz, *Semiconductor Research Third Quarterly Report, Jan. 1, to March 31, 1952*, PRF-746, p 28–31. See also thesis of J. H. Forster, Purdue University, 1953 (unpublished).

aging may occur during this waiting period, the curves do not necessarily represent conditions existing immediately after the specimen and holder are removed from the reactor. Typical log R vs $1/T$ curves after bombardment are compared with their original curves in Fig. 2 for three widely different values of p_0. The curve in Fig. 2*a* was taken 3.5 days after an exposure to 1.3×10^{17} fast neutrons/cm^2 at 60°C on a specimen with $p_0 = 3.4 \times 10^{18}$ cm^{-3}, that in Fig. 2*b* was obtained 6 days after $nvt_f = 5.6 \times 10^{16}$ cm^{-2} at 60°C with $p_0 = 7.0 \times 10^{16}$ cm^{-3}, and that in Fig. 2*c* 19 hr after $nvt_f = 2.2 \times 10^{16}$ cm^{-2} at 60°C with $p_0 = 7.3 \times 10^{14}$ cm^{-3}. The dashed curves are after exposure.

The curve in Fig. 2*a* indicates that bombardment decreases the hole concentration over the entire temperature range. This behavior is borne out by the observed conductivity change during exposure. Further irradiation was found to produce an additional decrease in σ toward a limiting value. In Fig. 2*b*, the curve after exposure crosses the original curve and indicates an increase in p above 250°K and a decrease in p at lower temperatures. The behavior in these two cases is qualitatively what is expected according to the model employed. In the case of small p_0, however, indications of Fig. 2*c* are that there is an increase in p over the entire temperature range despite the value of ζ^* indicating that the two curves should cross at $T^* = 166$°K. Furthermore, the curvature after bombardment suggests a wide distribution of acceptor-level energies from an appreciable value at room temperature to a value near zero at liquid-nitrogen temperature. These results indicate that, although there is qualitative agreement with the model at high values of p, there is a serious lack of agreement for small hole concentrations. The discrepancy cannot reasonably be explained by the initial introduction of an appreciable concentration of very shallow acceptors during bombardment, since they would, to a large extent, mask the presence of hole traps indicated by studies of initial behavior (see above). Rather, it is necessary to assume that the apparent low acceptor ionization energy results from some process which occurs during bombardment or during the aging period at room temperature. The same two processes mentioned above appear to be probable, namely, trapping of minority carriers or differential annealing of interstitials and vacancies. Evidence for these two processes will be treated in turn.

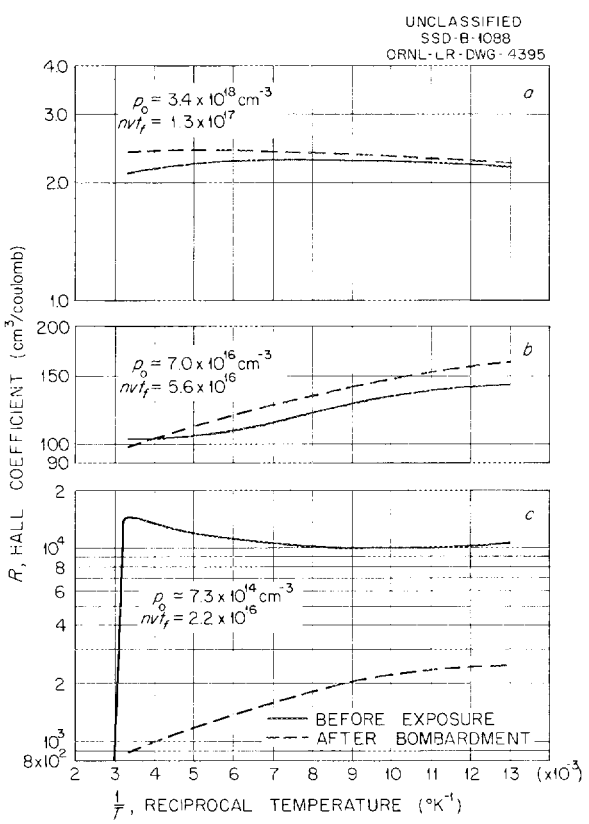

Fig. 2. Hall Coefficient vs Reciprocal Temperature for *p*-Type Germanium Before and After Exposure.

On close examination it was found that, at liquid-nitrogen temperature, the Hall coefficient and resistivity of irradiated samples were appreciably photosensitive. All the data, however, were taken on specimens wrapped with several layers of linen tape and mounted in a narrow-neck Dewar, the mouth of which was plugged with glass wool. Consequently, the amount of ambient light incident on the specimen was quite small. It was impossible, however, to exclude the gamma and beta radiation which resulted from radioactive decay of the specimen, leads, and holder. This radiation, even though of relatively low intensity, is efficient in producing electron hole pairs. Therefore measurements at low temperature taken shortly after removal from the reactor undoubtedly include photo effects. This process, however, cannot be solely responsible for the discrepancy,

since, after the activity in the specimen and its surroundings had essentially completely decayed, the difference between the observed and expected curve persisted.

The possible alteration of the distribution of energy levels was examined by following the process of aging at room temperature and slightly above. Both specimens studied showed a flattening of the log R vs $1/T$ curve while standing at room temperature. In one, the curve after exposure crossed the original one, and it was difficult to decide whether the flattening of the curve was a result of uniform annealing of the vacancies or an alteration of the energy-level distribution. The second specimen gave a curve similar to that of Fig. 2c, and its interpretation is less ambiguous. The results of the study are shown in Fig. 3. Curve I is the log R vs $1/T$ curve before bombardment, curve II is that 10 hr after an nvt_f of 2.6×10^{16} cm^{-2}, curve III is that after an additional 96 hr, and curve IV was obtained after subsequently warming to 140°C for 10 min. The curvature of curve II is such that, if its trend continues, it will not intersect curve I. R and ρ, measured during subsequent aging, showed a slow decrease at 77°K. After 106 hr of total aging, the changes were very slow, and curve III resulted. If both interstitials and vacancies were removed at

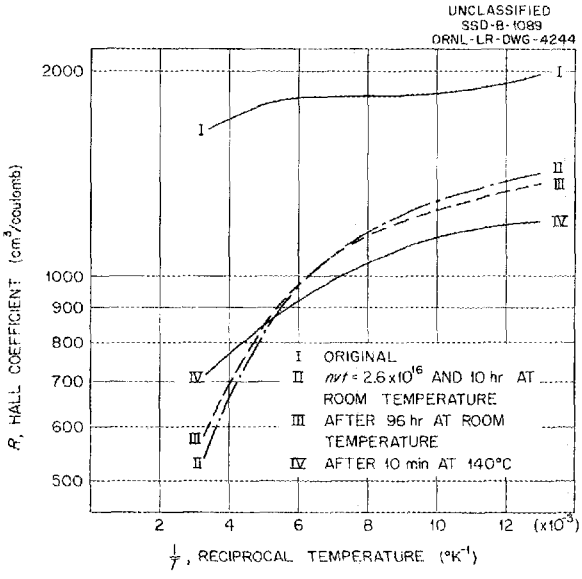

Fig. 3. Hall Coefficient vs Reciprocal Temperature for p-Type Germanium.

the same rate, the curves after bombardment would be expected to approach the original one rather uniformly over the entire range. Comparison of curves II and III, however, shows that this is not the case. Instead, the decrease at low temperature and the increase at high temperature indicate that the distribution of acceptors is shifted toward lower ionization energy. In addition, since a rotation, instead of a general lowering, of curve III with respect to curve II occurs, the total concentration of acceptors apparently decreases during aging. It is evident from curve IV that after the specimen was heated at 140°C for 10 min the process is accelerated and a marked flattening of the curve occurs.

In view of these observations it is not unreasonable to assume that similar annealing occurs during exposure. According to the model in question a vacancy introduces two low-lying empty states which are filled by electrons from a doubly ionized interstitial. If an interstitial is removed by some process, such as clustering or trapping in the vicinity of a dislocation, two shallow acceptors are produced. Since a decrease in total acceptor concentration is also observed, recombination of interstitials and vacancies must also be postulated. It is noteworthy that these assumptions require the interstitial atom to be the mobile component of the Frenkel defect. These considerations receive support from observations[11] on low-temperature aging of irradiated n-type germanium and from quenching experiments of Mayburg.[12]

The temperature dependence of hole concentration (see ref. 5) after successive periods of bombardment at approximately 40°C was determined from Hall-coefficient measurements on one p-type specimen ($p_0 = 1.8 \times 10^{15}$ cm^{-3}). Representative p vs T curves after various exposures are shown in Fig. 4. All the curves after bombardment are characterized by a sigmoid involution, with their inflection points centered in the vicinity of 145°K, superimposed on an almost linear increase in p with T. The almost linear increase of p indicates a broad distribution of acceptor ionization energies, whereas the sigmoid step reveals the presence of a discrete level or closely grouped

[11] J. W. Cleland and J. H. Crawford, Jr., *Solid State Semiann. Prog. Rep. Aug. 30, 1954*, ORNL-1762, p 71–75.

[12] S. Mayburg, *Phys. Rev.* **95**, 38 (1954).

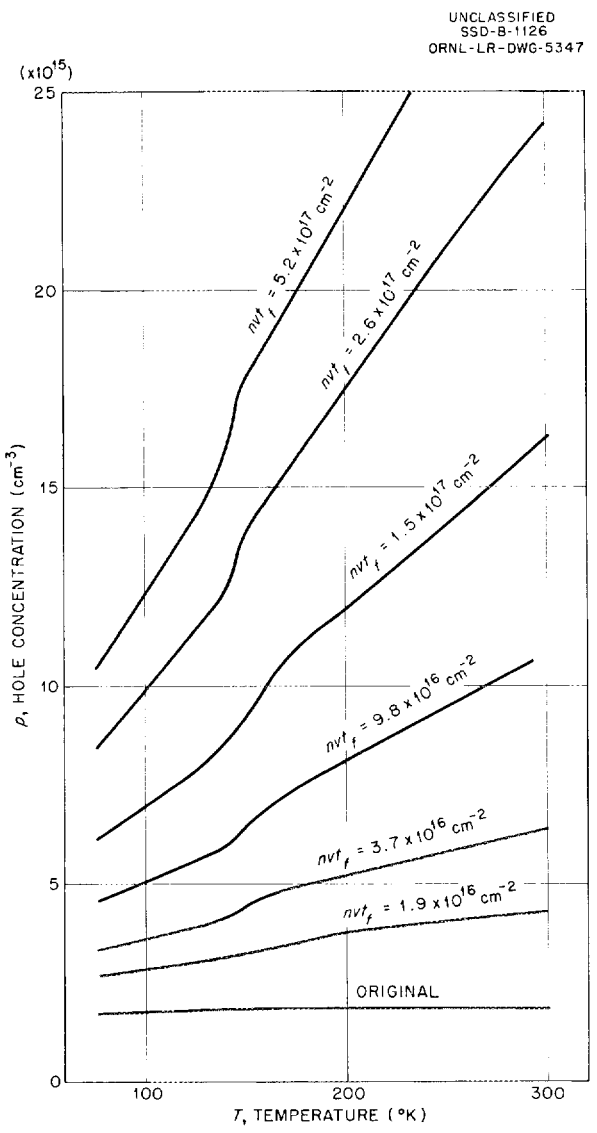

Fig. 4. Hole Concentration vs Temperature after Successive Periods of Bombardment.

set of levels superimposed on the broad distribution. Although it is possible to obtain acceptable fits to these curves by using arbitrarily chosen acceptor distributions,[13] such fits require the use of at least four adjustable parameters. Consequently, little can be learned concerning the nature of the broad distribution by these means. Such calculations, however, indicate that the discrete level or bump in the distribution lies in the vicinity of 0.10 ev above the band edge.[13]

In the case of an n-type specimen converted to p-type by bombardment, the resulting energy-level distribution may be examined without complications produced by holes initially present. Log R vs $1/T$ curves obtained after bombardment on an originally n-type specimen ($n_0 = 7.5 \times 10^{15}$ cm^{-3}) are shown in Fig. 5. Curve I was obtained after an $nvt_f = 1.0 \times 10^{16}$ cm^{-2}, curve II after an $nvt_f = 2.2 \times 10^{16}$ cm^{-2}, curve III after a 40-day anneal at room temperature, and curve IV after

[13] The authors have employed with good results a uniform distribution extending from the edge to the center of the forbidden band with a superimposed discrete level centered ~0.10 ev above the band edge (J. W. Cleland, J. H. Crawford, and J. C. Pigg, *Solid State Quar. Prog. Rep. Feb. 10, 1953*, ORNL-1506, p 43). In addition, I. M. Katz (*Solid State Semiann. Prog. Rep. Aug. 31, 1953*, ORNL-1606, p 68) has obtained an excellent fit by using a Gaussian distribution of levels of 0.236-ev half width centered at the middle of the forbidden band with a superimposed discrete level at ~0.09 ev.

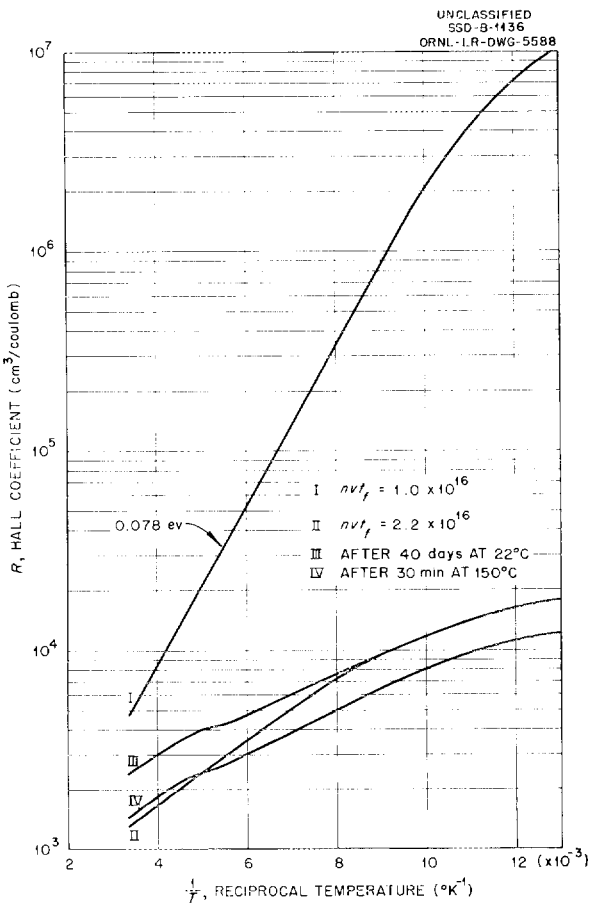

Fig. 5. Hall Coefficient vs Reciprocal Temperature of Germanium after Irradiations and Anneals.

annealing for 30 min at 150°C. Shortly after conversion to p-type, the slope of the log R vs $1/T$ curve (curve I) is linear over most of the range, with a slope corresponding to an acceptor ionization energy of about 0.08 ev. This level probably corresponds to the one that produced the step in Fig. 4. The curvature toward lower slope near 77°K indicates the presence of more shallow levels. After additional irradiation (curve II), the shift of acceptor ionization toward lower values is evident. After the 40-day room-temperature anneal (curve III), behavior is observed which is similar to that of initially p-type specimens. The room-temperature aging process is essentially complete after 40 days, as is evidenced by the uniform decrease of p over the entire range which accompanies the 150°C annealing period (curve IV).

The level at 0.08 ev may presumably be identified with the deep trap determined from the dry-ice experiments discussed above.

EFFECT OF BOMBARDMENT ON HOLE MOBILITY IN p-TYPE GERMANIUM

J. W. Cleland J. H. Crawford, Jr.
J. C. Pigg

Studies[14] of n-type germanium reveal that fast-neutron bombardment markedly decreases electron mobility. Moreover, the additional scattering was found to possess a greater temperature dependence than that predicted by the usual theories of ionized impurity scattering. Similar studies have been carried out on p-type germanium.

In Fig. 6 the mobility,[15] μ_h, is plotted against temperature for the specimen of Fig. 4 ($p_0 = 1.8 \times 10^{15}$ cm^{-3}) after several exposures. Values of nvt_f for each exposure are indicated on the curves. The slope of the curve before irradiation at high temperature is −2.1, in reasonable agreement with the reported temperature dependence for lattice scattering in p-type germanium.[16, 17] Furthermore, the initial curve shows the expected onset of the ionized impurity scattering at low

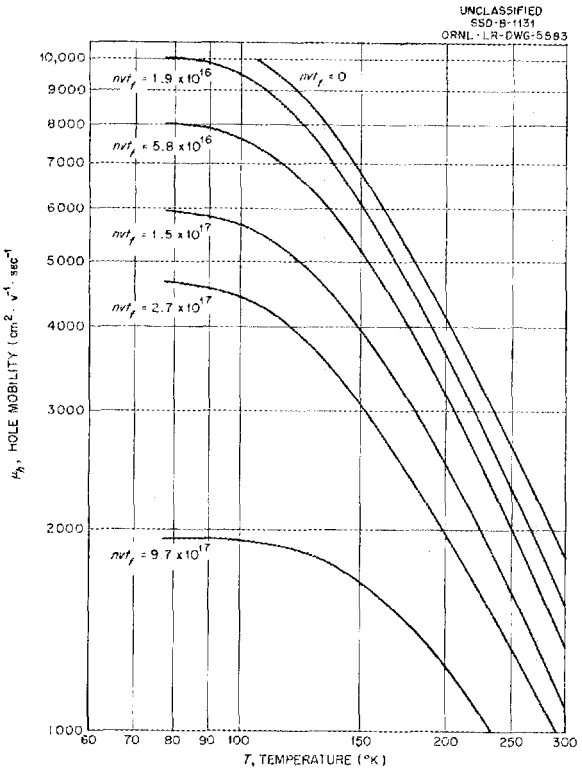

Fig. 6. Hole Mobility vs Temperature for Irradiated p-Type Germanium.

temperatures, which is not sufficiently great at this concentration to produce a maximum in the curve in this temperature range (77 to 300°K). On bombardment, μ_h decreases over the entire temperature range and decreases somewhat greater at low temperature. It is interesting to note that, even after appreciable bombardment, no discernible maximum is produced. If the additional bombardment-induced scattering were strictly of the charge-center type, a maximum which moves toward higher temperature with increasing defect introduction might be expected to appear. The lack of such a maximum may be taken as tentative evidence that the scattering associated with lattice damage of this type may not be amenable to treatment in terms of ionized impurity scattering.[18–20] It is noteworthy, however, that the excessively large

[14] J. W. Cleland and J. H. Crawford, Jr., *Solid State Semiann. Prog. Rep. Aug. 30, 1954*, ORNL-1762, p 75.

[15] As used here, $\mu_h = R/rp$, where the Hall parameter r is taken to be $3\pi/8$, the same value as that used in deriving p. Although the true value of r may be quite different from this (see ref. 5), it is desirable to use the same value throughout, since r is thus effectively eliminated when $1/\mu_h$ is compared with p (Fig. 7).

[16] M. B. Prince, *Phys. Rev.* 92, 681 (1953).

[17] F. J. Morin, *Phys. Rev.* 93, 62 (1954).

[18] E. Conwell and V. F. Weisskopf, *Phys. Rev.* 77, 388 (1950).

[19] H. Brooks, *Phys. Rev.* 83, 879 (1951).

[20] P. P. Debye and E. M. Conwell, *Phys. Rev.* 93, 693 (1954).

temperature dependence of electron mobility observed in bombarded n-type germanium[21] is absent in p-type germanium. Similar behavior to that shown in Fig. 6 was observed with a number of other specimens. In no case was a maximum observed which was not already present before exposure.

Since the curves of Fig. 6 indicate that μ_b at 77°K is limited predominantly by scattering processes other than lattice scattering, the reciprocal of this value, $1/\mu_{77}$, is expected to be approximately proportional to the scattering probability of these processes at that temperature. The dependence of the scattering probability on defect concentration is shown in Fig. 7, where $1/\mu_{77}$ is plotted against the hole concentration at 77°K. The convenient use of p_{77} as an index of disorder is possible because it increases approximately linearly with exposure. After the initial exposure, all points fall on a straight line, whose slope is 2.1×10^{-20} in appropriate units. Since the same value of the Hall parameter was used in determining both μ and p, the correlation should be independent of its value (see ref. 15).

[21] J. W. Cleland and J. H. Crawford, Jr., *Solid State Semiann. Prog. Rep. Aug. 30, 1954*, ORNL-1762, p 71–75.

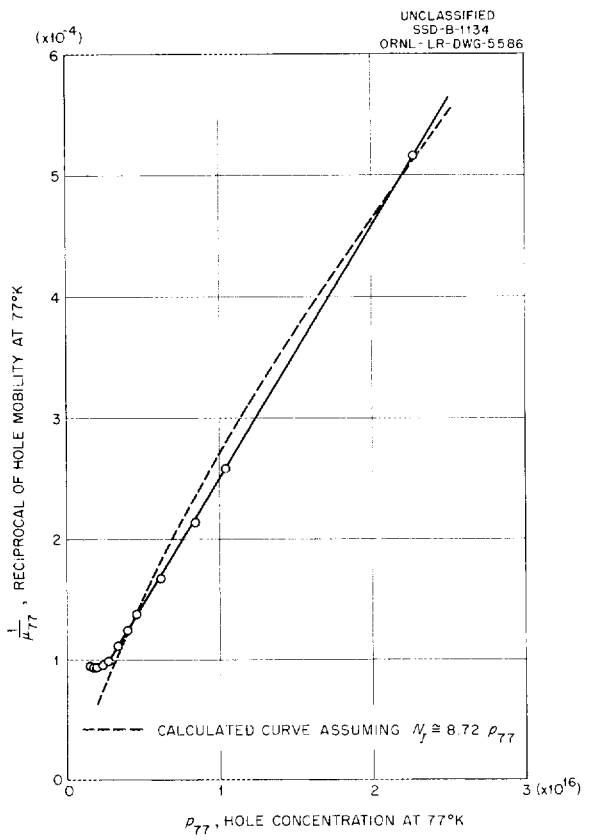

Fig. 7. Reciprocal of Hole Mobility vs Hole Concentration at 77°K in Irradiated p-Type Germanium.

Although it was indicated above that the scattering mechanism of the defects may not be of the ionized-impurity type, it can be shown that the data of Fig. 7 are not completely inconsistent with such a model. According to the Frenkel-defect energy-level model,[22] it is reasonable to expect the concentration of ionized scattering centers to be considerably larger than p_{77}. Moreover, the model suggests that an appreciable fraction of these may be doubly rather than singly charged. For a mixture of scattering charges, it is necessary to write the Conwell-Weisskopf formula[18] in a more general form.[23] In terms of the measure of scattering probability used here,

$$(12) \qquad \frac{1}{\mu_{77}} = A\overline{Z^2}N_I \ln\left(1 + \frac{B}{\overline{Z^2}N_I^{2/3}}\right) ,$$

where

$$A = \frac{\pi^{3/2}m^{*1/2}e^3}{2^{7/2}\kappa^2(kT)^{3/2}} ,$$

$$B = \left(\frac{3kT}{e^2}\right)^2 ,$$

N_I is the total concentration of all ionized scatterers regardless of magnitude of charge, and $\overline{Z^2}$ is the mean square of the charges,

$$(13) \qquad \overline{Z^2} = (\Sigma_i z_i^2 N_i)N_I ,$$

and the subscript i refers to those ions of the same charge magnitude.

It was shown in the previous section that, presumably because of different annealing kinetics of the interstitials and vacancies, the energy-level model begins to break down after appreciable exposure. Consequently, it is useless to attempt

[22] H. M. James and K. Lark-Horovitz, *Z. physik. Chem.* 198, 107 (1951).

[23] W. Shockley, *Electrons and Holes in Semiconductors*, p 264, Van Nostrand, New York, 1950.

to evaluate $\overline{Z^2}$ on the basis of the model. However, the product $\overline{Z^2}N_I = N_I'$ can be determined approximately from experiment by setting $\overline{Z^2}N_I^{2/3} = N_I'^{2/3}$ in the logarithmic term. This approximation would tend to make N_I' too small;[24] however, since, for a maximum charge of two units, $\overline{Z_1^2} < 4$, the error is probably less than a factor of 1.5. The ratio of N_I', the effective concentration of singly charged scatters required to produce the observed scattering probability, to p_{77} was obtained by matching the experimental curve of Fig. 7. The dashed curve shows the results obtained by using $m^* = 0.3\ m_0$ and $N_I'/p_{77} = 8.72$. A reasonable agreement with regard to magnitude was obtained, but the calculated curve shows a distinct curvature which is not apparent in the experimental one.

PHOTOCONDUCTIVITY AND MINORITY-CARRIER TRAPS IN BOMBARDED n-TYPE GERMANIUM

J. W. Cleland J. H. Crawford, Jr.
J. C. Pigg

In an earlier report[25] a peculiar oscillatory behavior was noted in the conductivity vs temperature curve obtained on n-type specimens during warming after low-temperature bombardment. Attempts were made to explain the successive maxima in terms of low-temperature annealing processes which involved the rearrangement of lattice disorders. Recent work by experimenters at Bell Laboratories[26] has shown that low-temperature electron bombardment of both n- and p-type germanium introduces minority-carrier traps which give rise to appreciable photoconductivity at low temperature. In view of their findings, previous data[25] have been re-examined. In the present discussion, only those data obtained during warming, when the reactor was not in operation, will be considered. The results are reprinted for convenience in Fig. 8.

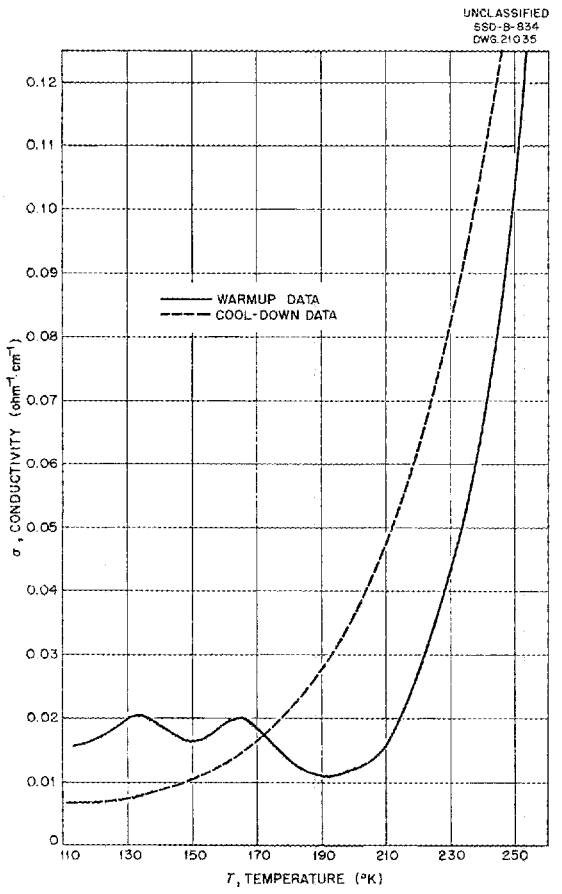

Fig. 8. Conductivity vs Temperature for n-Type Germanium Sample S-1-4-1 after 1125-min Exposure at −157(±2)°C.

After the sample had been irradiated (nvt_f = 2.4 × 10^{16} cm^{-2}) and had been maintained at 114°K for 40 min, it was warmed in the reactor at a relatively uniform rate (~1°C min^{-1}) to 260°K and then recooled. The σ vs T curves are shown in Fig. 8; the solid and dashed curves refer to the warming and cooling operations, respectively. Two well-defined maxima falling at 134 and 165°K are observed during warming. After the second maximum σ falls to a minimum value at ~195°K, it increases rapidly with further heating. The oscillatory behavior is interpreted as the successive escape of trapped holes (and their subsequent recombination with excess electrons) from two discrete trapping levels of different depth. Since the warming was conducted in the reactor, it is assumed that at 114°K the gamma-ray intensity

[24] There is another factor which has the opposite effect. The Conwell-Weisskopf scattering formula does not include screening effects. These are apt to become important even in this concentration range when $N_I > p$, thus decreasing the screening and increasing the scattering power of the ions (see ref. 20). The error involved in the approximation is expected to be compensated to some extent by the neglect of screening.

[25] J. W. Cleland, J. H. Crawford, Jr., and J. C. Pigg, *Solid State Semiann. Prog. Rep. Aug. 31, 1953*, ORNL-1606, p 67, Figs. 57 and 58.

[26] W. L. Brown, R. C. Fletcher, and K. A. Wright, *Phys. Rev.* 96, 834 (1954).

is sufficient to saturate these traps and that the rate of heating is sufficiently low to preserve steady-state conditions. As the temperature is raised, a point is reached at which the rate of release of holes from traps becomes comparable to the rate of trapping, and saturation is no longer possible. With further heating, the traps empty rapidly and the transition from a filled to an empty condition occurs over a relatively narrow temperature range. Although it is possible in principle to calculate the trap depth ϵ_t from the position of the inflection point,[27] the situation is complicated in the present case by the strong and unknown temperature dependences of mobility μ_e and electron concentration n in the range of interest. Consequently, it is impossible to make a reliable estimate of the trap depths in question.

When the sample is cooled at about the same rate, the reappearance of the same maxima under steady-state conditions of excitation would be expected, provided that the traps are still present and that the gamma-ray intensity is unchanged. The cooling curve in Fig. 8 shows no such behavior, and it is concluded that those traps which are responsible for the oscillatory behavior of the warming curve have annealed. This result is consistent with the findings on electron-bombarded Ge[22]. That some sort of annealing has occurred during the temperature excursion is evident from the position of the cooling curve relative to the heating curve. The cooling curve lies appreciably above the warming curve at temperatures above 173°K. It crosses the warming curve at that point and attains a value at 113°K of only about half the value before heating. The increase in σ in the range above 173°K can be caused either by an improvement in μ_e which had been decreased by bombardment or by the annealing of a portion of the defects responsible for removing electrons, or more probably by both. After heating, a decrease in σ at the low-temperature end of the curve is expected if the hole traps have annealed, since an important source of photoconductivity is thereby removed. It was possible to retrace the cooling curve at least as high as 200°K by subsequent warming.

The behavior attributed to trapping described above was confirmed by the warming of an n-type sample in which σ was reduced from 52 to 2.3 $ohm^{-1} \cdot cm^{-1}$ by bombardment at 116°K. Again, two maxima in the same temperature range of the σ vs T curve were observed during warming. It is interesting to note in this connection that one sample, which was bombarded almost to the conductivity minimum and hence was essentially intrinsic, showed only a small indication of the first maximum and none at all of the second. Such behavior would be expected when the Fermi level lies deep in the forbidden band or near one of the trapping levels.[27]

[27] H. Y. Fan, *Phys. Rev.* 92, 1424 (1953).

ANNEALING OF IRRADIATED GERMANIUM

J. W. Cleland J. H. Crawford, Jr.
J. C. Pigg

It is well known that nearly all the effects of fast-neutron bombardment on the conductivity σ and Hall coefficient R can be removed by suitable annealing. Heat treatment of irradiated specimens at approximately 450°C for periods in excess of 12 hr causes the conductivity and the Hall coefficient to revert to their values before exposure, provided that effects associated with transmutation-produced impurities are accounted for.[28] In addition to complete annealing of lattice damage introduced at or near room temperature, it has been shown[29] that, during warming, a considerable fraction of the changes in σ and R produced by bombardment at temperatures below −100°C anneal at a point well below room temperature. Recently, studies of energy levels in both n- and p-type germanium indicate that annealing of effects introduced at or near room temperature during room-temperature storage is also important.[30] Moreover, this annealing produces an effect opposite to that normally expected in that the property change is observed to increase rather than decrease with time.

In order to study the effect in greater detail, an n-type specimen was irradiated at 35°C until its room-temperature σ was decreased by a factor of approximately 8. After the sample was removed from the reactor, R and σ were measured as a function of temperature in the range from liquid-

[28] J. W. Cleland *et al.*, *Phys. Rev.* 83, 312 (1951).

[29] J. W. Cleland, J. H. Crawford, and J. C. Pigg, *Solid State Quar. Prog. Rep. Aug. 10, 1952*, ORNL-1359, p 36; *ibid., Solid State Semiann. Prog. Rep. Aug. 31, 1953*, ORNL-1606, p 62.

[30] J. W. Cleland and J. H. Crawford, Jr., *Solid State Semiann. Prog. Rep. Aug. 30, 1954*, ORNL-1762, p 71; see also p 6, this report.

nitrogen to room temperature. Immediately thereafter, the specimen was subjected to isothermal anneals at successively high temperatures in the range from 0 to 100°C. The results of these anneals are shown in Fig. 9, where curves of σ vs annealing time at the various temperatures are shown. The two lowest temperature anneals (0 and 23.3°C) indeed show a further decrease in σ. Hall-coefficient measurements as a function of temperature obtained after exposure (curve I) and subsequent to annealing at 0 and 23.3°C (curve II) are compared in Fig. 10. These data reveal that a further decrease in electron concentration has resulted from the annealing.

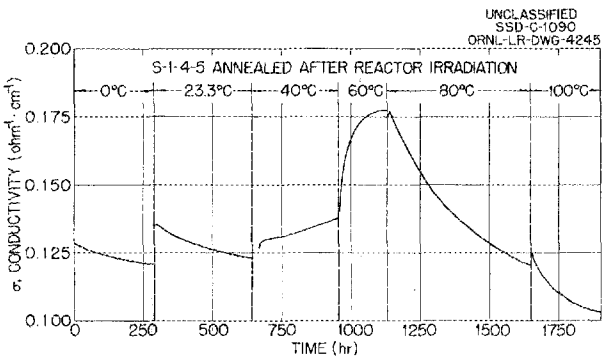

Fig. 9. Conductivity vs Annealing Time at Various Temperatures for n-Type Germanium.

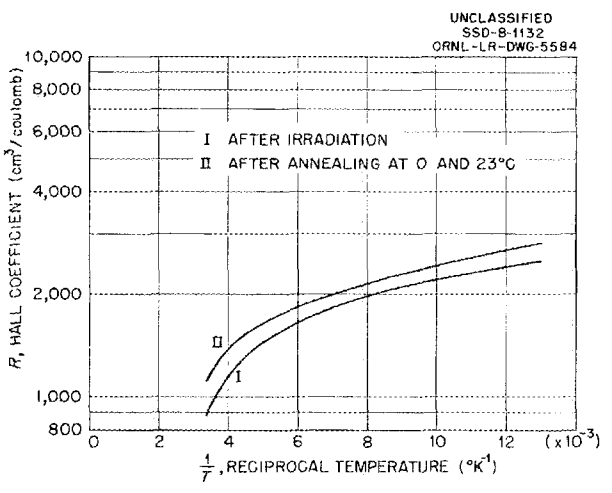

Fig. 10. Hall Coefficient vs Reciprocal Temperature of Irradiated Germanium.

Annealing at 40°C, on the other hand, produces an increase in σ, and at 60°C the rate of increase is greatly intensified but, as the annealing proceeds, appears to saturate. The additional anneals at 80 and 100°C once again produce marked decreases in σ. These results indicate that at least two and probably three kinetic processes occur in this temperature range. In consequence, a separation of the various effects and analysis of the annealing kinetics involved in each will be quite difficult.

It is possible, however, to postulate tentative hypotheses for the increase and decrease of σ during annealing, based on the Frenkel-defect energy-level model of James and Lark-Horovitz, as was done for the case of p-type germanium. Removal of the interstitial atoms by some process such as clustering or migration toward dislocations presumably decreases the concentration of shallow electron traps and in effect replaces them by much deeper traps situated below the middle of the forbidden band. Such a process would produce a further decrease in n. Much additional information is necessary, however, before the sequence of events depicted in Fig. 9 and the detailed nature of the processes underlying them can be understood.

DETERMINATION OF ENERGY LEVELS IN GERMANIUM BY TRANSMUTATION DOPING

J. W. Cleland J. C. Pigg
J. H. Crawford, Jr. H. C. Schweinler

It is possible in principle to determine the position of energy levels in semiconductors from the behavior of the Fermi level or Fermi energy ζ. In general, ζ is defined as the normalizing parameter in the Fermi-Dirac distribution function

$$(1) \qquad F_{F.D.} = \left\{ 1 + \exp\left[\frac{(\epsilon - \zeta)}{kT}\right] \right\}^{-1}$$

and hence is the value of energy for which the value of the distribution function is one half. It can readily be shown that ζ is essentially identical with the chemical potential. In a semiconductor, provided that the electron concentration in the conduction band is sufficiently low for the classical statistics to be valid, ζ is related to the electron concentration n by

$$(2) \qquad n = \frac{2(2\pi m^* kT)^{3/2}}{h^3} \exp \frac{\zeta - (\epsilon_g/2)}{kT} ,$$

where the zero of energy is taken at the middle of the forbidden-energy gap ϵ_g. Similarly for free holes, ζ is given by

$$(3) \qquad p = \frac{2(2\pi m^* kT)^{3/2}}{h^3} \exp \frac{\zeta + (\epsilon_g/2)}{kT} .$$

In considering a semiconductor containing a set of donor states located at ϵ_D, if effects caused by spin are neglected, the probability of finding a donor state occupied will be given by Eq. 1 for $\epsilon = \epsilon_D$. Consequently, when $\zeta > \epsilon_D + 2kT$, the donors will be essentially filled, whereas when $\zeta < \epsilon_D - 2kT$, the donors will be essentially empty. In general, it is possible to vary ζ in two ways: by varying the temperature and by varying the conduction electron (or hole) concentration by some agency. The first method has long been used to determine the position of energy levels. By varying the temperature over a wide range, ζ can be made to traverse a given energy level. As the level empties or fills, the rate of change of ζ with temperature will be markedly accelerated, and the position of the level may be determined by the inflection point of the ζ vs T curve. This method of energy-level spectrometry suffers from two difficulties: (1) the temperature of the inflection, particularly for deep-lying levels, may be quite high and quite near the intrinsic range, and (2) the half width of the inflection is approximately $2kT$. Therefore for high temperatures, resolution is poor, and it is difficult to locate levels with any degree of accuracy even if they can be found. The second method is not subject to these limitations, but, until recently, no reliable methods were available, particularly for the diamond-lattice semiconductors, for conveniently carrying out the measurements.

Nuclear doping provides an excellent means of varying ζ in germanium. Neutron capture produces two important activities which, on decay, produce both a donor and an acceptor impurity.[31] Germanium-71 decays with an 11.4-day half life to Ga^{71}, an acceptor impurity, and Ge^{75} decays with an 82-min half life to yield As^{75}, a donor impurity. Because of differences in capture cross section, after decay, the quantity of gallium produced is three times that of arsenic, thus making it possible to convert n-type Ge to p-type by sufficient slow-neutron exposure. The large difference in half life makes it possible to follow the motion of ζ across the forbidden-energy band by measurements of either σ or R on a convenient time scale. Since the ionization energy of the transmutation acceptors corresponds to an energy level quite near the top of the valence band, it is possible in principle to determine the positions of energy levels over the entire range of the forbidden band to within a few multiples of kT of the band edges.

The expected behavior of ζ with acceptor concentration for an initially n-type specimen originally containing 10^{14} electrons/cm^3 and a concentration of donors of 10^{14} located at 0.175 ev at 77°K is shown in Fig. 11. The ζ vs N_A curve was calculated from Eqs. 2 and 3 and under the assumptions that the donor level in question was the only one present and that the extra electrons come from completely ionized chemical donors. The inflection caused by the 0.175-ev level is readily apparent and is indicated by an arrow on the figure. The resolution of the method at this temperature (77°K) is about 1.3×10^{-2} ev. Consequently, positions of levels whose spacings are larger than this value should be readily determined.

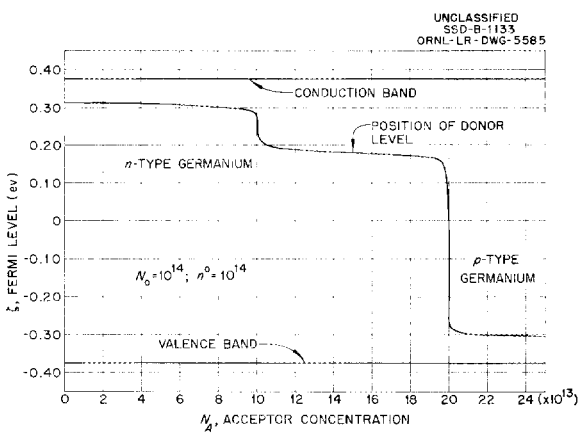

Fig. 11. Fermi Level vs Acceptor Concentration for n-Type Germanium with Donor Level at 0.175 ev.

In practice, two difficulties inherent in the method might be anticipated. They are the production of the transmutation impurity in other than a normal lattice site and the complications associated with photoeffects. The first of these possibilities arises

[31] J. W. Cleland, K. Lark-Horovitz, and J. C. Pigg, *Phys. Rev.* 78, 814 (1950).

from recoil produced by emission of capture gamma rays or decaying radiation. For the two activities in question, that is, Ge^{71} and Ge^{75}, the recoil energy that results from decaying radiation is not sufficiently large to displace the emitting atoms. On the other hand, the capture gamma-ray energy spectrum for the various germanium isotopes is not known, and it is indeed possible that the capture gamma-ray energy may be sufficient to displace from normal to interstitial positions those atoms that capture a thermal neutron. The concern on this point is that there is no assurance that an interstitial gallium or arsenic atom will any longer act as an acceptor or donor. Furthermore, the vacancies produced by the displacement process will introduce an additional complication. In order to investigate this possibility, an extremely high-purity n-type germanium sample ($n_0 \sim 10^{13}$ cm^{-3}) was exposed in the animal tunnel of the ORNL Graphite Reactor. In this position the thermal flux is estimated to be approximately 1×10^9 neutrons/cm^2 and the cadmium ratio to be approximately 10^3. After several hours of exposure, the specimen was converted to p-type behavior, which indicated an appreciable concentration of lattice defects. A second exposure with the specimen shielded with cadmium foil yielded essentially the same results. Consequently, it was concluded that the conductivity change resulted from a fast-neutron flux that was greater than had been expected. Conductivity measurements during radioactive decay showed that acceptor atoms were produced at the rate to be expected from the half life of Ge^{71}. This behavior also indicated that the introduced gallium behaved, according to expectation, as an acceptor impurity.

This method of energy-level determination is most useful for studying deep-lying levels. It should be of considerable value in determining multiple energy-level structures in germanium doped with more unusual impurities, such as Cu, Ag, Au, Ni, Co, Fe, etc., and, in particular, in determining the energy levels that result from nucleon bombardment. Preliminary experiments have been carried out on fast-neutron bombarded germanium. The procedure used is as follows: The specimen, previously characterized, is first exposed to the desired thermal-neutron flux and is then heat treated to remove the effects of fast neutrons. By virtue of the anneal, it is now possible to introduce the desired concentration of bombardment defects by a subsequent exposure. In order to be able to follow the behavior of ζ in the interesting region, it is necessary that these operations be performed in a period not much greater than 24 hr. After the final exposure the conductivity during radioactive decay is recorded at constant temperature. The results of one such run carried out at 77°K are shown in Fig. 12, in which σ is plotted against time. Initially, there is a rapid decrease in σ; then, after additional decay, σ shows a much more moderate decrease and appears to approach saturation. These data do not indicate conversion to p-type, and, in addition, there are no fluctuations in the curve (nor in a plot of log σ vs time) to indicate the presence of any discrete energy levels. Examination of the temperature dependence and photosensitivity of the specimen after decay reveals that a very large concentration of photoelectrons is present, presumably as a result of trapped minority carriers. Although the specimen was well shielded against light, the intensity of decaying radiation of the specimen, lead wires, and holder was apparently sufficient to saturate the minority carrier traps and to produce an excess electron concentration which, at the end of the decay period, was several orders of magnitude larger than the expected equilibrium concentration.

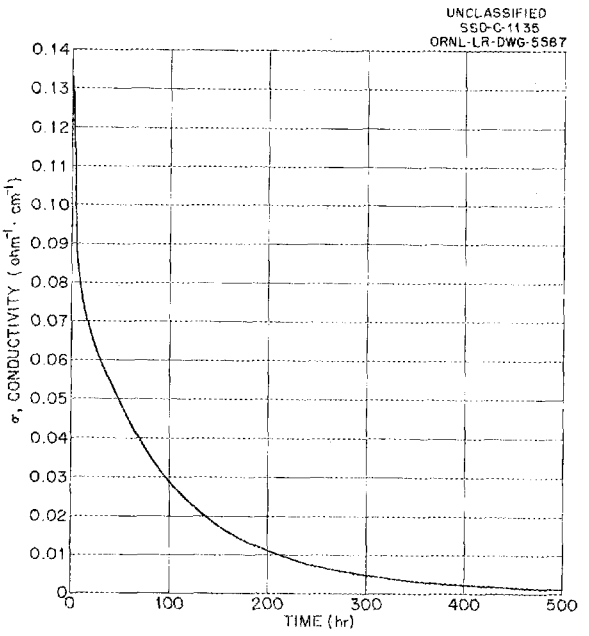

Fig. 12. Conductivity vs Time at 77°K During Radioactive Decay of Ge^{71}.

The presence of such a high concentration of excess carriers would completely mask the presence of discrete energy levels. However, the temperature dependence of the photosensitivity is such that at dry-ice temperature the excess electron concentration is negligible. Therefore, although some resolution is lost at the higher temperature, the discrete levels should be detectable at −78°C. It is planned to investigate the effects of decay at this temperature in the near future.

Studies of gold-doped germanium[32,33] reveal a complex energy-level structure with at least two deep-lying levels present. Since minority-carrier trapping effects in this material may be much less important, it is planned to carry out similar studies on several specimens furnished by W. C. Dunlap of the General Electric Research Laboratories. Future plans also include the investigation of specimens with other unusual doping agents.

RADIATION EFFECTS IN GALLIUM ANTIMONIDE

J. W. Cleland J. H. Crawford, Jr.

The semiconducting properties of the intermetallic compound GaSb have recently been extensively investigated.[34–37] This material is one of a series of compounds that can be formed between elements of the third and fifth columns of the periodic table and is characterized by a zinc-blende lattice structure, a forbidden-energy gap of about 0.7 ev at room temperature, and electron and hole mobilities of approximately 2000 and approximately 800 $cm^2 \cdot volt^{-1} \cdot sec^{-2}$, respectively. The best pure material currently reported is *p*-type, which may be doped with tellurium to produce *n*-type material.

The effect of irradiation in the ORNL Graphite Reactor on the conductivity, carrier concentration, and mobility of both *n*- and *p*-type samples is reported here.[38] The samples were rectangular plates of about 1 × 0.3 × 0.1 cm, on which a determination of the Hall coefficient and resistivity was made before and after reactor exposure. The conductivity was recorded during exposure. Some of the samples were wrapped with thin layers of indium and cadmium foils to shield out thermal and resonance neutrons that would cause transmutation of the gallium and antimony to germanium and tellurium, respectively, since they would act as donor atoms in the GaSb lattice.

The effect of reactor radiation on the conductivity of representative samples of shielded and unshielded *n*- and *p*-type GaSb is indicated in Fig. 13, and the initial carrier concentration, the temperature of exposure, and the initial rate of removal of current carriers are listed in Table 2. These data indicate that the conductivity of both *n*- and *p*-type samples, shielded or unshielded, decreases monotonically during irradiation. The removal rate of current

[32] W. C. Dunlap, Jr., *Phys. Rev.* **91**, 208 (1953).

[33] J. W. Cleland, J. H. Crawford, Jr., and E. S. Schwartz, *Solid State Semiann. Prog. Rep. Aug. 31, 1953*, ORNL-1606, p 70.

[34] H. Welker, *Z. Naturforsch.* **7a**, 744 (1952); *ibid.*, **8a**, 248 (1953).

[35] D. P. Detwiler, *Phys. Rev.* **94**, 1431 (1954).

[36] H. N. Liefer and W. C. Dunlap, Jr., *Phys. Rev.* **95**, 51 (1954).

[37] R. F. Blunt, W. R. Hosler, and H. P. R. Frederikse, *Phys. Rev.* **96**, 576 (1954).

[38] We are indebted to R. L. Smith of the Franklin Institute for the *p*-type samples and to H. P. R. Frederikse of the National Bureau of Standards for the *n*-type samples used in these experiments.

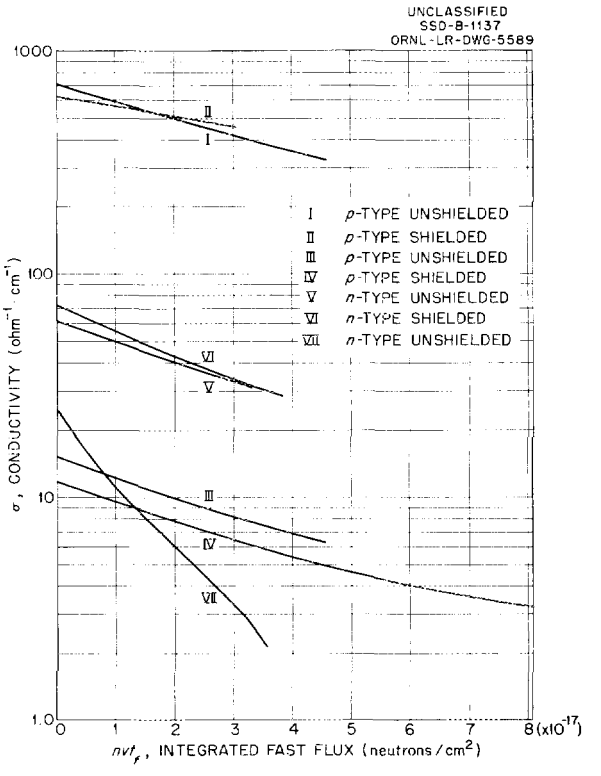

Fig. 13. Effect of Reactor Radiation on the Conductivity of Shielded and Unshielded GaSb.

TABLE 2. ORIGINAL MEASUREMENTS ON GaSb SAMPLES AND CONDITIONS OF IRRADIATION

Sample No.	Type	Shielded	Original Carrier Concentration (cm^{-3})	Temperature of Exposure (°C)	$\left[\frac{dn_0}{d(nvt_f)}\right]_{t=0}$ Removal Rate
I	p	No	14.25×10^{17}	37	2.57
II	p	Yes	12.95×10^{17}	46	1.40
III	p	No	2.59×10^{17}	42	0.68
IV	p	Yes	1.36×10^{17}	47	0.41
V	n	No	18.50×10^{17}	24	4.90
VI	n	Yes	12.30×10^{17}	41	2.97
VII	n	No	5.80×10^{17}	29	4.40

carriers is quite temperature dependent but is approximately equal for all samples of high carrier concentration. The initial removal rate of holes for p-type material is less for a sample of low initial carrier concentration, whereas the initial removal rate of electrons for n-type material is not dependent upon initial carrier concentration and does not appear to approach a saturation condition. Slow-neutron-produced donor atoms would be expected to increase slightly the removal rate of holes from p-type material and to decrease slightly the removal rate of electrons from n-type material, and this effect does appear to be indicated for the four samples of highest conductivity. The temperature difference of exposure of the two purest p-type samples may mask any effect that could be attributed to transmutations.

The Hall-coefficient and resistivity data for a typical p-type sample are shown in Figs. 14 and 15. The original activation energy as determined from the slope of the Hall curve is about 0.018 ev. Prolonged irradiation apparently introduces a sizable number of rather deep-lying hole traps which increase the activation energy to about 0.14 ev. That some of these hole traps are thermally annealable is indicated by the fact that a relatively short (~ 1 hr) low-temperature (~ 140°C) heat treatment increased the carrier concentration and conductivity considerably and reduced the activation energy to approximately 0.12 ev.

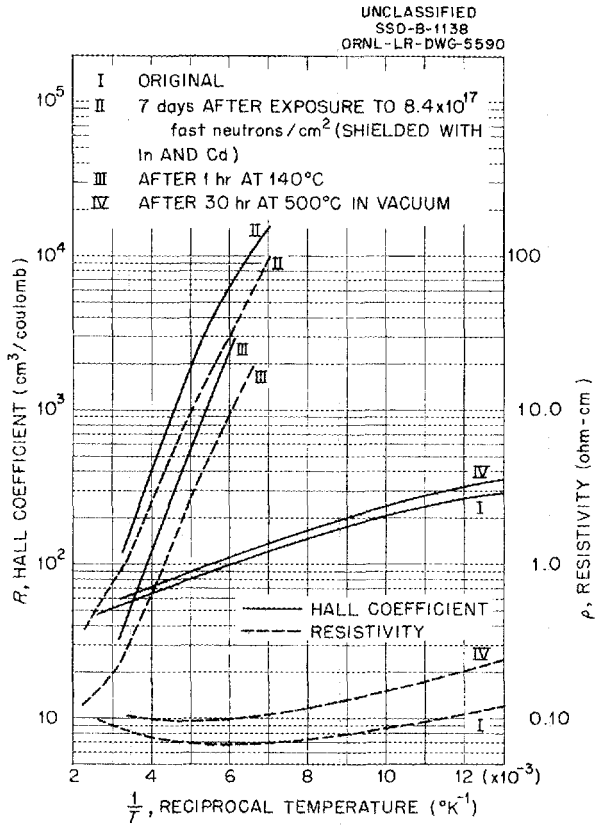

Fig. 14. Hall Coefficient and Resistivity of p-Type GaSb as a Function of Temperature — Curves I Through IV.

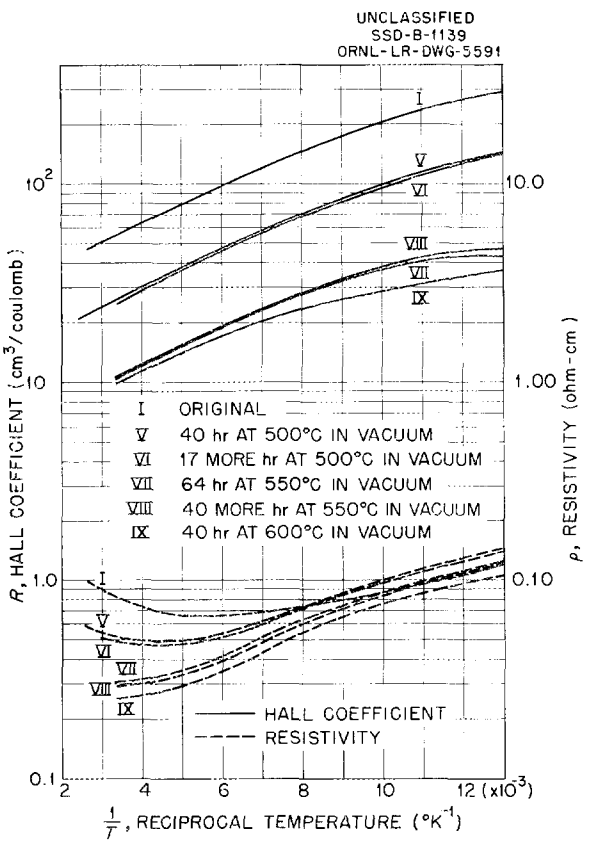

Fig. 15. Hall Coefficient and Resistivity of *p*-Type GaSb as a Function of Temperature – Curves V Through IX.

It has been shown previously[39,40] that vacuum heat treatment at about 500°C for germanium and about 350°C for InSb removes the major portion of any fast-neutron-introduced donors and acceptors and leaves only those donor or acceptor atoms that result from nuclear transmutations. The behavior of GaSb, however, is more complicated under similar conditions. Curves IV of Fig. 14 might be interpreted as an indication that an extended high-temperature vacuum anneal removes most of the irradiation-produced acceptors, but all curves of Fig. 15, obtained after successive periods of vacuum anneal at increasing temperatures, indicate that a large number of additional current carriers are being introduced by some mechanism.

The purest GaSb currently available is *p*-type, with an initial carrier concentration of approximately 10^{17} cm^{-3}. A slight departure from true stoichiometry in the original melt that amounts to an excess of 1 part in 10^5 of antimony vacancies has been suggested as the cause of this initial *p*-type character.[41] Moreover, Detweiler[42] has reported that vacuum annealing in the temperature range from 700 to 900°C resulted in the deposit of free antimony on the cool portions of the furnace tube. Consequently, it would appear reasonable to assume that evaporation of antimony from the surface of a GaSb sample during the successive anneals might be accompanied by the introduction of Schottky-type defects in the antimony superlattice. These defects would be expected to act as acceptor states and would increase the *p*-type character of the specimens. In addition to this possibility, the introduction of an acceptor-type impurity by diffusion during the annealing process or by differential annealing of the interstitials and vacancies produced by irradiation might also explain the increase in *p*-type character that results from extensive high-temperature annealing.

In order to differentiate between the various possibilities outlined above, a companion sample to the one shown in Figs. 14 and 15 was subjected to the same type of series of extended high-temperature vacuum anneals without being previously irradiated. The results, as shown in Fig. 16, indicate that there is no large increase in acceptor concentration for a sample that has not been irradiated. It is believed that this rules out the possibility of either the evaporation of antimony from the surface or the introduction of an acceptor-type impurity by diffusion as a mechanism for increasing the acceptor concentration at this annealing temperature, since these two processes should work equally well for both irradiated and unirradiated material. The mechanism of differential annealing of radiation-produced interstitials and vacancies must therefore be employed to explain the experimental results obtained here and to examine this type of mechanism more closely.

The Hall-coefficient and resistivity data for a typical *n*-type sample are shown in Fig. 17. The decrease in carrier concentration and conductivity

[39] J. W. Cleland, K. Lark-Horovitz, and J. C. Pigg, *Phys. Quar. Prog. Rep. March 15, 1950*, ORNL-694, p 56.

[40] J. W. Cleland and J. H. Crawford, Jr., *Solid State Semiann. Prog. Rep. Aug. 30, 1954*, ORNL-1762, p 65.

[41] H. J. Hrostowski, personal communication.

[42] D. P. Detweiler, *Study of Rectifying Contacts Between Semiconductors*, F-2337-2 (also submitted to *Phys. Rev.*).

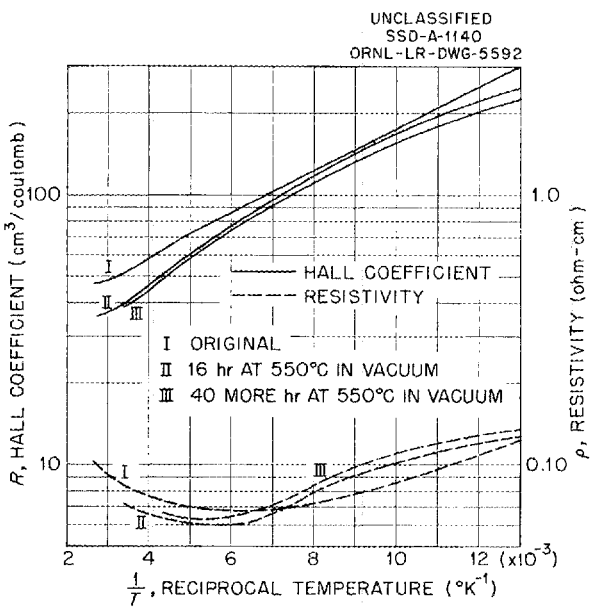

Fig. 16. Hall Coefficient and Resistivity of Unirradiated GaSb as a Function of Temperature.

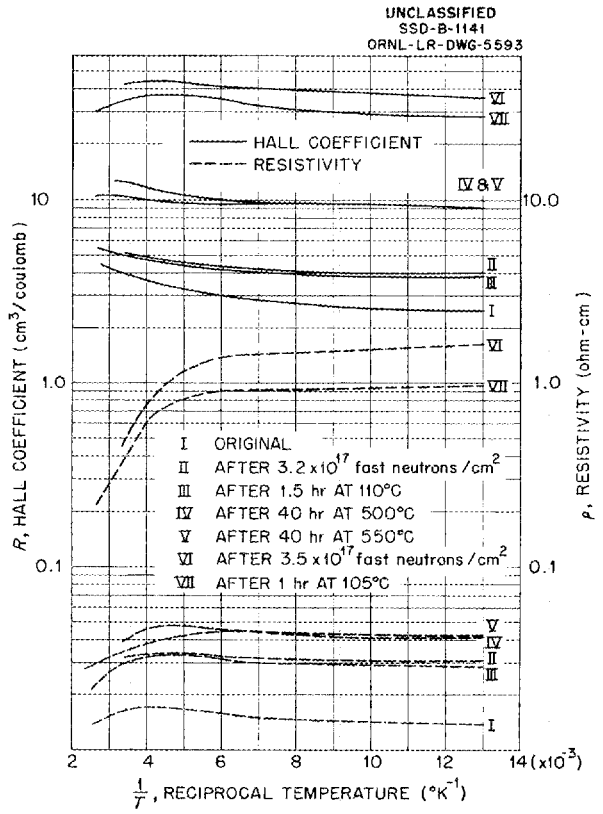

Fig. 17. Hall Coefficient and Resistivity of a Typical *n*-Type GaSb as a Function of Temperature.

as a result of irradiation indicates that electron traps are produced. That some of these electron traps are also thermally annealable is indicated by the fact that a 1.5-hr heat treatment at 110°C slightly increased the carrier concentration and conductivity. Curves IV and V of Fig. 17 indicate that an extended high-temperature vacuum anneal of irradiated *n*-type samples of GaSb decreases greatly the net effective donor concentration of such material. This is presumably the same type of behavior as that observed with *p*-type samples and can therefore be considered as the differential annealing of irradiation-produced interstitials and vacancies. The net result of irradiation and heat treatment of an *n*-type sample of GaSb, therefore, is the production of a sample with lower carrier concentration. Reirradiation of such a sample further decreases the net effective donor concentration, as is shown in curves VI of Fig. 17, and curves VII indicate again that some of the irradiation-produced electron traps are thermally annealable.

Since irradiation and heat treatment of an *n*-type sample of GaSb result in a lower carrier concentration, the sample shown in Fig. 17 was also employed to obtain curve VII of Fig. 13 and the data on sample VII of Table 2. These results show that the removal rate of current electrons in *n*-type material is not dependent upon initial carrier concentration, although, as was previously indicated, the removal rate of holes in *p*-type material decreases rapidly for material of lower initial hole concentration.

Fast-neutron radiation reduces the mobility of both *n*- and *p*-type samples of GaSb, an effect similar to that previously observed for other semiconductors; however, the effect of heat treatment after irradiation is to improve the mobility of the *n*-type samples considered here to an even higher value than the original one. The *p*-type mobility, on the other hand, not only was less than the original value after the irradiation and initial high-temperature heat treatment but also was further decreased by each succeeding higher-temperature vacuum anneal.

It is not yet possible, on the basis of the experimental data presented here, to formulate a

detailed model of the energy-level spectrum associated with irradiation-produced defects in GaSb. Because of its binary nature, an interstitial can be either a gallium or an antimony atom, and a vacancy can be either type of vacant lattice site. Thus, four possible simple defects can exist. In addition, a forbidden-energy gap width of 0.71 ev at room temperature[43] and a dielectric constant[44] of 14 are both very analogous to those of germanium, for which, application of the hydrogenic model has indicated the possibility of multiple ionization. It is therefore possible that states corresponding to both the first and second ionization energies of each of the two possible interstitial atoms and states corresponding to the first and second ionization energies of each of the two vacant lattice sites will lie in the forbidden-energy gap and will participate in altering the carrier concentration as a result of irradiation.

Several general conclusions, however, can be obtained from the behavior of GaSb as a result of fast-neutron irradiation. The rate of decrease in conductivity during irradiation is about the same for *n*- and *p*-type samples of high carrier concentration. This would indicate the introduction of approximately equal numbers of acceptors and donors whose center of gravity is apparently near the middle of the forbidden-energy band. The fact that the removal rate of electrons from *n*-type material is independent of carrier concentration would seem to indicate that the donor atoms, which are presumably interstitials, ionize and lose electrons to the lower-lying acceptor states, which are presumably lattice vacancies. These donors can therefore act as electron traps in *n*-type material, whereas the low-lying filled acceptor states can act as hole traps in *p*-type material. One of these hole traps can be tentatively located at about 0.14 ev above the filled band.

MAGNETIC SUSCEPTIBILITY OF INDIUM ANTIMONIDE

D. K. Stevens J. H. Crawford, Jr.

A new sample furnace which permits measurement of magnetic susceptibility in the range from room temperature to 400°C has been constructed. The apparatus consists of a vacuum-jacketed furnace tube of copper with a Nichrome heater winding and the necessary thermocouples. The new assembly may be attached to the susceptibility equipment instead of to the liquid-nitrogen cryostat. This furnace has been used to extend susceptibility data[45] on *p*-type InSb to 636°K. In addition, measurements have been made on an *n*-type specimen from 293 to 634°K.

Susceptibility, χ, vs temperature, T, curves for these specimens are shown in Fig. 18. Both curves exhibit an increase in diamagnetism with temperature. Hall-coefficient measurements on plates cut adjacent to these specimens reveal that they are intrinsic in behavior well below room temperature.[46] Consequently, the increase in diamagnetism with temperature may be attributed almost entirely to intrinsic carriers. Since at the high-temperature end of the range the carrier concentrations in the two specimens should be almost identical, the susceptibility is expected to be the same. It is evident from Fig. 18 that this is not the case. Because of the calibration technique employed, however, a difference in absolute value of 0.6% for the two curves is not surprising;[47] the difference at the high-temperature end is 1.2%. In addition to the difference in magnitude, the two curves show an unexpected difference in temperature dependence. This discrepancy may be associated with thermal expansion of the molybdenum sample-suspension fiber and will be discussed below in greater detail.

The temperature range of measurements on the *p*-type specimen is sufficiently extensive to permit a tentative analysis of the data to be made. Studies of the magnetoresistance of InSb seem to indicate that the energy surfaces of electrons and holes in momentum space are essentially spherical.[48] Consequently, the effective mass should be represented by a scalar and should be independent of the method of determination. Electrical measurements[49] indicate that for any electron

[43] H. N. Liefer and W. C. Dunlap, Jr., *Phys. Rev.* 95, 51 (1954).

[44] H. B. Briggs, R. F. Cummings, H. J. Hrostowski, and M. Tanenbaum, *Phys. Rev.* 93, 912 (1954).

[45] D. K. Stevens, *Solid State Semiann. Prog. Rep. Aug. 30, 1954*, ORNL-1762, p 81.

[46] J. W. Cleland and J. H. Crawford, Jr., *Solid State Semiann. Prog. Rep. Aug. 30, 1954*, ORNL-1762, curves P_0 and N_0 of Fig. 61, p 68.

[47] D. K. Stevens, *Magnetic Susceptibility of Annealed and Fast-Neutron Bombarded Germanium*, ORNL-1599, p 22 (Feb. 17, 1954).

[48] G. L. Pearson and M. Tanenbaum, *Phys. Rev.* 90, 153 (1953).

[49] R. G. Breckenridge *et al.*, *Phys. Rev.* 96, 571 (1954).

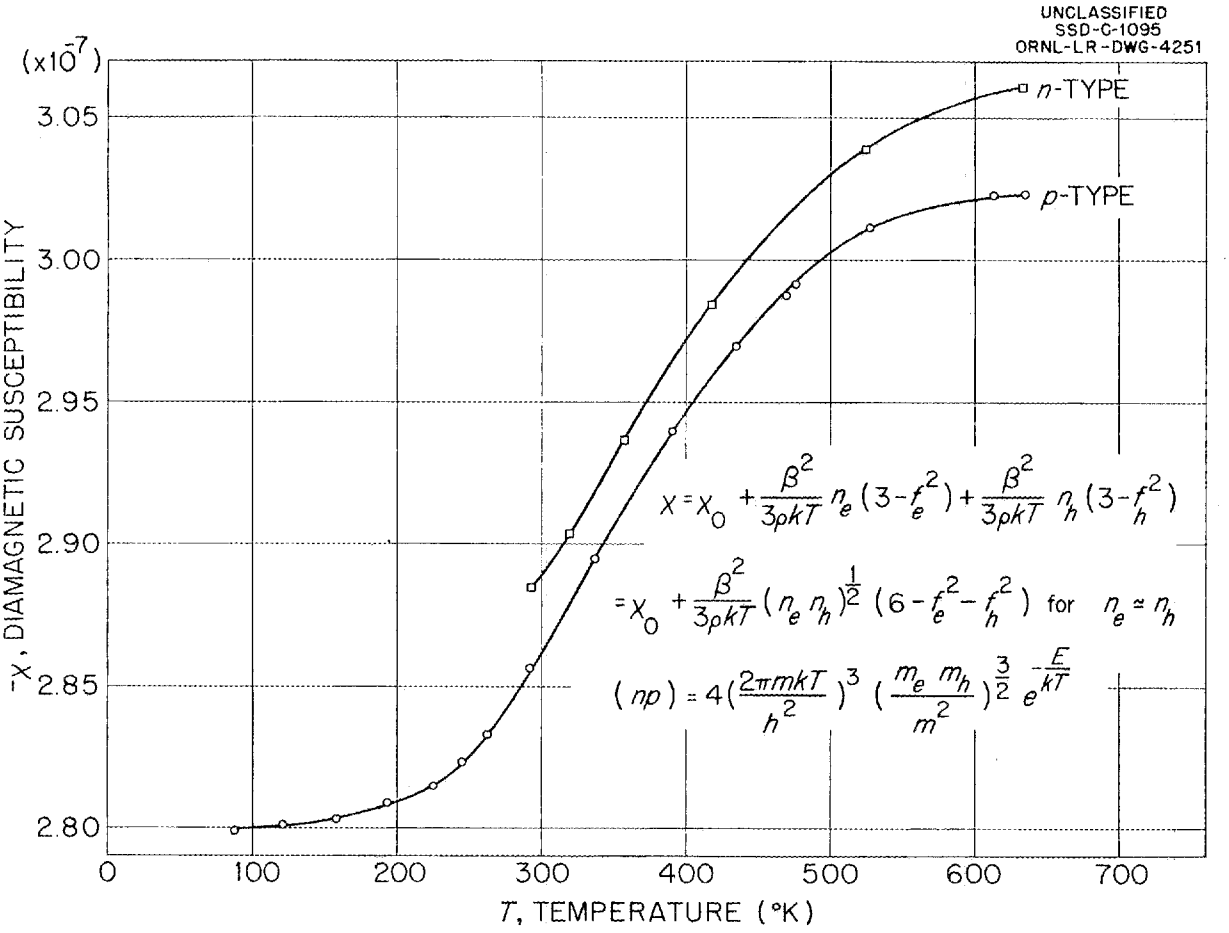

Fig. 18. Diamagnetic Susceptibility of Indium Antimonide.

the effective mass $m_e = 0.04\ m_0$ and the effective mass of a hole $m_h = 0.15\ m_0$, where m_0 is the rest mass of an electron. In view of the comparatively large effective mass of holes and the small concentration of holes in the extrinsic range ($p_0 = 1 \times 10^{16}$ cm^{-3}), it can be reasonably assumed that the low-temperature value of χ is that due to the InSb lattice alone. By subtracting this value from the rest of the curve, the contribution $\Delta\chi$ of the carriers is obtained. Consequently, it is possible to compare the observed carrier contribution with that expected theoretically.

When both electrons and holes are present, the carrier susceptibility is given by the sum of their individual contributions:[50]

$$(1) \quad \Delta\chi = \frac{\beta^2}{3\rho kT} [n(3 - f_e^2) + p(3 - f_h^2)] ,$$

where β is the Bohr magneton, ρ is the density, n and p are, respectively, the electron and hole concentrations, $f_e = m_0/m_e$, and $f_h = m_0/m_h$. It is assumed that the contribution of impurity atoms is negligible. If the specimen is completely intrinsic,

$$(2) \quad n = p = \frac{2(2\pi\bar{m}^* kT)^{3/2}}{h^3} e^{-\epsilon_g/2kT} ,$$

where $\bar{m}^* = (m_e m_h)^{1/2}$ and ϵ_g is the forbidden-energy gap. By substituting Eq. 2 in Eq. 1,

$$(3) \quad \Delta\chi = \frac{2\beta^2 (2\pi\bar{m}^*)^{3/2} (kT)^{1/2}}{3\rho} (6 - f_e^2 - f_h^2)\, e^{-\epsilon_g/2kT} ,$$

[50] D. K. Stevens, *Magnetic Susceptibility of Annealed and Fast-Neutron Bombarded Germanium*, ORNL-1599, p 26 (Feb. 17, 1954).

and it is evident that log $\Delta\chi T^{-1/2}$ plotted against $1/T$ should yield a straight line of slope $-\epsilon_g/2k$. Such a curve is shown in Fig. 19. In the high-temperature range (1.6×10^{-3} to 5×10^{-3} on the $1/T$ scale), except for some concave downward curvature at the highest end of the range, the curve is fitted approximately by a straight line whose slope corresponds to 0.095 ev. This is in only fair agreement with the reported value[49] of $\epsilon_g/2$ of 0.115 ev. The curvature at the high-temperature end of the range is presumably due to the onset of electron degeneracy. This is to be expected because of the high concentration of intrinsic electrons and the very small effective mass.[51] The linear portion of the curve at low temperatures with smaller slope is neither expected nor understood. This behavior may result from a wrong choice of the value used for the lattice susceptibility.

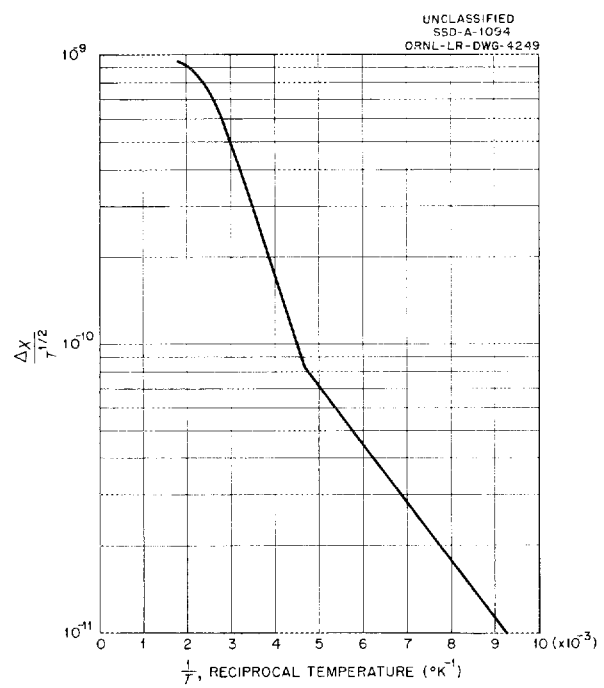

Fig. 19. Intrinsic Carrier Contribution to Magnetic Susceptibility of *p*-Type Indium Antimonide.

It was mentioned above that the discrepancy between the *n*- and *p*-type curves might be associated with thermal expansion of the suspension fiber. Because of the large variation of the magnetic field square gradient $H(dH/dz)$ with distance, even a small variation in the position of the sample can produce a significant variation in measured susceptibility. If the thermal expansion coefficient of molybdenum and the heated length of the fiber are used, it can be shown that a variation in position of approximately 0.2 mm is to be expected. This possibility was further checked by means of a fused silica specimen. The susceptibility of this specimen, which is expected to be very slightly temperature dependent, was measured over the entire temperature range for initial positioning both above and below the position of maximum $H(dH/dz)$. An increase in the apparent value of χ with temperature was observed when the specimen was above the maximum, and an opposite change was observed when the specimen was below the maximum. Since the suspension length may vary from specimen to specimen by as much as 2 mm and since the maximum of $H(dH/dz)$ occurs over a very small interval of distance, these results indicate strongly that this effect could adequately explain the different temperature dependences of the *n*- and *p*-type curves of Fig. 18. The maximum variation of observed χ which could be attributed to suspension expansion over the range from 25 to 400°C was found to be 0.7%. Consequently, because it was obtained by subtracting the large contribution of the lattice, the $\Delta\chi$ data of Fig. 19 might be expected to exhibit a maximum spurious temperature dependence of about 8% in the same temperature range. Such a discrepancy could affect slightly the measured slope in the intrinsic range and might possibly explain the smaller-than-expected value of $\epsilon_g/2$. Steps are being taken to correct this deficiency.

LOW-TEMPERATURE APPARATUS FOR MAGNETIC-SUSCEPTIBILITY MEASUREMENTS

D. K. Stevens

An apparatus designed to cover the entire temperature range from 300°K to pumped liquid-helium temperatures (~1°K minimum) has been designed and constructed. Figure 20 is a schematic illustration of the apparatus. In essence, the sample S is suspended along the axis of a nest of concentric copper thimbles $T_{1...4}$, which are separated from each other by spaces that individually may be evacuated or filled with an atmosphere of helium (for heat transfer) through ports $P_{1...3}$. The outside diameter of T_4 is $1\frac{5}{16}$ in. and fits between

[51] E. Burstein, *Phys. Rev.* 93, 632 (1954).

the poles of the ADL magnet; T_3, which is joined to a tank filled with liquid nitrogen, provides a thermal shield, T_2, which extends down from the liquid-helium container. Quartz pins and spheres are used to center T_2, T_3, and T_4 relative to each other. The sample thimble, T_1, is hard soldered to a length of 0.003-in. wall, ½-in. dia, cupro-nickel tubing which extends to the top of the apparatus. A copper collar, C, centers the sample tube relative to T_2 and provides a thermal connection between the two. Longitudinal holes through the collar permit evacuation of the intervening space and passage of leads to thermocouples and heaters attached to the copper sample thimble. These leads are brought out through a multiple Kovar-to-glass seal at P_4. Stainless steel bellows (not shown) have been used where necessary to allow for unequal contraction upon cooling.

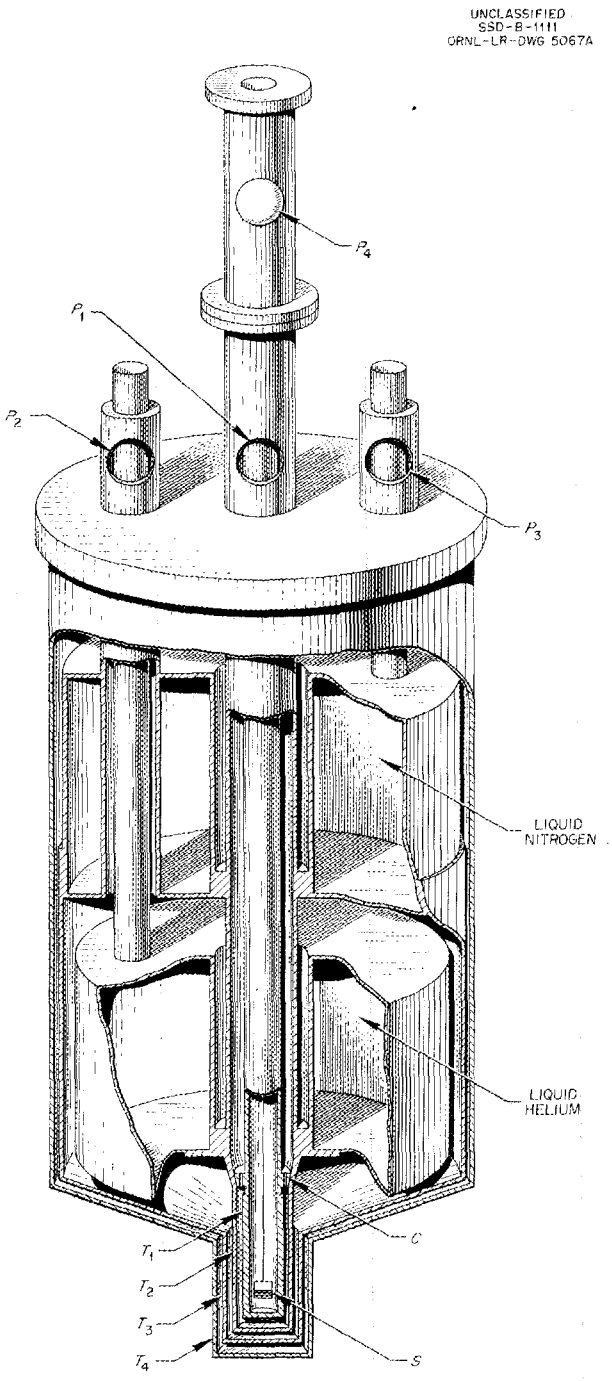

Fig. 20. Low-Temperature Apparatus for Magnetic-Susceptibility Measurements.

An atmosphere of helium at a pressure of 120 μ of mercury will provide heat transfer between the sample and the walls of T_1. If either liquid nitrogen or liquid helium is used in the liquid-helium container and if the proper heater power is selected, this equipment should permit the adjustment of the sample temperature to any desired value from approximately 1°K to room temperature.

The apparatus has been built and leak tested but the outside vacuum plumbing is incomplete. The heaters and thermometers have yet to be installed and calibrated. This apparatus will be used in conjunction with the magnetic-susceptibility equipment previously described[52] but will replace the liquid-nitrogen cryostat.

RADIATION EFFECTS IN IONIC CRYSTALS

C. M. Nelson

Electrical conductivity studies on ionic crystals have been continued. As in the past, potassium chloride has been the main interest. Since the previous results[53] indicated that there were changes in conductivity upon annealing, even for unirradiated crystals, attention has been focused upon them. Other alkali halide crystals were also examined, and similar behaviors upon heating were observed.

The technique used in these studies was to heat the crystal at approximately 10°C/min for 50 to 100°C intervals. However, instead of annealing the crystal at the end of the interval, the heating was stopped. The temperature dropped rapidly

[52] D. K. Stevens, *Magnetic Susceptibility of Annealed and Fast-Neutron Bombarded Germanium*, ORNL-1599 (Feb. 17, 1954).

[53] C. M. Nelson, *Solid State Semiann. Prog. Rep. Aug. 30, 1954*, ORNL-1762, p 79.

because of heat leak. After the crystal reached room temperature, it was heated again over a higher temperature interval. The highest temperature used was 400°C, since previous work had indicated that painted electrodes suffered at higher temperatures and also because there should not be appreciable diffusion to contribute to the intrinsic conductivity up to this temperature.

It was observed by this technique that there were only small differences in conductivity between heating cycles until the temperature range of 250 to 300°C was reached. The whole curve is shifted upward by as much as a factor of 10 after this temperature is reached. Plotted in Fig. 21 is a curve showing the ionic conductivity of a KCl crystal that was heated directly to 400°C with no stops and subsequently heated after cooling to room temperature. Inflection points which indicate different species contributing to the conductivity can be noted. The apparent decrease in activation energy at approximately 240°C was not expected. If this behavior, which has been observed in a number of samples, is real, the species contributing to the conductivity at lower temperatures is apparently a different one and has a lower activation energy (from 0.8 to 0.5 ev).

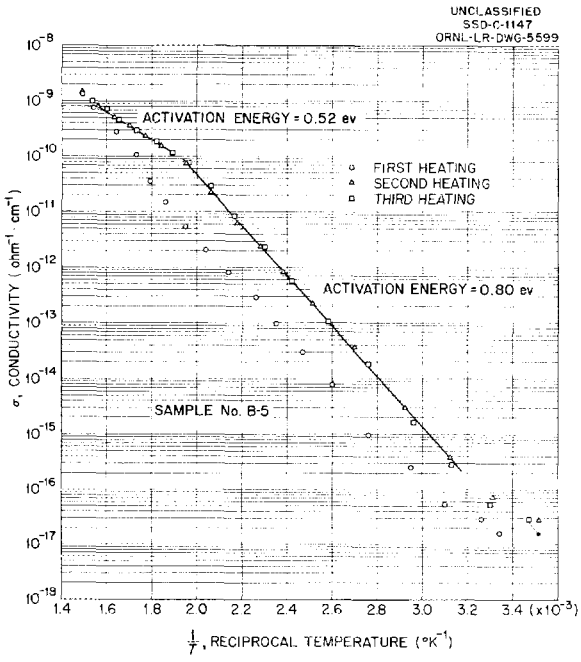

Fig. 21. Annealing Cycles for KCl.

Other alkali halides were examined by use of the same technique, and similar results were obtained. When NaCl, KBr, and LiF were heated to 400°C, the conductivity curves shifted upward in a manner similar to that observed for KCl. Further work with some other alkali halides will be done to see whether an explanation can be found for this behavior.

The ionic-conductivity apparatus appears to be performing satisfactorily. In order to check whether this d-c method was giving results comparable to an a-c method, a new switch for reversing polarity of the current was added. A 1-rpm Bodine motor was used to reverse the polarity and to give the crystal a pulsed voltage. The sequence used was as follows: current on 6 sec, off 9 sec; then reversed current on 6 sec, off 9 sec. The results obtained when this switch was used gave data not significantly different from those obtained by the usual technique.

Optical spectra of irradiated KCl have been obtained with a Cary recording spectrophotometer. The V_3 band at 2150 Å is of particular interest, since it apparently is associated with holes trapped at positive ion vacancies. The ionic conductivity, of course, is influenced by positive ion vacancies. Both reactor-irradiated and Co^{60}-irradiated samples were examined. Preliminary results seem to indicate that these studies may yield important information about the relation between V centers and the type of radiation used.

OPTICAL SPECTRA OF IRRADIATED QUARTZ AND SILICA

C. M. Nelson

In connection with other studies of radiation effects in both fused and crystalline silica, optical-absorption studies have been initiated. Reactor-bombarded quartz is too intensely colored in most cases for the samples used in other investigations to be used for optical measurements because of the limitations of the instrument used. The samples must be cut on a diamond saw and polished with diamond dust for optical measurements. Very pure fused silica samples of various thicknesses have been obtained from the Corning Glass Works. Optical absorption curves were taken on one of these samples after various bombardments, and the results are shown in Fig. 22. There was no absorption in the visible spectrum, and apparently only one absorption band occurred at 2150 Å in the

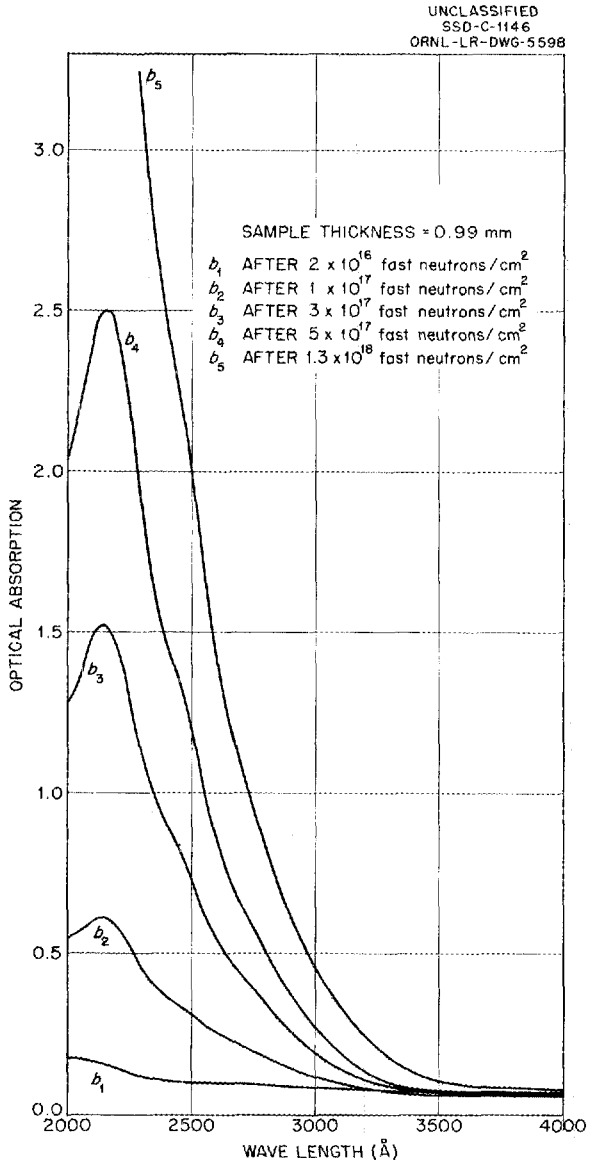

Fig. 22. Reactor-Induced Growth of Ultraviolet Bands for Corning Pure Fused Silica.

ultraviolet spectrum. The optical density is approximately proportional to the length of bombardment. This work is being continued and will be extended to crystalline silica.

[54] R. Berman, *Proc. Roy. Soc. (London)* A208, 90 (1951).

[55] R. Berman, *Advances in Phys.* 2, 103 (1953).

[56] M. Wittels, *Phys. Rev.* 89, 656 (1953).

[57] M. Wittels and F. A. Sherrill, *Phys. Rev.* 93, 1117 (1954).

FAST-NEUTRON EFFECTS IN SOME REFRACTORY SINGLE CRYSTALS

M. C. Wittels F. A. Sherrill

Earlier observations[54–57] on fast-neutron effects in silica structures revealed the vulnerability of the silicon-oxygen bond to neutron irradiation and the apparent efficiency with which oxygen atoms are displaced and frozen in at room temperatures. As a result of these observations a group of natural insulator-type crystals having oxygen atoms dominating their structures and in which the binding is partially covalent were selected for similar irradiation studies. Single crystals of zircon, beryl, chrysoberyl, phenacite, topaz, and garnet were exposed to fission-spectrum neutrons at a temperature of approximately 100°C and were then examined by conventional x-ray diffraction methods.

In a previous report[58] some effects of the irradiation on zircon were described. Continued bombardment of zircon to fluxes as high as 3.6 $\times 10^{20}$ fast neutrons/cm^2 indicates that considerable long-range order is still retained in the crystal lattice after this irradiation. The anomalous reflections seen in Laue transmission photographs were still observed after the maximum irradiation, and, in order to determine the possibility of a thermal origin for these diffuse reflections, diffraction patterns were taken at liquid-nitrogen temperatures. These low-temperature photographs were essentially the same as those taken at room temperature, and the anomalous reflections were still observed with undiminished intensities. The "extra" reflections, it is noted, are observed when the incident x-ray beam is directed along a major crystal axis, usually parallel to a heavily populated lattice plane of low index. In order for such planes to fulfill the Bragg conditions for reflection, there must be some angle between the reflecting plane and the incident radiation. It is felt that this result is achieved in zircon by a bombardment-induced bending or warping of large mosaic blocks in the crystal lattice while long-range order is retained. The maximum angular deviation of these "warps" from the normal lattice positions in zircon for (200) and (101) are 6.2 and 4.6 deg as measured with molybdenum radiation.

[58] M. Wittels and F. A. Sherrill, *Solid State Semiann. Prog. Rep. Aug. 30, 1954*, ORNL-1762, p 85.

Beryl, chrysoberyl, and phenacite were irradiated with successive dosages of fast-neutron flux up to 3.6×10^{20} neutrons/cm^2. Single-crystal x-ray-diffraction studies reveal that beryl, as compared with the other two beryllium-bearing crystals, has the least stable structure under neutron bombardment, all single-crystal reflection being destroyed after the last irradiation. Figure 23 shows the successive structural disintegration of beryl upon neutron irradiation. Here again are the "extra" reflections that appear in the central portion of the Laue photographs. These reflections, as in zircon, are not of thermal origin, as determined by low-temperature diffraction studies, but result from the bombardment-induced warping of lattice planes. In beryl this amounts to at least 4.6 deg in (110) and at least 2.6 deg in (100). Figure 24 shows the similar anomalous reflections that appear in the center of the Laue photographs of a quartz single crystal bombarded with an integrated flux of 7.8×10^{19} neutrons/cm^2. Warping in (100) as high as 4.6 deg and as much as 5.8 deg in (101) was measured. There are striking similarities between the bombardment effects in beryl and those observed in quartz. The displacements produced in both these open structures are easily trapped in the irregular *c*-axis channels and give rise to an anisotropic lattice expansion that follows a structure dependence. Also, neither crystal exhibits any macroscopic defects in large single crystals despite these large distortions.

Chrysoberyl has its oxygen atoms in a hexagonally close-packed system. As a result of fast-neutron bombardment, this crystal undergoes a lattice expansion exceeding 1% in the *c* direction, with little or no distortion observed. The same type of effect is observed in phenacite, which has an open hexagonal lattice with *c*-axis interstitial channels that is more structurally similar to that of quartz and beryl. Bombardment of phenacite with 3.6×10^{20} neutrons/cm^2 produces an *a*-axis expansion of 0.7% with no measurable expansion in the *c* axis. Little or no distortion of the expanded lattice was seen in single-crystal x-ray-diffraction patterns. The expansion, it is seen, has a pronounced structure dependence.

The production of displacements and the lattice expansion observed in beryl, chrysoberyl, and phenacite following fast-neutron bombardment indicate that oxygen atoms are readily displaced and frozen in at room temperature in this type of insulator crystal. The expansion effects are clearly structure dependent, and it seems likely that the beryllium-oxygen bonds, when disrupted, may be re-formed at relatively low temperatures. The latter interpretation stems from the observation of crystal perfection retained in chrysoberyl and phenacite, which have a very high ratio of beryllium-oxygen binding as compared with beryl.

Fast-neutron effects in garnet and topaz are similar to those found in zircon. Expansion and distortion in both crystal lattices are of the same order of magnitude as in zircon. In topaz the distortion gives rise to a random stacking of certain atomic layers, seen as streaks in Weissenberg patterns.

A pronounced structure dependence for displacements is exhibited by all the crystals examined in this investigation. Interstitial positions, which are the most likely sites for trapped displacements, usually are found to satisfy this condition, with oxygen serving as the most probable trapped atom. Other prominent features include lattice expansions with or without large lattice distortions, varying degrees of disorder, the formation of mosaic blocks in single crystals, and bombardment-induced defects with a high thermal stability. Further investigation of these crystals is in progress.

X-RAY SCATTERING FROM COVALENT SINGLE CRYSTALS

M. C. Wittels F. A. Sherrill

Preliminary theoretical calculations by H. C. Schweinler have led to the search for the so-called "forbidden" reflections in diamond, germanium, and silicon. It can be reported that the (200) is observed in neutron-irradiated diamond, together with an increase in intensity of the anomalous (222) reflection. Similarly, (200), (222), and (420) have been observed in unirradiated antimony-doped germanium, and the (200) has been found in unirradiated germanium crystals of extremely high purity.

With the collaboration of H. C. Schweinler an extensive x-ray-diffraction investigation of these crystals and other semiconductors is now in progress.

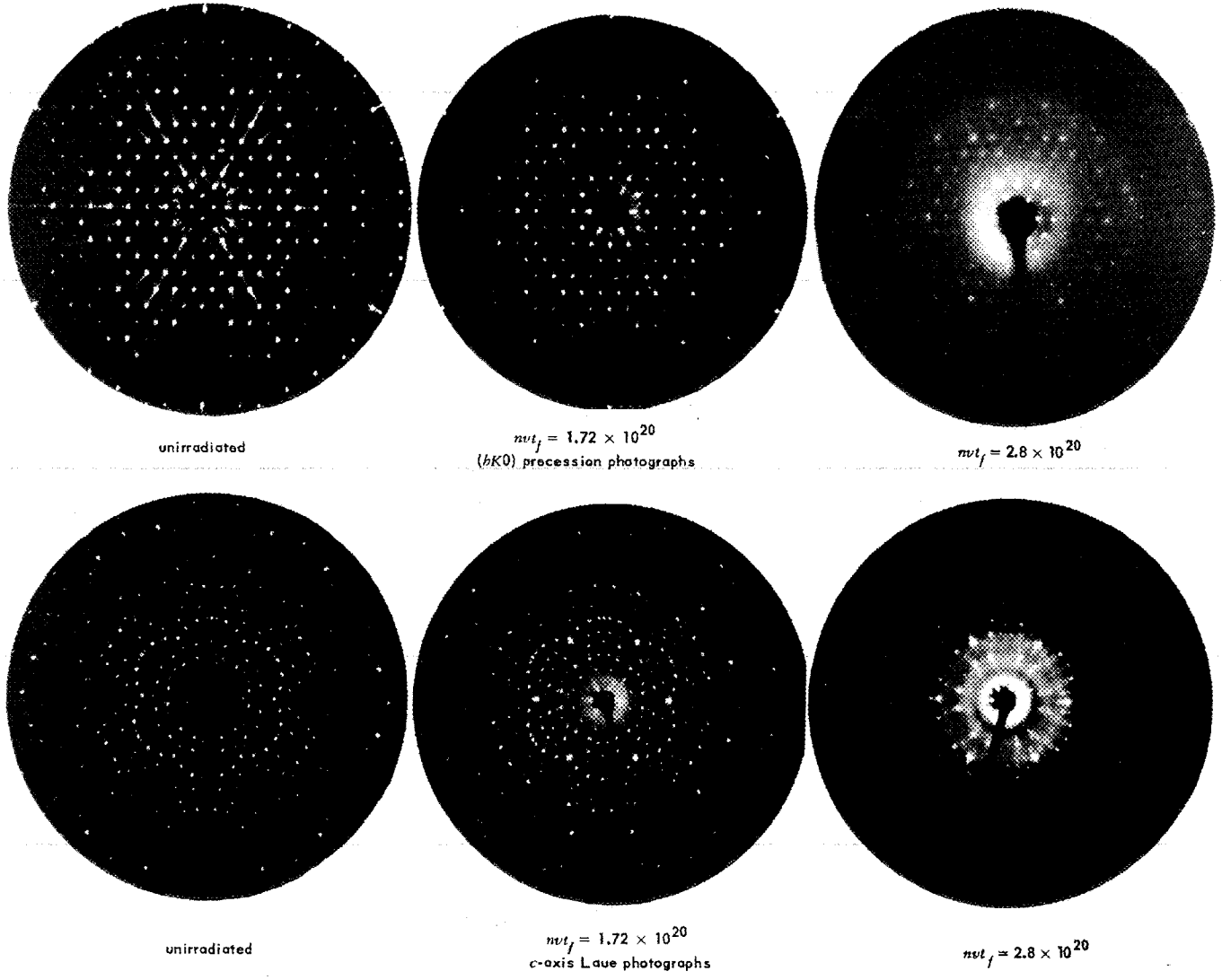

Fig. 23. Precession and Laue Photographs of Beryl after Irradiation.

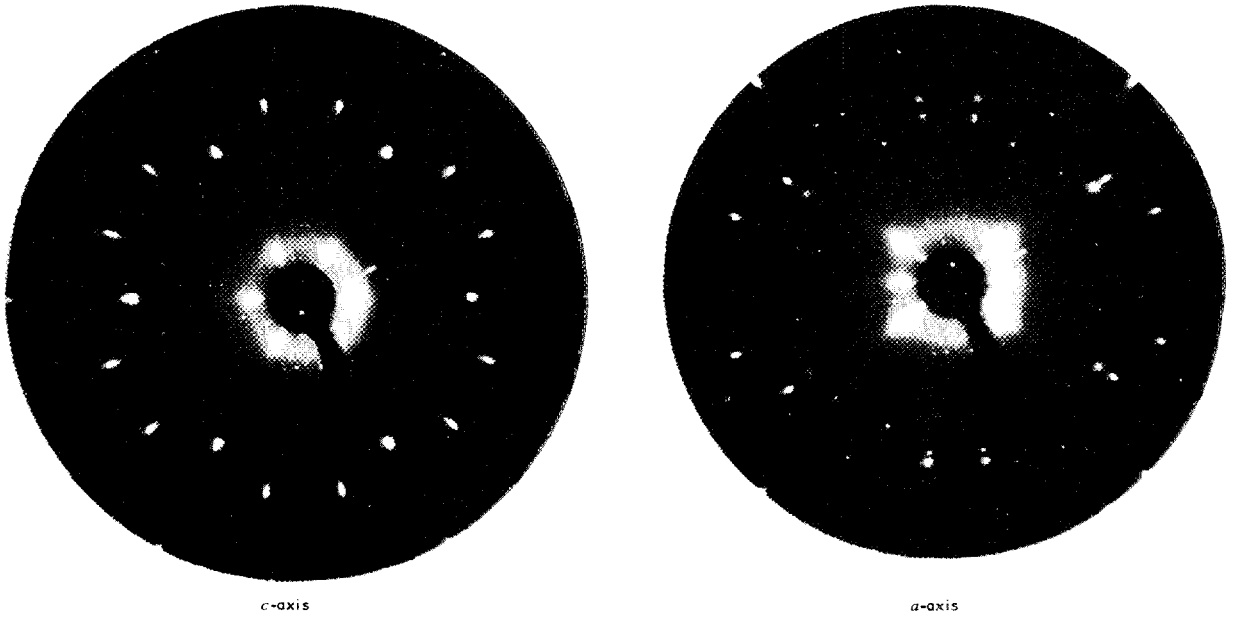

Fig. 24. Laue Transmission Photographs of Irradiated Quartz ($nvt_f \approx 7.8 \times 10^{19}$).

ENGINEERING PROPERTIES

RADIATION EFFECTS ON THE THERMAL CONDUCTIVITY OF CERAMICS

O. Sisman C. D. Bopp
R. L. Towns

The thermal conductivity at about 40°C has been measured for irradiated ceramic specimens.[1] Crystalline materials, for which an x-ray diffraction study indicated disordering (see "X-Ray Examination of Ceramic Samples," this report), are decreased in thermal conductivity (Table 3) more rapidly than are materials for which there is small order before irradiation (such as glasses). In some cases a change in thermal conductivity is detectable at exposures for which the x-ray diffraction pattern is not yet changed.

Zircon irradiated with 2×10^{20} neutrons/cm^2 gave very low and poorly reproducible thermal conductivities before a thin, soft surface coating was removed by scraping. The results of Table 3 are for the scraped material. (There were no crystalline peaks in the x-ray diffraction pattern after this exposure, either before or after scraping.)

For many of the materials, there was not much additional change in thermal conductivity for the longer exposure (2×10^{20} neutrons/cm^2), although there was a change for the shorter exposure (1×10^{20} neutrons/cm^2). Possibly the change is approaching saturation.

[1] C. D. Bopp, O. Sisman, and R. L. Towns, *Solid State Semiann. Prog. Rep. Aug. 30, 1954*, ORNL-1762, p 90.

TABLE 3. THERMAL CONDUCTIVITIES[a] OF IRRADIATED CERAMICS[b]

Material	Thermal Conductivity (10^{-4} cal·sec^{-1}·cm^{-1}·°C^{-1})		
	Preirradiation	Postirradiation[c]	
		$nvt = 1 \times 10^{20}$	$nvt = 2 \times 10^{20}$
Silica glass	35		35
Single-crystal Al_2O_3	>300		>300
Hot-pressed Al_2O_3	>300		>300
BeO	>300		>300
TiO_2	200	120	110
Spinel	>170	100	100
Forsterite No. 243	180	43	43
Cordierite No. 202	77	23	21
HfO_2	80	30	30
Steatite No. 228	60	28	28
Mica	21	14	13
ZrO_2 No. 550	33		25
Zircon No. 475	120		21
Zircon No. 71	49		28
Plate glass	30	30	30
Pyrex glass	36	30	20
Lead glass	16	10	10

[a] In the temperature range from 35 to 45°C.

[b] C. D. Bopp, O. Sisman, and R. L. Towns, *Solid State Semiann. Prog. Rep. Aug. 30, 1954*, ORNL-1672, p 90.

[c] Exposures are given in epithermal neutrons.

The specimens were in the form of wafers about $\frac{3}{4}$ in. in diameter by 20 mils thick. In order to create a temperature gradient across them, they were sandwiched between mercury pools, as shown in Fig. 25. The top mercury pool is heated electrically; the heat passes through the specimen and the bottom pool to a large base plate, which is at room temperature. In order to reduce convection losses the apparatus is enclosed in an evacuated chamber. The mercury containers and the thermocouple wells are constructed of stainless steel. Joints are welded where possible; soldered joints are protected from mercury attack by paint.

The small temperature drop, the small area of the top mercury chamber, the polished surface of the cell, and the thinness of the specimens (20 to 40 mils) all aided in holding heat losses to a minimum. The losses were estimated by substituting several thicknesses of glass cloth for a test specimen. Since very little heat passes through this poor conductor, the power which is necessary to maintain a temperature gradient is equal to the losses. The losses were less than 5% of the energy input for all the specimens tested.

With the losses neglected,

$$q = \frac{A}{t/k + 1/h} , \tag{1}$$

where

q = the electrical power divided by the temperature difference,

A = the area of the test specimen,

t = the thickness,

k = the thermal conductivity,

$1/h$ = the thermal resistance between the thermocouples and the surfaces of the test specimen (Fig. 25).

The thermal resistance $1/h$ is governed both by the distance from the thermocouple wells to the specimen and by the size of the thermocouple wells. It is necessary that specimens be nearly flat in order that the thickness of mercury between the thermocouples and the specimen remain constant. In order to keep the mercury free of lint and moisture, it was replaced frequently. (Dirty mercury tends to trap air bubbles at the mercury-specimen interface.) The effect of surface roughness was examined by surfacing specimens with both No. 320 and No. 100 carborundum grits; there

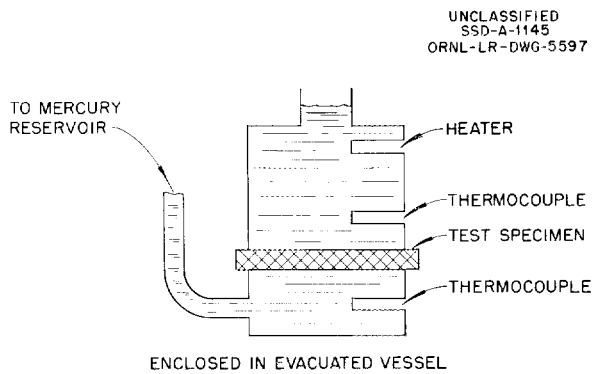

Fig. 25. Thermal-Conductivity Apparatus.

was no appreciable difference between these two degrees of roughness. When silica glass specimens were polished to a smoother finish, there was more of a tendency for air bubbles to be trapped; however, little trouble with trapping of air bubbles was encountered with either shiny mica or metal surfaces.

The effect of temperature was examined by heating the apparatus to about 10°C above room temperature and by using a test specimen of carbon stock thin enough to have $t/k \ll 1/h$. Since q varied less than 5% over this temperature range, $1/h$ was taken as nearly temperature independent for this work.

In order to evaluate the resistance $1/h$, a number of different thicknesses of carbon were tested at the power input which was used for all the measurements (carbon has a thermal conductivity low enough for this purpose). Aluminum was used as a check. Both results are given in Fig. 26. Equation 1 may now be written

$$\frac{A}{q} = \frac{t}{k} + \frac{1}{h} . \tag{2}$$

If A/q is plotted vs t, as in Fig. 26, the intercept at $t = 0$ equals $1/h$. This evaluation of $1/h$ permits the following calculation of k from Eq. 1:

$$k = \frac{t}{A/q - 1/h} . \tag{3}$$

The sensitivity of the method is limited by fluctuations in $1/h$ that result from variations in surface roughness and from the above-mentioned trapping of air bubbles. The thermal conductivity determined for silica glass checks within 5% the

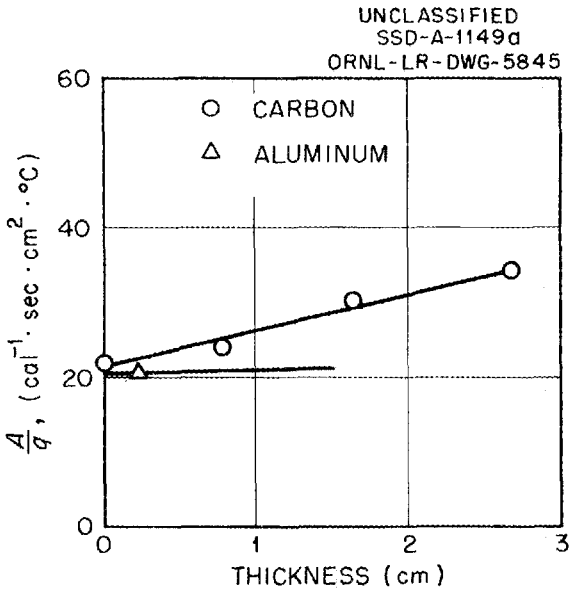

Fig. 26. Determination of $1/b$ for a Heat Flux of 0.24 cal·sec^{-1}·cm^{-2}.

value reported by another author[2] for quartz glass of comparable density. The specimen of silica glass was a wafer, $\frac{3}{4}$ in. in diameter by 20 mils thick. The thermal conductivity was calculated for the area of the mercury interface, 2.2 cm^2, since, for specimens of these dimensions, the portion of the specimen outside the interface conducts less than 5% of the total heat.[3] The sensitivity is less for better conductors than silica glass, owing to the larger effect of $1/b$. For specimens as thin as 20 mils, it is difficult to estimate thermal conductivities greater than 0.03 cal·sec^{-1}·cm^{-1}·°C^{-1} with this apparatus.

X-RAY EXAMINATION OF CERAMIC SAMPLES

G. E. Klein

Diffractometer patterns were obtained of a series of ceramic disks which had been subjected to irradiations of 1×10^{20} and 2×10^{20} neutrons/cm^2, respectively, by use of the shielded x-ray diffractometer.

The patterns of the irradiated specimens were qualitatively compared with the patterns of the corresponding samples before irradiation, and the results are listed in Table 4.

The method of x-ray analysis for polycrystalline samples with a high activity count is not so sensitive in detecting weak x-ray reflections as the method used for small single crystals of the same material. Consequently, where the method used in this study would indicate the absence of detectable diffraction lines in certain cases, the single-crystal analysis might still indicate a few weak reflections remaining in the film pattern after a comparatively long-exposure time. Wherever the data are comparable, the observed results are in agreement with those obtained by Wittels and Sherrill[4] and others. Furthermore, the ceramic disks (the same specimens as were used for the thermal-conductivity measurements) were fabricated from materials which in most cases contained a higher degree of impurity content than is generally found in natural single crystals. This would also have some effect on the resulting x-ray patterns.

A CORRELATION OF THE RADIATION STABILITY OF PLASTICS WITH THE YOUNG'S MODULUS

O. Sisman C. D. Bopp
R. L. Towns

The changes produced by high-energy radiation in the mechanical properties of irradiated plastics and elastomers depend upon the rates of crosslinking and cleavage. The relative rates at which these reactions proceed are governed by the chemical structure of the polymer and may also be affected by the strength of the van der Waals forces. For uncrosslinked polymers, Young's modulus is in part a measure of the van der Waals forces. For materials of like chemical structure a correlation may be expected between the Young's modulus and the rate of crosslinking.

The commercial plastics previously tested[5,6] have been grouped according to rigidity and are listed in Table 5. The order of ranking the plastics in Table 5 is given approximately by the preirradiation value of Young's modulus. This order is

[2] J. H. Perry, *Chemical Engineers Handbook*, p 1548, 3d ed., McGraw-Hill, New York, 1950.

[3] J. C. Jaeger and A. Beck, *Brit. J. Appl. Phys.* 6, 15 (1955).

[4] M. C. Wittels and F. A. Sherrill, *Solid State Semiann. Prog. Rep. Aug. 30, 1954*, ORNL-1762, p 85.

[5] O. Sisman and C. D. Bopp, *Physical Properties of Irradiated Plastics*, ORNL-928 (June 29, 1951).

[6] C. D. Bopp and O. Sisman, *Radiation Stability of Plastics and Elastomers*, ORNL-1373 (July 23, 1953).

TABLE 4. X-RAY EXAMINATION OF CERAMIC SAMPLES

Sample	Results When Irradiated with 1×10^{20} neutrons/cm^2	Activity (at 1 cm)	Results When Irradiated with 2×10^{20} neutrons/cm^2	Activity (at 1 cm)
Single-crystal Al_2O_3	No change in pattern	1.5 mr/hr	No change in pattern	1.5 mr/hr
Hot-pressed Al_2O_3	No change in pattern	6 mr/hr	No change in pattern	10 mr/hr
Spinel	No change in pattern	1.5 mr/hr	No change in pattern	5 mr/hr
Forsterite	No change in pattern	15 mr/hr	No change in pattern	60 mr/hr
Porcelain	No change in pattern	40 mr/hr	No change in pattern	40 mr/hr
Steatite	No change in pattern	80 mr/hr	No change in pattern	80 mr/hr
TiO_2	No change in pattern	170 mr/hr	No change in pattern	230 mr/hr
Silica glass	Halo broadening	2 mr/hr	Halo broadening	2 mr/hr
Plate glass	Halo broadening	10 mr/hr	Halo broadening	15 mr/hr
Pyrex glass	Halo broadening	10 mr/hr	Dimunition in halo intensity; broadening	30 mr/hr
Lead glass*	Lead plus other devitrification products	500 mr/hr	Lead plus other devitrification products	900 mr/hr
Mica	Line broadening; 1.3% expansion in c_0	120 mr/hr	Line broadening; 1.7% expansion in c_0	170 mr/hr
Enamel ground coat	Loss in crystallinity	6.7 r/hr	Loss in crystallinity	11 r/hr 7 r/hr (gamma)
ZrO_2	No change in pattern	6 r/hr	0.28% expansion in a_0	10.4 r/hr 600 mr/hr (gamma)
Hf-free ZrO_2	Dimunition in monoclinic phase	800 mr/hr	Monoclinic phase disappears; cubic phase remains	1.2 r/hr
Zircon	1.9% expansion; large loss in crystallinity	2.2 r/hr	No lines detectable; large loss in crystallinity	6.8 r/hr
SiC	Line broadening; 0.3% expansion	10 mr/hr	Expansion and loss in crystallinity	10 mr/hr
BeO	Very slight expansion in c_0	9 mr/hr	Approximately 0.3% expansion in c_0; none in a_0	25 mr/hr
Lava	Loss in crystallinity	170 mr/hr	No lines detectable	220 mr/hr
Cordierite	No change in pattern	100 mr/hr	Line broadening	150 mr/hr
MgO	No change in pattern	15 mr/hr	$MgO + MgO{\cdot}4CO_2{\cdot}5H_2O + MgCO_3{\cdot}3H_2O$	15 mr/hr
$BaTiO_3$	2.03% expansion in a_0	80 mr/hr	2.87% expansion in a_0; reflections broadened	170 mr/hr

*Confirmed by petrographic analysis.

TABLE 5. RADIATION STABILITY OF PLASTICS

Group Designation and Type of Plastic	Energy Absorption* (rad/10^9 nvt)	Exposure (rad) for 50% Decrease				Young's Modulus	
		Shear Strength	Impact Strength	Tensile Strength	Elongation	Initial Value (10^5 psi)	Change
A – Highly rigid mineral-polymer mixtures							
Plaskon alkyd (polyester)	0.4	>4	>4	>4	>4	32	Small
Asbestos fiber phenolic	0.4	>4	>4	4	>4	25	Small
Asbestos fabric phenolic	0.4	>4	>30	4	>4	18	Small
Karbate (phenolic)	0.3	>3	>30	3	>3	18	Small
Haveg 41 (phenolic)	0.3		>3	3	>3	10	Small
Duralon (furan)	0.3		>3	3	>3	8	Small
Melmac 592 (amino)	0.4	>4					Small
B – Highly rigid unfilled polymers							
Araldite, type B	0.7	>4					Small
Triallyl cyanurate polymer	0.7	>10					Small
Polyvinyl carbazole	0.7	>10	>10	>10	>10	6	Small
Aniline formaldehyde polymer	0.7	10	10	10	10	6	Small
C – Highly rigid paper or linen laminates							
Paper-base phenolic	0.7	2	2	0.2	0.2	16	
Micarta (phenolic laminate)	0.7		0.1	0.5	0.1	10	
Linen-fabric phenolic	0.7		0.02	0.4	0.02	10	
D – Moderately rigid polymers							
Catalin (unfilled phenolic)	0.7	1	1	1	2	6	Small
Casein	1	0.4	0.1	0.4	0.4	6	Small
Polystyrenes (amphenol, styrons 637, 671, and 411C)	0.7	>30	>30	>30	>30	5	Small
Polyalphamethyl styrene	0.7	0.4					Small
Lucite (methyl methacrylate)	0.7	0.1	0.1	0.05	0.05	5	Small
Polyvinyl formal	1			10	10	5	Decreases

TABLE 5 (continued)

Group Designation and Type of Plastic	Energy Absorption* (rad/10^9 nvt)	Exposure (rad) for 50% Decrease				Young's Modulus	
		Shear Strength	Impact Strength	Tensile Strength	Elongation	Initial Value (10^5 psi)	Change
D – Moderately rigid polymers							
Vinyl chloride acetate polymer	2.5	5	10	5	5	4.8	Decreases
Cellulose nitrate	0.7	0.1	0.1	0.1	0.04	3.6	Small
CR-39 (allyl diglycol carbonate polymer)	0.9	8	8	3	7	2.8	Decreases
Pliotuf (butadiene-styrene, rubber blend)	0.8	>10	2	>10	2	2.7	Small
E – Nonrigid polymers							
Styron 475 (high impact polystyrene)	0.8	>30	0.4	>30	0.04	2.6	Increases
Cellulose acetate	0.7	0.2	0.07	0.2	0.07	2.6	Small
Royalite (styrene copolymer)	0.8	>10		>10	1	2	Increases
Silicon-varnished glass cloth	0.6	4					Increases
Nylon	1	>10	0.05	>10	0.1	2	Increases
Ethocel (ethyl cellulose)	0.7	0.07	0.03	0.05	0.02	2.0	Increases
Cellulose propionate	0.7	0.04	0.04	0.04	0.04	2.0	Small
Fluorothene	1	0.2	0.05	0.1	0.05	1.8	Small
Cellulose acetate butyrate	0.7	0.07	0.05	0.07	0.05	1.6	Small
Teflon	1	0.1	0.1	0.07	0.003	1.0	Small
Mylar	1			2	1		Small
Selectron 5038 (polyester)	0.8	>10	3	>10	0.1	0.6	Increases
Saran B-115 (vinyl chloride polymer)	2.5	1	0.5	1	0.5	0.6	Small
Geon 2046 (vinyl chloride polymer)	2.5			4	0.4	0.5	Small
Polyethylene	1	>10	0.5	>10	0.5	0.3	Increases
Butacite (polyvinyl butyral)	1			0.6	0.6	0.04	Increases

*The data were abstracted from ORNL-928[5] and ORNL-1373,[6] which give the exposures in thermal neutrons/cm^2 in the ORNL Graphite Reactor. These factors convert the nvt numbers to rad. For practical purposes a rad is equivalent to a rep, which is discussed on p 56 of *Solid State Semiann. Prog. Rep. Feb. 28, 1954*, ORNL-1677.

significant for many applications of plastics and may also be related to the radiation sensitivity of Young's modulus. For materials of like composition (such as vinyl chloride polymers or polyesters), those falling in group D may be predominantly cleaved, those in group E, crosslinked. The Young's modulus of the plastics was determined from the initial slope of the tensile curve. The Young's modulus is fairly sensitive to crosslinking – not so sensitive, however, as the change in solubility – but may be less sensitive to cleavage. A more pronounced effect of cleavage is to cause a decrease in breaking strength.

Although low exposure in a radiation field often improves certain mechanical properties, longer exposure usually decreases the ultimate strength. In certain applications for nonrigid materials the change produced in rigidity is important. In Table 5 the materials tested are compared on the basis of the exposure required to decrease the elongation and the strength by 50%.

Group A includes plastics having a high rigidity, which is partly due to a large amount of mineral filler. Group B includes unfilled plastics that have such high rigidity as to break with a glass-like fracture. Group C includes polymer and paper (or cloth) combinations that have high rigidity. Group D includes plastics that are less rigid than group B but not sufficiently nonrigid to show high values of elongation in the tensile test. (The tensile curves of group D plastics usually show a small amount of curvature, just before the breaking point.) Group E includes plastics that give high elongation in the tensile test.

The plastics in groups A or B show small change in either Young's modulus or breaking strength for the maximum exposures. Often there is uncertainty as to whether an apparent change in tensile strength is real or the result of poor statistics for these rigid materials. It is planned to resolve this matter by employing greater exposures.

Since the paper constitutes a sizable portion of the group C plastics, any damage to the paper weakens the plastic.

The different group D plastics encompass a large stability range. There is little crosslinking for these moderately rigid plastics; however, the cleavage may be large or small, depending on the chemical composition.

Group E plastics, like group D plastics, may show a large or small amount of cleavage, depending on the chemical composition; however, for group E plastics the crosslinking is always sizable in the absence of large cleavage. In certain group E plastics the change in hardness is not great because there is an equalization of the cleavage and the crosslinking processes; however, in this case the breaking strength is decreased. For certain of the materials which are least sensitive to radiation, the maximum exposure given is listed and is prefixed by the symbol >. Whether the Young's modulus is increased or decreased appreciably before the strength is decreased is also indicated.

An explanation has been developed which accounts for the differences in effects for different materials. Sufficient experimental evidence is lacking to fully substantiate these ideas; however, presenting them in their present form is of aid in planning future experiments and in predicting radiation effects for untested polymers.

The rate of the volume change that accompanies the cooling of a high polymer is controlled by a diffusion process, which becomes so slow at the second-order transition temperature that it introduces a discontinuity in the temperature-specific volume relation as it is ordinarily measured. Perhaps if a sufficiently long waiting period were allowed between changing the temperature and measuring the volume, the volume-temperature relation would be linear to absolute zero. Analogously, the rate of crosslinking may be diffusion controlled, since, during crosslinking, hydrogen diffuses out of the polymer and the molecular segments diffuse close together.

It may be speculated that, in a polymer exposed in a radiation field, there exist ionized and excited molecular segments which crosslink as they diffuse together. The rate of crosslinking will be proportional to the energy absorption under two conditions: first, that the rate of crosslinking is proportional both to the rate of diffusion and to the concentration of ionized and excited molecular segments; second, that the concentration of ionized and excited molecular segments is proportional to the intensity of the radiation field. The likelihood that the second condition will fail may possibly be greater for rigid materials with low rates of diffusion because there is a slower rate of deactivation of excited or ionized radicals by crosslinking. However, there exists another possibility: deactivation is predominantly by a decay process which is independent of crosslinking. In the intensity range from 10^4 to 10^7 rad/hr the changes

produced in nonrigid materials showed very little dependence on radiation intensity. Polystyrene was exposed at even higher intensities, and there was still no measurable change in its mechanical properties; but this is only a qualitative observation.

That diffusion determines the rate of approach to the equilibrium value of deformation is apparent from the broad spectrum of retardation times of many polymers. The retardation time[7,8] τ is defined by the expression $y = y_0 (1 - e^{-t/\tau})$, where y is the deformation at time t after the application of stress, and y_0 is the equilibrium value of deformation. Rarely is it possible to fit experimental data with only one retardation time, and it is customary to use a smooth distribution of retardation times.

The distribution of retardation times is often sensitive to the rate of dissipation of frictional energy and for this reason may be dependent on the dimensions of the specimen. On the other hand, the free volume is often important in governing the rate of diffusional processes, and for this reason the distribution of retardation times is usually sensitive to the temperature.

A third factor which may affect the retardation time spectrum is crosslinking. In fact, the crosslinking effect on Young's modulus may be explained in terms of increased retardation times, since seldom is the measured value of Young's modulus independent of the rate of loading.

In order to explain that the rate of crosslinking is nearly constant in the early stages of crosslinking (though the retardation times are increased), it is necessary to postulate that crosslinking does not microscopically restrict the diffusion of neighboring molecular segments except perhaps very close to the crosslinking site. The effect on the retardation times must then be largely due to the formation of a network structure. Thus, it is possible for the macroscopic retardation times to be affected by crosslinking without affecting the microscopic diffusion rate of a large portion of the molecular segments.

From these considerations it appears necessary to restrict the correlation between rigidity and the rate of crosslinking to noncrosslinked polymers. Even in the absence of crosslinking, the correlation based on Young's modulus is only an approximation, since clearly the microscopic rate of diffusion may be only very roughly estimated from Young's modulus.

---

[7] R. N. Howard, *Chemistry & Industry* 62, 495 (1943).

[8] T. Alfrey, *The Mechanical Behavior of High Polymers*, Interscience, New York, 1948.

CRYSTAL PHYSICS

LOW-TEMPERATURE IN-PILE CRYOSTAT

T. H. Blewitt R. R. Coltman
J. W. Cleland W. E. Busby
J. T. Howe

During the past few years it has become increasingly evident that a more complete understanding of radiation damage might be obtained through studies of bombardments at low temperatures. For the past three years a facility has been available in which bombardments can be made at −160°C and from which specimens can be removed without warming to above about −120°C prior to storage in liquid nitrogen and subsequent controlled annealing experiments. Recent results of bombardments on copper in this facility have indicated that some neutron-induced defects are mobile at temperatures lower than −160°C. Until recently, the amount of refrigeration required to obtain bombardments at very low temperatures proved to be financially prohibitive. This was due to the physical size of the cryostat required, the operating temperature of the reactor, and the gamma-ray heating effects.

Six months ago the laboratory acquired a surplus helium refrigerator with a rated capacity of 120 w of heat load at an operating temperature of 20°K. The machine will circulate cold helium gas through a cryostat, which will be placed in vertical hole 12 of the ORNL Graphite Reactor.

An aluminum cryostat has been constructed and has been tested outside the reactor. With the refrigerator operating inefficiently at about half its rated output, the cryostat reached 20°K, which indicated that the heat load it presented to the machine was not excessive. The cryostat has a sample chamber $1\frac{1}{4}$ in. in diameter, and the usable length inside the heat exchanger, which will be in the center of the reactor, is 18 in. long. The total length of the cryostat is 22 ft, and the lower 15 ft is made entirely of 2S aluminum.

A modification now under way will increase the capacity of the refrigerator to approximately 300 w at 20°K. Since calculations show that the heat load inside the reactor will be about twice the heat load outside, it is believed that this amount of refrigeration will be sufficient to perform bombardments at 20°K and possibly lower.

The design and working drawings of the new shielding for the cryostat and shield support are completed.

THE CRITICAL SHEAR STRESS IN ALPHA BRASS AS A FUNCTION OF ZINC CONCENTRATION AND TEMPERATURE

R. E. Jamison F. A. Sherrill

The data presented here are the result of preliminary work in a study of neutron-radiation effects on the mechanical and electrical properties of alpha-brass single crystals. Although there is no development in dislocation theory to explain the temperature dependence shown, the results are believed to be interesting, and they supplement early room-temperature data[1,2] and more recent data[3] on beta brass in the range 78 to 673°K.

High-purity copper (99.999%) and zinc (99.99%) were inserted in the approximate proportion desired[4,5] into a closed graphite mold, which, in turn, was sealed at 400°C in a fused-quartz carrier under a vacuum of approximately 2×10^{-5} mm Hg. The carrier was then placed in a furnace mounted on a horizontal axis, the metals were melted and homogeneized, and the crystals were grown by the Bridgman technique with a minimum of dezincification. Spectrographic analysis indicated an extremely minute addition of impurities during this process. The Laue x-ray back reflections from which orientations were determined showed only samples 2 and 8 to be mosaic. The crystals were in the shape of tensile specimens, with the gage length $1\frac{1}{2}$ in. long and $\frac{7}{32}$ in. in diameter.

After the crystals were grown, they were removed from the carrier and crucible (in which some deformation occurred during cooling) and were etched; then they were sealed again in a closed carrier under vacuum and annealed for 17 hr at 550°C. They were then pulled in an Instron tensile testing machine, with the rate of extension equal to 0.02 in./min and rapid-response load indication, at various temperatures in the following order: 297,

[1] V. Göler and G. Sachs, *Z. Physik* **55**, 581 (1929).

[2] M. Masima and G. Sachs, *Z. Physik* **50**, 161 (1928).

[3] G. W. Ardley and A. H. Cottrell, *Proc. Roy. Soc. (London)* **219A**, 328 (1953).

[4] E. A. Owen and G. D. Preston, *Proc. Phys. Soc. (London)* **36**, 49 (1923).

[5] A. Westgren and G. Phragmén, *Phil. Mag.* **50**, 311 (1925).

78, 4.2, 297, and 195°K. The samples were not allowed to exceed 78°K between the pull at 78°K and the pull at 4.2°K. During each pull the samples were extended just enough to obtain the elastic limit. After these five pulls the samples were again annealed (72 hr at 550°C) and were pulled again at the various temperatures to check the first measurements and to note the height and nature of existing yield points. Total extension before the second anneal was never more than 1% and was generally less than 0.5%.

After all measurements were made, sections from the ends of the samples were removed for single-crystal lattice-parameter measurements. These measurements were accurate to ±0.001 Å.[6] Some samples varied in zinc concentration from end to end, in which case the measurements were interpolated to the region where slip occurred in the gage length.

Since the concentration dependence of the critical shear stress at room temperature is well known and since a relative value of the critical shear stress is much more accurately determined, the ratio of the critical shear stress at each of the lower temperatures to that at room temperature is plotted in Figs. 27 and 28. The value at room temperature is listed in Table 6, along with a value which is taken from a smooth curve drawn as an average through all data available.[1-3]

It is pretty well established that, to within 10%, the critical shear stress in pure copper is independent of temperature.[7,8] It is unfortunate that, because of the indefinite yield point, the data on the pure metal are not more accurate. It could be assumed that the critical shear stress in pure copper is actually lower at 4.2°K than at 78°K by 6 or 7%; or it could be assumed that the critical shear stress is really independent of temperature. Either assumption is difficult to make, since the first would mean that there is anomalous behavior in the pure metal, and the second would mean that there is an even more anomalous behavior in the copper with small percentages of zinc.

Although a portion of the curve for 4.2°K in Fig. 27 is shown to be indefinite and although the

[6] R. J. Fox, F. A. Sherrill, and M. C. Wittels, *A Single-Crystal Adapter for the Norelco Wide-Range Diffractometer*, ORNL-1807 (Jan. 6, 1955).

[7] P. W. Neurath and J. S. Koehler, *J. Appl. Phys.* 22, 621 (1951).

[8] T. H. Blewitt, *Phys. Rev.* 91, 1115 (1953).

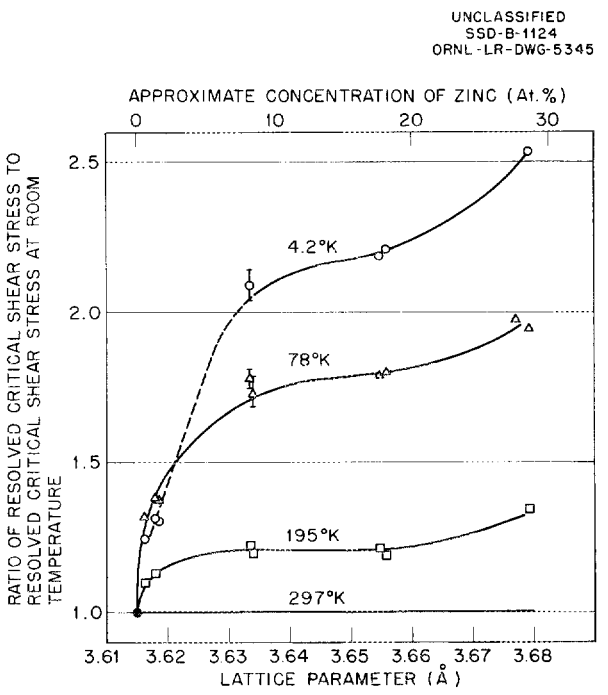

Fig. 27. The Resolved Critical Shear Stress of Alpha Brass as a Function of Lattice Parameter and Temperature.

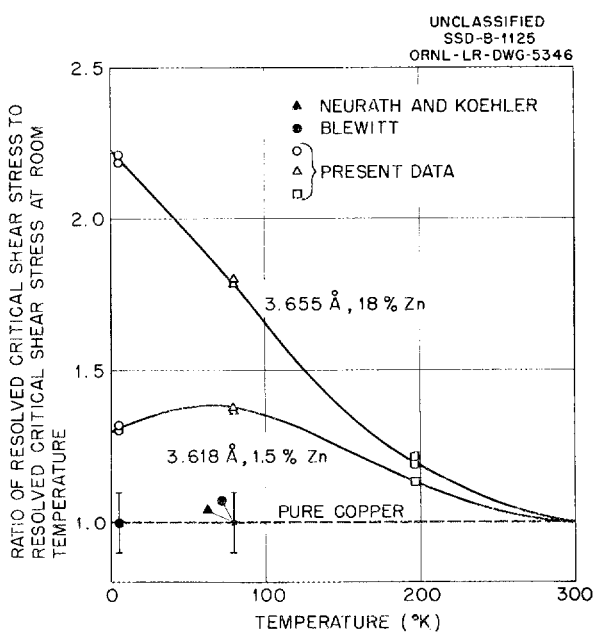

Fig. 28. The Resolved Critical Shear Stress of Alpha Brass as a Function of Temperature for Two Concentrations of Zinc.

TABLE 6. CRITICAL RESOLVED SHEAR STRESS AT ROOM TEMPERATURE, ORIENTATION, LATTICE PARAMETER, AND APPROXIMATE COMPOSITION

Sample[a]	Orientation[b] (deg)	Lattice Parameter (Å)	Approximate Composition[c] (at. % Zn)	Critical Resolved Shear Stress at Room Temperature (kg/mm^2)	
				Measured	Corrected[d]
CuZn 1	30 , 63 , 78	3.6792 ± 0.0010	28.7	1.52 ± 0.15	1.43
CuZn 2	46 , 56½, 63	3.6770 ± 0.0010	27.6	1.56 ± 0.15	1.425
CuZn 3	43 , 53 , 73 43½, 51½, 72½	3.6548 ± 0.0005	17.8	1.49 ± 0.13	1.33
CuZn 5A	41 , 56½, 70	3.6335 ± 0.0005	8.3	1.08 ± 0.12	1.07
CuZn 5B	41 , 56½, 70 Assumed	3.6340 ± 0.0005	8.6	1.03 ± 0.12	1.08
CuZn 6	4½, 86½, 87	3.6162 ± 0.0005	0.7	0.51 ± 0.08	0.50
CuZn 7A	43½, 48½, 79½	3.6179 ± 0.0005	1.4	0.76 ± 0.10	0.64
CuZn 7B	44 , 48 , 82	3.6185 ± 0.0005	1.6	0.72 ± 0.10	0.67
CuZn 8	17½, 73 , 84	3.6558 ± 0.0010	18.2	1.31 ± 0.13	1.34

[a]Samples 5A and 5B and samples 7A and 7B were grown together.

[b]The angles between the specimen axis and the three [100]-type poles.

[c]From refs 1, 4, and 5.

[d]These values are from a smooth curve, drawn through the plot of data from ref 1, 2, and 3 and the author's own values. They would be very reasonable values to use in determining the actual resolved shear stress from the ratio plotted in Figs. 27 and 28.

other two curves might not really run through a common point, it should be emphasized that, as shown in both Figs. 27 and 28, the critical shear stress at 4.2°K in this region of small zinc percentages is definitely lower than that at 78°K.

The standard annealing temperature was 550°C, but in some instances (CuZn 3 and CuZn 5A) the second anneal was made at 850°C, which caused a rise in the ratio at 78°K, while the actual critical shear stress was lowered at room temperature and at 195°K. On annealing again at 550°C for 72 hr, the ratio at 78°K returned to nearly its normal value. This effect is believed to be due to excess dezincification at the higher temperatures and to trapping of an increased number of vacancies during the more rapid cooling.

When sample CuZn 1 was pulled at 4.2°K, it yielded discontinuously and with an audible click. This was definitely a real effect and is thought to be more like the phenomenon reported for irradiated copper[9] at 78°K and for deformed copper[10] at 4.2°K than like the discontinuous slip reported[11] for alpha brass at 200°C.

The curve plotted in Fig. 28 for samples CuZn 3 and CuZn 8 is very similar to the same curve plotted for pure copper after an irradiation of approximately 3×10^{18} fast neutrons/cm^2.

As Ardley and Cottrell found,[11] sharp upper yield points existed at room temperature in the samples where zinc concentration was more than about 1 at. %, and the height of these yield points increased with concentration. However, no consistent temperature dependence was observed, and the expected increased effect at low temperatures did not exist. The existence of an upper yield point in any pull seemed to be more dependent on small amounts of previous deformation, the temperature of that deformation, and the aging temperature between deformations than upon the temperature of the pull itself.

[9]R. E. Jamison and T. H. Blewitt, *Phys. Rev.* **91**, 237 (1953).

[10]T. H. Blewitt, J. K. Redman, F. A. Sherrill, and R. R. Coltman, *Bull. Am. Phys. Soc.* **30** (2), 32 (1955).

[11]G. W. Ardley and A. H. Cottrell, *Proc. Roy. Soc. (London)* **219A**, 328 (1953).

SPECIAL PROJECTS

ELASTIC EFFECTS IN NEUTRON IRRADIATED LiF

W. J. Sturm D. Binder

In the interpretation of results of recent experiments[1] directed toward identification of the lattice defect introduced in large LiF single crystals by neutron irradiation, it has been customary to introduce the concept of surface-to-volume yield ratio, S, as a parameter in the analysis. This was done because measurement consisted primarily in comparing x-ray- and density-determined lattice parameters in which only surface properties are detected with x rays because of their small penetration, and only average volume effects are detected from density measurements because density is a bulk property. Since in some cases defects were produced in the crystal lattice by an (n,α) process having a high thermal-neutron cross section, attenuation of defects as a function of crystal dimension could be severe, and the surface-to-volume yield, S, had obvious significance in correcting measurements directed at the determination of a ratio of the two lattice parameters.

However, the correction factor,

$$S = \frac{\text{surface defect concentration}}{\text{mean defect concentration}} = \frac{c_s}{c_m},$$

would be fully appropriate only if the crystal were made up of many thin slabs free to slide over each other, as in Fig. 29*b*, in which the unit cell expands uniformly. Each slab would have approximately uniform damage (when edge effects are neglected); since x-ray measurements were made of the large surface in the xy plane (Fig. 29*a*), the lattice parameter measured was that along the z direction, a_z. Under these conditions, the expansive strain in any slab free to slide would be

$$e_{xx} = e_{yy} = e_{zz} = \beta c(z) ,$$

where β is the proportionality between defect concentration and strain and is assumed to be linear for moderate defect concentrations. It is also assumed that the crystal has cubic anisotropy; edge effects are ignored in the xz and yz planes. The problem then involves a "self-strained" system and is analogous to that of a slab deformed by a nonuniform temperature distribution equal to $c(z)$. Since

$$e_{xx} = \frac{p_{xx}}{E} - \frac{\sigma p_{yy}}{E} ,$$

$$e_{yy} = \frac{p_{yy}}{E} - \frac{\sigma p_{xx}}{E} ,$$

$$e_{zz} = -\frac{\sigma p_{xx}}{E} - \frac{\sigma p_{yy}}{E} ,$$

in which the p's are stresses, σ is Poisson's ratio, and E is Young's modulus, and since

$$p_{xx} = p_{yy}$$

by the nature of the system, the stresses required to bring the crystal back to its original width and breadth are

$$p_{xx} = p_{yy} = -\frac{\beta c(z) E}{1 - \sigma} .$$

The resulting strain in the z direction is

$$e_{zz} = \frac{2\beta c(z)\sigma}{1 - \sigma} .$$

The actual crystal, with unrelieved reactive stresses, would be represented by welding the slabs together at this stage (Fig. 29*c*); as a result of this process the unit cell expansion is entirely in the z direction. If the reactive stresses are relieved, there is a reduction in the z strain (Fig. 29*d*) which produces a further change in the strain:

$$e_{zz} = -\frac{2\beta c_m \sigma}{1 - \sigma} ,$$

where c_m is the average defect concentration. The net strain, then, is

$$e_{zz} = \frac{\beta}{1 - \sigma} c(z)(1 + \sigma) - 2\sigma c_m ;$$

and at the surface, if $c(z)$ is replaced with c_s, the experimental slope, S', is

$$S' = \frac{\Delta a_x}{\Delta a_\rho} = \frac{1 + \sigma}{1 - \sigma} S - \frac{2\sigma}{1 - \sigma} ,$$

where a_x and a_ρ are the lattice parameters determined by x-ray and density measurements.

[1] D. Binder and W. J. Sturm, *Solid State Semiann. Prog. Rep. Aug. 30, 1954*, ORNL-1762, p 111.

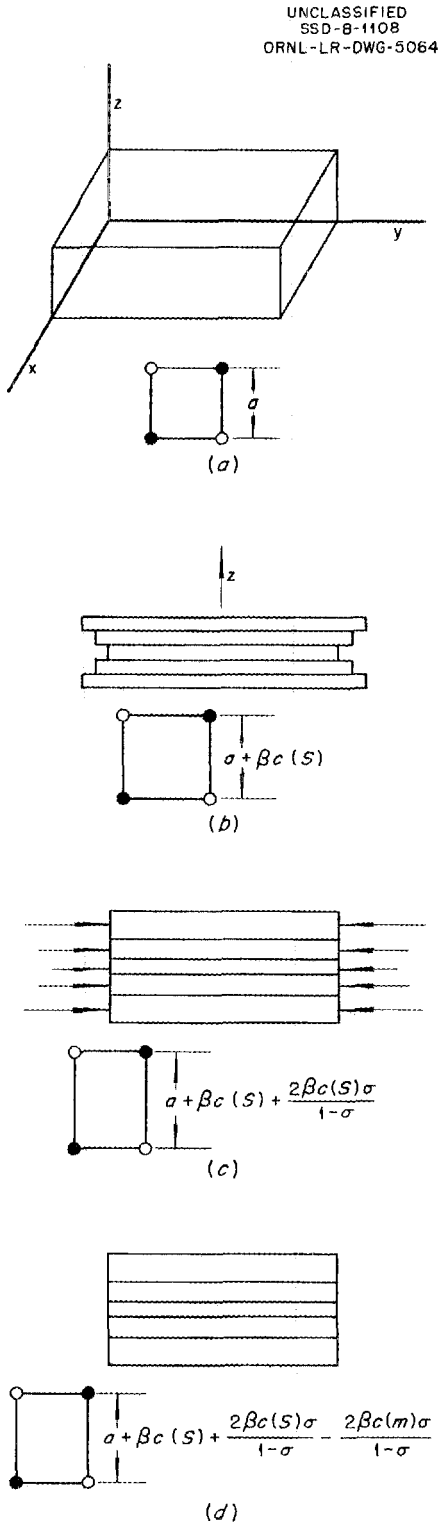

Fig. 29. Strains Induced in an Irradiated Crystal and in a Unit Cell at the Surface by Nonuniform Defect Distribution.

A recent determination[2] of σ has been used in applying this interpretation to all the recent measurements, and the results have been published.[3]

TWO-STAGE ANNEALING PROCESS IN NEUTRON-IRRADIATED LiF

D. Binder W. J. Sturm

An LiF crystal (obtained from the Harshaw Chemical Co.) was irradiated for 2×10^{16} neutrons/cm^2 in the ORNL Graphite Reactor. Before-and-after measurements of x-ray line breadth were made by using the 200 and 400 reflections of the copper K_β line and the 200 reflection of the chromium K_β line. The copper radiation has a wave length of 20 and 44 deg, and the chromium reflection is at 31 deg. The three lines are then suited to an experiment to determine variation of x-ray line broadening with angle and give some indication of a variation with wave length.

The initial broadening caused by irradiation was observed to follow a tan θ law, so-called "strain broadening." This result has been reported by Warren,[4] who used the 200, 400, 600, 800, and 1000 reflections of molybdenum radiation. When the irradiated crystal was annealed, a two-stage process was observed. For step anneals at successively higher temperatures from 300 to 400°C, the line breadths remained the same or tended toward the original values. The accuracy of the measurement needs to be improved before a definite statement on the behavior of line breadth in this range of temperatures can be made. Lattice-parameter measurements were also made. The irradiated crystal displayed an expansion of 0.075 ± 0.010%, which decreased monotonically on annealing to 0.009 ± 0.010% at the 400°C anneal.

Further anneals from 425 to 500°C showed a second stage in the annealing process. The line breadth actually increased, reached a peak around 450°C, and then decreased toward the unirradiated value. The increase was marked: the 400 reflection of copper K_β radiation was 1.4 times as broad as the reflection from unirradiated material.

If neutron irradiation introduces a uniform distribution of Frenkel defects (vacancy-interstitial

[2] S. Rao, *Current Sci.* 18, 336 (1949).

[3] D. Binder and W. J. Sturm, *Phys. Rev.* 96, 1519 (1954).

[4] B. E. Warren, *X-Ray Study of Radiation Damage*, NYO-6508 (Jan. 31, 1954) p 4.

pairs), the lattice-parameter change is probably proportional to their concentration in the "perfect" regions of the crystal. "Perfect" regions may be taken as the interior of mosaic blocks. The first stage of the annealing in which the lattice parameter returns to its initial value is, then, the disappearance of Frenkel defects from perfect regions. The initial lattice-parameter change of 0.075% indicates a concentration of about 0.075% of vacancy-interstitial pairs. Annealing sets the defects into motion, and, on the assumption of a random walk process, a vacancy will meet an interstitial every 1300 steps. This means that the pair will be annihilated within $1300^{1/2}$ steps or about 40 interatomic distances from its original position. The mosaic blocks of the crystal under study are 400 or more interatomic distances across, so that the initial stage of annealing involves mostly the inside of a mosaic block.

In the second stage, the lattice-parameter change has decreased by a factor of 8 or more, so that the boundary of the block may play an important role. The defect may now travel longer distances before annihilation and may be affected by mosaic-block boundaries or by other large defects at comparable distances.

The variation of line breadth with angle in the second stage is inconsistent with a tan θ law or any combination of a tan θ law and a λ sec θ law (mosaic-block broadening). A new type of broadening, possibly a result of a disordered mosaic-block boundary, is in evidence.

A STUDY OF LATTICE DEFECTS IN GOLD-CADMIUM ALLOY

M. S. Wechsler

It has been recognized for same time that many of the important properties of crystalline solids do not depend on the structure of the individual atoms nor even on the arrangement of the atoms in the crystal lattice. Instead, these properties depend upon the way in which the solid deviates from perfect crystallinity, that is, on the number and types of imperfections present in the crystal. In order to study these imperfections, it is convenient to introduce by external means a larger concentration of lattice defects than would normally be present in the material. Several ways of doing this are in current use. One way is to deform the material mechanically. Another approach is to introduce imperfections by irradiation. A third method is to freeze into the material the imperfection structure that is characteristic of a high temperature by quenching from the high temperature to a temperature at which atomic mobilities are negligibly low. This report deals with the effect of quench on the structure of gold-cadmium alloys.

An investigation of the effect of quench on the resistivity of gold-cadmium alloys was started several years ago at Columbia University under the direction of T. A. Read. It was found that quenches from 450°C cause increases of more than 10% in the electrical resistivity of gold-cadmium alloys of approximately 50 at. % composition. An investigation has been in progress at ORNL since July 1954 in order to gain some insight into the cause of this increase in resistivity and the mechanism by which the increase subsequently anneals out. A polycrystalline sample was used of composition 49 at. %; it was rod-shaped, about 3 mm in diameter, and several inches long. After quenching, a series of isothermal annealing experiments were carried out at various temperatures. The resistivity was measured with a Kelvin bridge. The sample was quenched each time from 450°C into water at 40°C; the melting temperature of the alloy is about 620°C. A plot of the raw data for an isothermal annealing run at 69.5°C is shown in Fig. 30. If it is assumed that the decay curve starts off with zero slope, an initial resistivity,

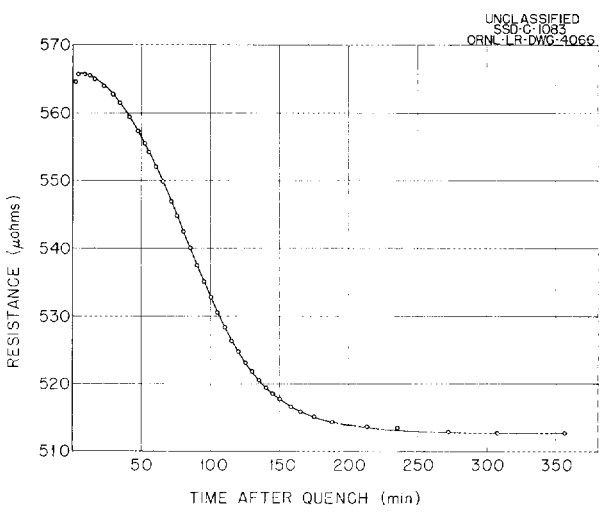

Fig. 30. Resistance at 69.5°C of Au-Cd (49 at. % Cd, Specimen RW-1) after Quench from 450°C.

R_i, can be assigned. Similarly, the final resistivity, R_f, can be determined. The fraction

$$f = \frac{R - R_f}{R_i - R_f}$$

is, then, a measure of the fractional amount from completion of the process. A plot of f vs time after quench for isothermal relaxation at various temperatures is shown in Fig. 31. Relaxation times corresponding to various values of f may be obtained from this figure. In Fig. 32 these times are plotted vs the reciprocal of the absolute temperature. From the slopes of the curves in Fig. 32, it is found that the defects frozen in by the quench have an activation energy for movement of about 0.6 ev. A quantitative analysis of the kinetics of the relaxation process has been hampered by the fairly large thermal lag in the present apparatus. Several modifications in the apparatus are being considered that will enable a more accurate determination of the decay curve in the first few minutes of the process.

At temperatures several degrees above room temperature, Au-Cd in the 50 at. % region exhibits an ordered CsCl structure. In the absence of

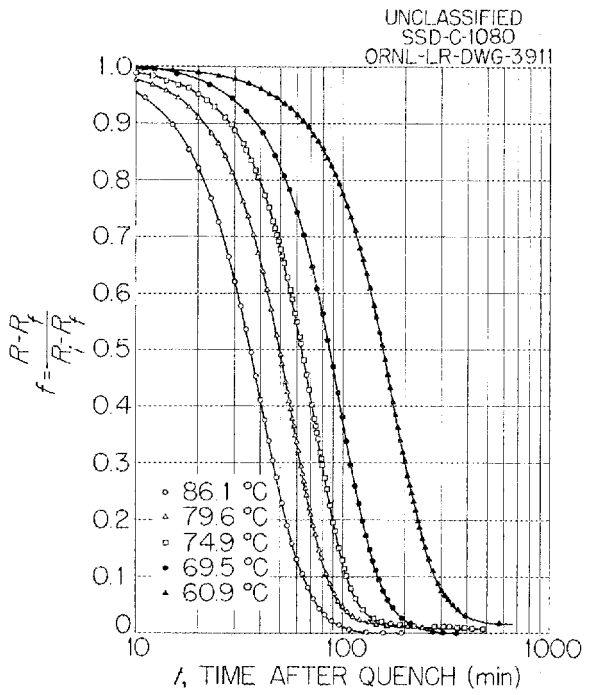

Fig. 31. Isothermal Relaxation Curves of the Resistivity of Au-Cd (49 at. % Cd) after Quench from 450°C.

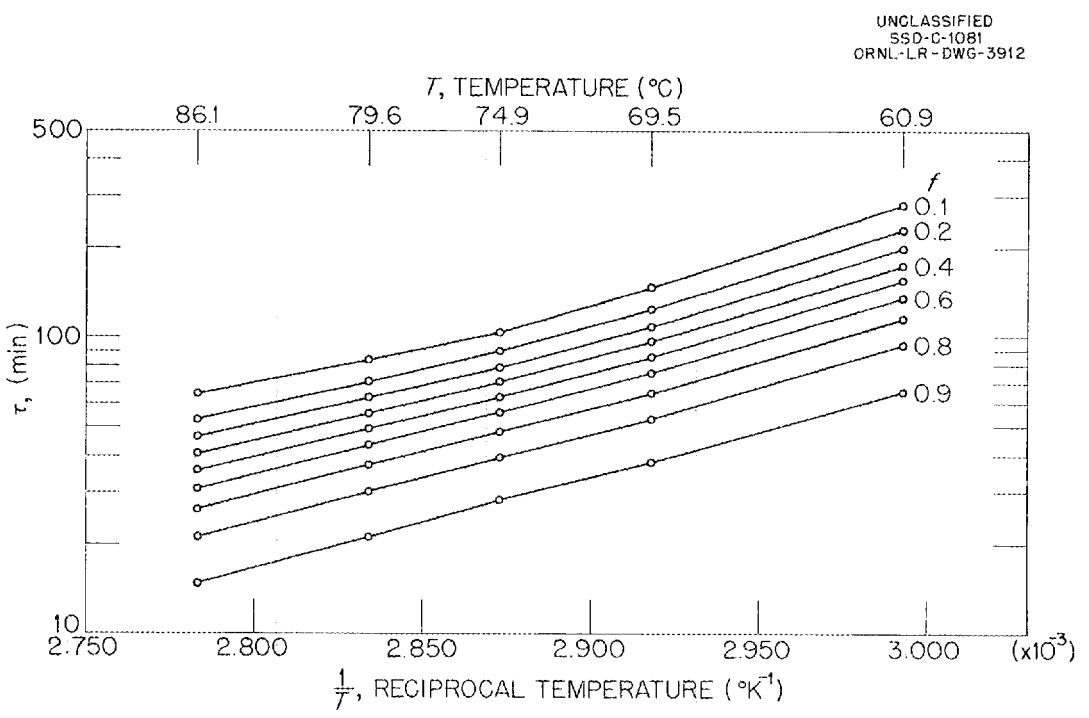

Fig. 32. Times (τ) for Fractional Amounts from Completion (f) from Relaxation Process at Various Temperatures.

evidence to the contrary, a possible explanation for the increase in resistivity is that a disordered structure characteristic of high temperature is frozen in upon quench. It could then be supposed that the alloy orders at the annealing temperatures, thereby decreasing the resistivity to its normal annealed value. To test this idea, experiments in collaboration with M. A. Bredig and R. D. Ellison were performed with a high-temperature x-ray spectrometer.[5] X-ray reflections were obtained at temperatures ranging from 40 to 600°C for the superstructure (100) reflection, as well as for several of the ordinary reflections. There was no indication of any decrease in the amount of order with increase in temperature. In fact, a well-defined (100) reflection was obtained only 20°C below the melting point. This would indicate that the alloy is certainly highly ordered at 450°C, thus eliminating the possibility of quenching in a disordered structure. Also, there was no indication of the formation of a new phase.

The question of the possible role of quenching stresses was also investigated. Quenching stresses are due to unequal rates of cooling of the surface and the interior of the sample, and therefore no quenching stresses would be expected for a thin foil. The experiment was repeated for a 1-mil foil of the same composition as the rod-shaped sample. Essentially the same effect was noted for the foil as for the rod.

Preliminary x-ray work has been done in collaboration with G. E. Klein on the effect of quench on the appearance of back-reflection Laue spots. It was found that there is a characteristic splitting of the spots associated with the quenched state. This is in essential agreement with a previous investigation[6] in which it was found that considerable broadening of the rocking-curve width is induced by the quench.

EFFECT OF NEUTRON RADIATION ON THE PRECIPITATION HARDENING REACTION

R. H. Kernohan D. S. Billington

The effect of neutron radiation on the precipitation hardening reaction in the copper-beryllium system has been a subject of investigation for several years.[7,8] From observations on the changes in electrical resistance and mechanical properties, Taylor and Murray, who made the most comprehensive study, concluded that neutron irradiation of copper-beryllium alloys was very similar to low-temperature precipitation hardening of the alloy. All the evidence was indirect, however, and it was not possible to establish from their observations that the precipitation of beryllium in the form of the gamma phase (BeCu) was actually enhanced. In other words, the appreciable changes observed could very easily be explained as being the result of precipitation; however, they do not exclude the possibility that other processes may be operative. A later irradiation of the alloy at liquid-nitrogen temperature confirmed the hypothesis that the changes occurring in the irradiated alloy were diffusion controlled.

The purpose of the present study was to determine whether it could be shown directly that more beryllium precipitated from solution as a result of irradiation, all other conditions being constant. It was decided to make use of the nickel-beryllium system, which is very similar to the copper-beryllium system, with the same percentage of beryllium concentration in solid solution. The advantage in using the Ni-Be system lies in the fact that its alloys are ferromagnetic. Thus magnetic measurements can be made which are not possible in the copper-beryllium alloys. For example, it has been shown by W. Gerlach[9] that the Curie temperature of an alloy in the nickel-beryllium system is a linear function of the amount of beryllium in solid solution. Therefore a determination of the Curie temperature of a nickel-beryllium alloy before and after irradiation would reveal whether more beryllium precipitated out of an irradiated specimen than out of a similar control specimen held at the same temperature for the same length of time outside a reactor.

An alloy of electrolytic nickel and high-purity beryllium was fabricated by the ORNL Metallurgy Division. The material was vacuum melted and

[5] M. A. Bredig, *Chem. Quar. Prog. Rep. March 31, 1951*, ORNL-1053, p 115.

[6] L. C. Chang, T. A. Read, and M. S. Wechsler, *Acta Cryst.* 6, 567 (1953).

[7] D. S. Billington and S. Siegel, *Metal Progr.* 58, 847 (1950).

[8] G. T. Murray and W. E. Taylor, *Acta Met.* 2, 52 (1954).

[9] W. Gerlach, *Z. Metallkunde* 28, 80–83 and 183–188 (1936); 29, 124–131 (1937).

cast, and a beryllium content of approximately 3% resulted. The ingot was first hot rolled at 900°C to a diameter of ⅜ in. and then cold swaged to ⅛-in. rounds. The round rods were finished by centerless grinding and were cut into 4-in. lengths. These rod specimens were then solution annealed by holding at 1150°C for 1 hr, then quenching them in water. Metallographic examination at this stage revealed that not all the beryllium was in solution; that is, the maximum solubility limit of beryllium is 2.9% at 1157°C. However, the excess beryllium in the form of Ni-Be is nonferromagnetic, and thus it does not influence subsequent measurements of Curie temperature.

Measurements of Curie temperature were made on an Anderson inductance bridge. One arm of the bridge consisted of a coil with a core just large enough to hold the ⅛-in.-dia specimen. The coil and specimen were situated in a stirred oil bath which could either be warmed with an immersion heater or cooled with the addition of dry ice. The bridge was operated at 1000 cycles, and measurements of the inductance of the coil containing the Ni-Be specimen were made as the temperature of the oil bath was slowly increased. The inductance of the coil is a measure of the permeability of the core. The measurements of inductance were an indication of the initial permeability, since only small currents were used in the bridge circuit; that is, only the first part of the normal magnetization curve was utilized.

The results of several inductance-temperature runs are shown in Fig. 33. The curve on the far left, designated in the legend as 1, is for one of five specimens annealed at 1150°C for 1 hr and quenched in water. The other four specimens gave similar results, with the variations being shown by the vertical and horizontal lines perpendicular to the curve. The straight-line portion of the curve may be extrapolated to the horizontal line at the bottom of the graph, which is the value of the inductance of the coil with no material in the core. The intersection for curve 1 at about −2°C may be defined as the ferromagnetic Curie temperature. This temperature corresponds to 17.3 at. % beryllium dissolved in the nickel.

Three of the five specimens available were irradiated in a hollow fuel element in the ORNL Graphite Reactor for one month ($nvt \sim 2 \times 10^{18}$) at a temperature of about 40°C. Measurements after irradiation indicated no change in the Curie

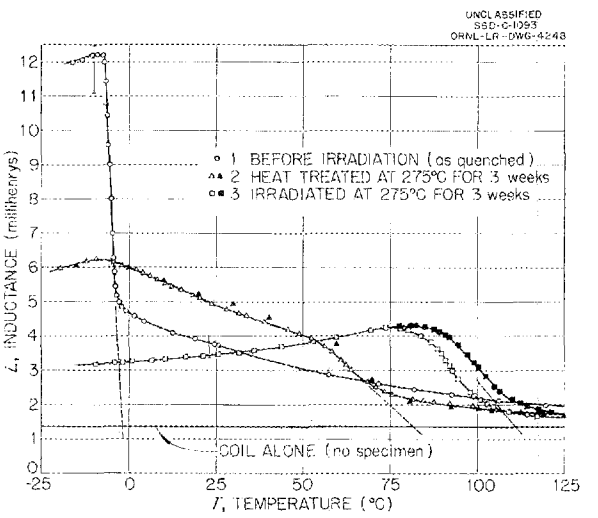

Fig. 33. Inductance vs Temperature Curves for Nickel-Beryllium Alloys.

temperature of the alloy. This result was probably to be expected, since the temperature of irradiation was several hundred degrees below normal precipitation temperature. It is unlikely that irradiation would be able to enhance diffusion at this temperature.

These three specimens were then placed in a capsule with a heater coil and were maintained at a temperature of 275°C in the reactor for three weeks ($nvt \sim 1.5 \times 10^{18}$). The other two specimens were used as controls; they were also maintained at 275°C for three weeks outside the reactor. The temperature of 275°C is about 200°C lower than the normal precipitation temperature, but it was considered to be sufficiently high to make the effect of radiation apparent. After the combined irradiation and heat treatment, all five specimens were again measured. The No. 2 curve is for the two control specimens, and the No. 3 curves are for the irradiated specimens.

The irradiated specimens were not all the same. Two of them followed the line marked with black squares, while the third followed the line marked with open squares. There may have been slight concentration differences in the specimens, or there may have been a small temperature difference between specimens during irradiation.

Extrapolation of the curve for the two control specimens indicates a Curie temperature of about 82°C, corresponding to 13.1 at. % dissolved beryllium. The Curie temperature for the irradiated

specimens is about 110°C, corresponding to 12 at. % dissolved beryllium. It is thus evident that neutron radiation at a temperature somewhat under the precipitation process range does appear to enhance the precipitation, probably through the mechanism of increased diffusion on a microscale.

As can be seen from Fig. 33, the maximum value of the permeability decreased for the heat-treated control specimens and even more so for the irradiated specimens. Permeability is a structure-sensitive property and as such would be sensitive to radiation damage. The actual value of the permeability has little to do with this method of determining the Curie temperature, although the smaller values make the drops in the curves less sharp and hence affect the accuracy. The decrease in permeability is probably associated with structure changes that result from the formation of the nonmagnetic Ni-Be phase. In future work with this alloy, it is planned to study permeability and other magnetic properties in addition to the Curie temperature.

REACTOR-INDUCED RESISTIVITY CHANGES IN COPPER-BASE SOLID SOLUTIONS

R. H. Kernohan A. B. Lewis
D. S. Billington

Bombardment of metals and alloys with nuclear particles furnishes a new technique, which, it is hoped, will lead to a better understanding of these materials. Reactor irradiations might be expected to produce very little effect in stable metals or alloys except for transmutations found upon lengthy bombardments. Furthermore, if merely the effect on electrical conductivity of metals is considered, it might be supposed that the effect of neutron bombardment would be in such a direction as to increase electrical resistivity by disruption of the atoms or by transmutation.

In order to find out what changes might occur in metals bombarded with neutrons, a number of copper alloys were investigated several years ago. In many cases the changes found were slight, but unexpected decreases in the electrical resistivity of stable brass and copper-aluminum solid-solution alloys were observed after the alloys were given comparatively short neutron irradiations in the ORNL Graphite Reactor.[10–12]

Since the resistance anomaly in brasses was difficult to explain and since the accuracy of the earlier work was not too high, it was decided to repeat the earlier experiments with more accurate measurements. Studies of the electrical resistivity of many dilute alloys of copper in the absence of irradiation had already been made,[13] and it was hoped that some correlation of radiation-induced resistance effects and the type of solute in copper could be found.

Pure copper and 23 copper-alloy specimens of high purity were available from previous experiments in the form of ⅛-in.-dia rods about 3 in. long. After a thorough cleaning, the specimens were annealed in a vacuum furnace at 700°C for 1 hr and were allowed to cool in the furnace. The Cu-Zn alloys were vacuum annealed at only 450°C for 1 hr to prevent excessive dezincification. Spectroscopic analysis of representative specimens indicated that the binary alloys were very clean, and the greatest impurity, other than the alloying constituent, was less than 0.01%. Chemical analysis and metallographic studies showed that the binary alloys were all within the solid-solubility range.

Three specimens of each alloy were chosen for resistance measurements. Potential leads were spot welded to these ⅛-in. rod specimens, and measurements of gage length and diameter were taken on each. A Rubicon microvolt potentiometer was used to measure the voltage drop across a fixed standard resistor and across the unknown. The resistance was calculated from the potential ratios. The temperature coefficient of the resistance of each alloy was determined by making measurements at three different temperatures: liquid nitrogen, room temperature, and 68.4°C. The values of resistance plotted vs temperature did not fall on a straight line, and so the three measurements for each specimen were fitted on a quadratic curve by use of the equation

$$R = a + bt + ct^2 .$$

From the dimensions of the specimen the resis-

[10] R. H. Kernohan, A. B. Lewis, and D. S. Billington, *Phys. Quar. Prog. Rep. Sept. 25, 1949*, ORNL-480, p 15.

[11] E. C. Miller and W. H. Bridges (eds.), *Met. Quar. Prog. Rep. July 31, 1950*, ORNL-827, p 72.

[12] W. E. Taylor, G. T. Murray, and F. M. Blacksher, *Phys. of Solids Inst. Quar. Prog. Rep. Jan. 31, 1951*, ORNL-1025, p 41.

[13] J. O. Linde, *Ann. Phys.* 15, 219 (1932).

tivity values were calculated. Thus

$$\rho_t = \rho_0 (1 + \alpha_0 t + \beta_0 t^2) ,$$

where

ρ = resistivity,
t = temperature of the material,
α_0, β_0 = temperature coefficients of resitivity.

All specimens were irradiated for one month in a hollow fuel element in the ORNL Graphite Reactor to increase the proportion of fast neutrons. The integrated flux was estimated to be 2×10^{18}; the temperature during irradiation was not monitored, but judging from previous experience it was probably in the range of 40 to 50°C. Since the highest neutron absorption cross section to be found among the alloying elements was only about 10 barns, the effect of transmutation impurities on the resistivity would be beyond the limits of detection.

The results of resistivity measurements are shown in Table 7; ρ_{20} is the preirradiation value and ρ'_{20} is the postirradiation value. The resistivity values are the average for three specimens measured at the three temperatures and corrected to 20°C. The estimate of error on any particular resistance reading in the data is 0.04%. The changes in resistivity were about the same order of magnitude at all three measurement temperatures except for the Cu-Mn alloys. For these alloys, not only was the resistivity decreased but also the temperature coefficients of resistivity were changed by neutron irradiation. The column labeled $\Delta\rho$ gives the average change in resistivity at the three temperatures for all the specimens of

TABLE 7. REACTOR-INDUCED RESISTIVITY CHANGES IN COPPER-BASE SOLID SOLUTIONS

Alloy	Solute (at. %)	Av ρ_{20} (μohm-cm)	Av ρ'_{20} (μohm-cm)	Av $\Delta\rho$ (μohm-cm $\times 10^2$)	Average Deviation from $\Delta\rho$ (μohm-cm $\times 10^2$)	Percentage Change, $\Delta\rho/\rho_{20}$
Pure Cu		1.6867	1.6905	+0.38	±0.07	+0.23
Cu-Zn	1.85	2.0467	2.0493	+0.25	±0.24	+0.12
Cu-Zn	4.3	2.7505	2.7437	−0.73	±0.11	−0.27
Cu-Zn	11.3	4.1794	4.1229	−5.86	±0.68	−1.40
Cu-Zn	12.9	4.3188	4.2646	−5.48	±0.30	−1.27
Cu-Ga	2.6	4.3024	4.2987	−0.28	±0.21	−0.07
Cu-Ga	4.4	6.7614	6.7517	−0.98	±0.32	−0.14
Cu-Ge	2.6	10.7226	10.7412	+1.97	±0.10	+0.18
Cu-Ge	4.4	15.590	15.605	+1.45	±0.15	+0.09
Cu-As	1.9	16.303	16.313	+0.97	±0.38	+0.06
Cu-As	3.8	29.427	29.476	+4.84	±0.16	+0.16
Cu-Al	1.2	3.0752	3.0729	−0.29	±0.06	−0.09
Cu-Al	5.8	7.3712	7.3425	−2.90	±0.13	−0.39
Cu-Al	9.6	9.0416	8.9531	−8.64	±0.22	−0.96
Cu-Si	3.3	13.859	13.855	−0.58	±0.31	−0.04
Cu-Si	5.6	19.752	19.732	−1.60	±0.44	−0.08
Cu-Sn	1.0	4.6021	4.6031	+0.17	±0.37	+0.04
Cu-Sn	2.4	7.7244	7.7295	+0.51	±0.26	+0.07
Cu-Sn	6.4	15.253	15.255	+0.33	±0.27	+0.02
Cu-Mn	0.73	4.8950	4.8826	−1.24		−0.25
Cu-Mn	6.0	19.628	19.575	−5.3		−0.27
Cu-Mn	8.9	29.103	29.004	−9.9		−0.34
Cu-Mn	17.1	52.552	52.222	−33.0		−0.63
Cu-Mn	22.0	68.103	67.846	−25.7		−0.38

a given alloy. The column of percentage changes in resistivity is the ratio of the average $\Delta\rho$ divided by the preirradiation resistivity at room temperature, ρ_{20}. The increase in resistivity found for pure copper agrees well with the results of Blewitt and Coltman in some of their earlier work. If only percentage changes in resistivity were considered, it would be obvious that all alloys decrease percentagewise with respect to pure copper. Also, since the absolute change in resistivity is about the same at the three temperatures of measurement, it is probable that the changes are in residual resistivity rather than in the temperature-dependent part of the resistivity. However, this is probably not true for the Cu-Mn alloys. The most interesting alloys of copper from an atomic point of view are those which follow copper in the periodic table, that is, Zn, Ga, Ge, and As, because they differ from copper only in mass and the number of outer electrons. The results for these alloys and a few others are shown graphically in Fig. 34.

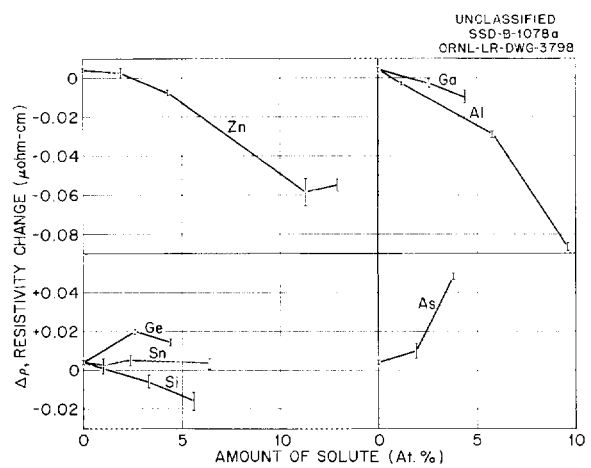

Fig. 34. Resistivity Changes in Copper Alloys Exposed to an *nvt* of 2 × 10^{18}.

When the values of ρ_{20} in Table 7 are used, the effect of the solute atoms on the resistivity of the unirradiated alloys is in good agreement with the results of Linde.[13] It can be shown that the value for the increase in resistivity over pure copper for 1 at. % of solute in copper is proportional to the square of the difference in valence between the solute atom and copper. This general rule is true for those elements which follow copper in the periodic table. The theory for the resistivity of substitutional alloys of copper developed by Mott[14] yields an expression which indicates that the increase in resistivity per atom per cent of foreign atom varies as the square of the valence difference.

An attempt can be made to form some general conclusions on the effects of neutron bombardment on copper alloys based on the data of Table 7. It is evident that as the type of solute atom is varied (Zn, Ga, Ge, As) from electropositive to electronegative there is a tendency to go from decreases in resistivity to increases in resistivity. Another trend to be noted is the variation of neutron-induced change with the amount of solute in any particular alloy group. With the exception of Cu-Ge and quite possibly Cu-Sn, it would appear that absolute values of $\Delta\rho$, as well as the percentage changes, are lower for the more dilute alloys. Still another correlation may have some significance. All negative values of $\Delta\rho$ are associated with solute atoms found near copper in the periodic table or with light atoms, for instance Al and Si, while positive values of $\Delta\rho$ are associated with atoms of relatively higher atomic weight, such as Ge, As, and Sn.

A satisfactory explanation for the decrease in resistivity has not been found. Investigators at Brookhaven National Laboratory have made measurements on copper and alpha brass and are of the opinion[15] that decreases in alpha brass are the result of short-range order.

It is well known that impurity or solute atoms in the copper lattice present larger scattering centers to the electron wave and thus increase the resistivity. Vacancies and interstitial atoms produced by fast neutrons should also leave more scattering centers in pure metals and should increase resistivity. Qualitatively, a vacancy in a copper ion lattice would be similar to an effective negatively charged region, whereas impurities of atoms initially having more than one outer electron would appear as net positively charged regions in a copper lattice. Thus, the possibility arises that the impurity or solute atom could trap the vacancies or that the impurity atom and vacancy could exist adjacently and in so doing present a less effective scattering region for the electron wave than would the impurity atom or vacancy alone.

---

[14] N. F. Mott, *Proc. Cambridge Phil. Soc.* **32**, 281 (1936).

[15] To be published.

LATTICE PARAMETERS OF SOME COPPER ALLOYS

F. A. Sherrill M. C. Wittels

Substitutional solid solutions are formed in those alloys whose solute atoms have approximately the same size as the atoms in the parent lattice. Vegard's law states that the lattice parameters of these kinds of solutions should vary in nearly a linear relation, with the composition expressed in atomic per cent.

Electrical resistivity measurements were made by R. H. Kernohan (see "Reactor-Induced Resistivity Changes in Copper-Base Solid Solutions") on a number of polycrystalline copper-alloy samples in the course of neutron-irradiation experiments. A few of these same copper-alloy samples were used for x-ray diffraction studies, and the atomic percentage of the solute was determined by the Analytical Chemistry Division at ORNL.

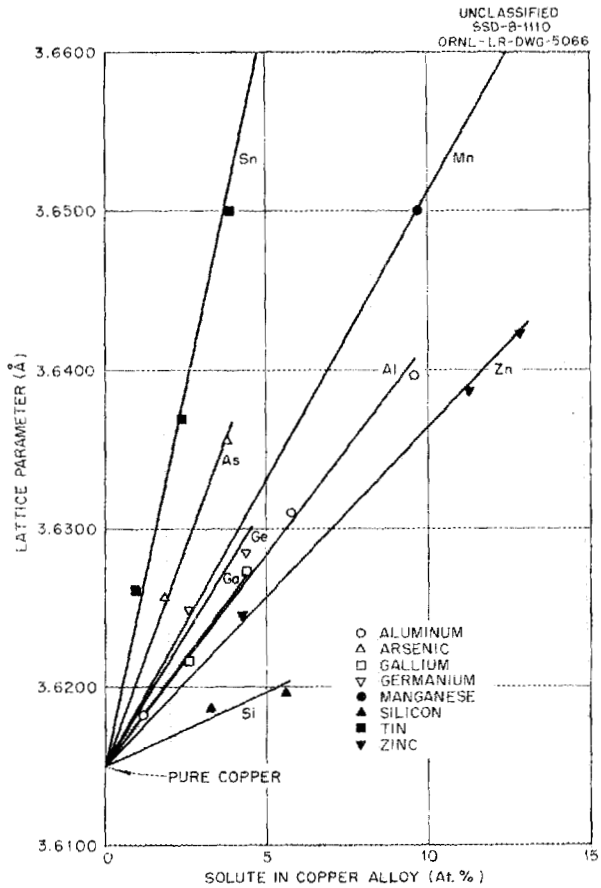

Fig. 35. Lattice Parameter vs Amount of Solute for Various Copper Alloys.

Lattice-parameter measurements were made with the North American Philips diffractometer, and, since the grain size was sufficiently large to employ single-crystal techniques, the Fox spinner[16] was employed to make the measurements at the maximum Bragg angles. Copper K_α radiation was used to obtain diffractions from the (420) or (331), and the lattice parameters were computed from these data with an estimated accuracy of ±0.03%.

Figure 35 shows the relation between lattice parameter and atomic composition in several binary alloys of copper. It can be seen that, at low percentages of solute, these alloys deviate only slightly from Vegard's law. It should also be mentioned that the two irradiated alloys studied, one with 12.9 at. % Zn in Cu and the other with 9.6 at. % Al in Cu, exhibited no lattice-parameter changes after a neutron irradiation with an integrated flux of 2×10^{18} neutrons/cm^2.

PARAMAGNETIC RESONANCES IN IRRADIATED MATERIALS

R. A. Weeks

A schematic plan of the paramagnetic-resonance apparatus is shown in Fig. 36. It is a transmission type employing a high-gain, narrow-band amplifier. The amplifier output is synchronously demodulated by a signal from the oscillator that supplies the modulation component of the magnetic field. The synchronously demodulated signal is rectified and chart recorded. The magnetic field is sine-wave modulated, and the modulation amplitude is variable. The signal appearing at the detector is composed of a d-c component and, in the neighborhood of a resonance, an a-c component at the frequency of the magnetic-field modulation. The amplitude of the a-c component to a first-order approximation is proportional to the first derivative of the resonance. With the narrow-band amplifier, only the fundamental of the a-c component is amplified. For modulation amplitudes that are small relative to the half-width of the resonance, the amplitude of the fundamental of the a-c signal is proportional to the first derivative of the resonance. The harmonics of the a-c signal make only a small contribution to the amplitude of the signal.

[16] R. J. Fox, F. A. Sherrill, and M. C. Wittels, *A Single-Crystal Adapter for the Norelco Wide-Range Diffractometer*, ORNL-1807 (Jan. 6, 1955).

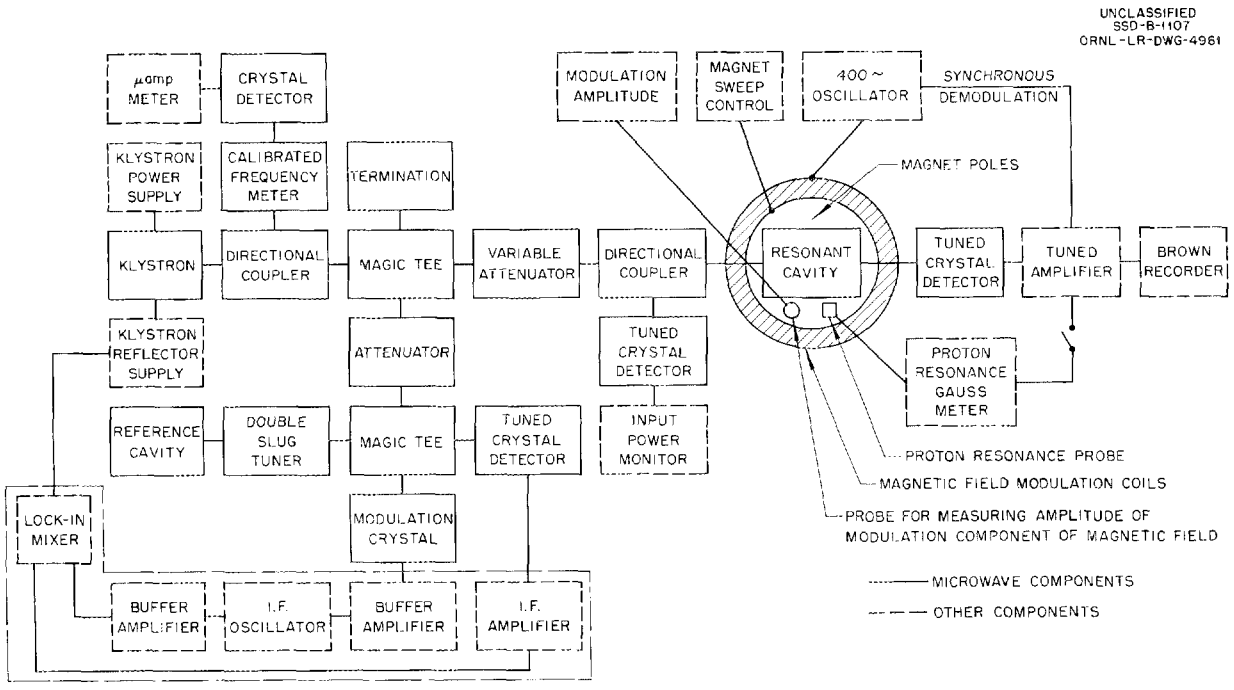

Fig. 36. Paramagnetic-Resonance Apparatus.

The amplifier was designed by K. H. Kline of the Instrument Division. It is based on a starved-circuit design. The synchronous detector preceded by a twin-T feedback network achieves the narrow band. The amplifier output is down 3 db at ±3 cps off the tuned frequency. The maximum gain is 1.5×10^8. A schematic diagram of the circuit is shown in Fig. 37.

The frequency source is stabilized with a Pound i-f system. The frequency stability is better than 1 part in 10^5 for periods of 1 hr or less. For longer periods the temperature cycle of the room affects the reference cavity; the stability is then 2 parts in 10^5. Usually, the time needed to trace out a resonance is considerably less than 1 hr. The circuitry of the Pound system is the same as that published in the literature.[17]

The intensity of the magnetic field is measured with a proton-resonance gauss meter. The resonance of the hydrogen proton in water is observed, and the frequency at which resonance occurs is determined with a BC-221-J frequency meter. The magnetic field is then calculated from this frequency. The accuracy of the meter is 2 parts in 10^5. Provision is made to chart record the first derivative of the proton resonance. The width of the resonance, approximately 0.2 gauss at half width, is due to inhomogeneities of the magnetic field. The proton resonance signal is amplified by a preamplifier and then fed into one of the inputs of the amplifier. The other input of the amplifier takes the output of the paramagnetic-resonance preamplifier. An oscilloscope can be substituted for the amplifier. On the scope the proton-resonance signal appears as a sine wave, with the frequency of the magnetic-field modulation for magnetic-field modulation amplitudes being small relative to resonance half-width. One advantage of the scope display is the ease with which the BC-221-J can be tuned to the frequency of the proton-resonance oscillator. The frequency of the BC-221-J is mixed with the oscillator frequency, and the beat frequency appears on the scope. The oscillator frequency is found by tuning the BC-221-J to zero beat. The circuitry of the gauss meter is of conventional design.

The amplitude of the modulation component of the magnetic field is determined from the voltage induced across the terminals of a probe coil of known turns and dimensions. The d-c component of the magnetic field is varied linearly by a motor-driven potentiometer. Over the width of the narrow

[17] R. V. Pound, *Proc. I.R.E.* 35, 1405–1415 (1947).

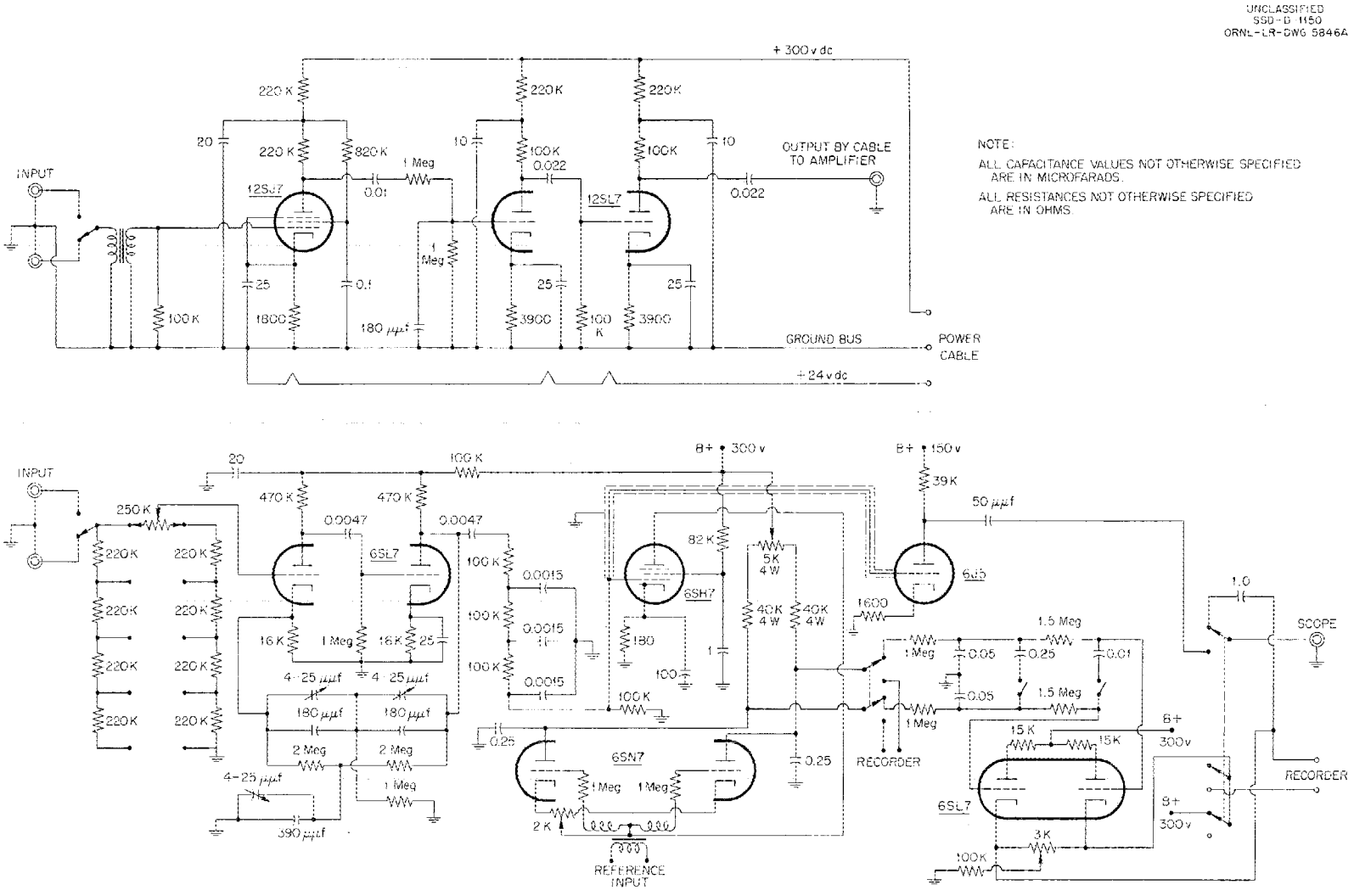

Fig. 37. Preamplifier and Amplifier with Synchronous Demodulation.

resonances thus far studied, the nonlinearity of the magnet is negligible, and a linear potentiometer is adequate.

Figure 38 shows some of the apparatus used for supporting the specimens in the cavity and for making observations at liquid-nitrogen temperatures. Provision is made for orienting the specimens relative to the magnetic field.

Paramagnetic resonances caused by irradiation of glass, vitreous silica, and quartz have been reported.[18,19] Measurements on the magnetic susceptibility of unirradiated and irradiated piezo quartz have also been reported.[20,21] These measurements show that paramagnetic centers are induced in the quartz as a result of irradiation. The paramagnetic resonances in two irradiated crystals on which magnetic-susceptibility measurements were made[21] have been observed. The first derivatives of the resonances of the quartz and of diphenyl-picryl-hydrazyl were chart recorded. These curves were then integrated with a planimeter. Figure 39 is a plot of the integrated curves vs the Landé g factor. The intensity of absorption is in arbitrary units. The hydrazyl curve was recorded with a modulation amplitude of 0.256-rms gauss, while the quartz curves were recorded with a modulation amplitude of 0.320-rms gauss. In order for the hydrazyl curve to be equivalent to the quartz curves, it should be increased by a factor of 1.25. Curve III′ is the result of this increase.

By integrating the curves in Fig. 39, a number proportional to the number of paramagnetic electrons is obtained, provided that the following assumptions are made:

The square of the detector-crystal direct current (off resonance) is proportional to the energy transmitted by the cavity. The detector-crystal direct current, off resonance, is set to the same value for each sample. The quartz crystals were rather

[18] J. Combrisson and J. Uebersfeld, *Compt. rend.* 238, 572–3 (1954).

[19] *ANL Mo. Prog. Rep. Nov. 1953*, ANL-5146.

[20] J. D. McClelland, *Effect of Neutron Bombardment upon the Magnetic Susceptibility of Various Oxides*, NAA-SR-263 (Nov. 15, 1953).

[21] D. K. Stevens, H. C. Schweinler, and M. C. Wittels, *Solid State Semiann. Prog. Rep. Aug. 30, 1954*, ORNL-1762, p 89.

UNCLASSIFIED
PHOTO 13677

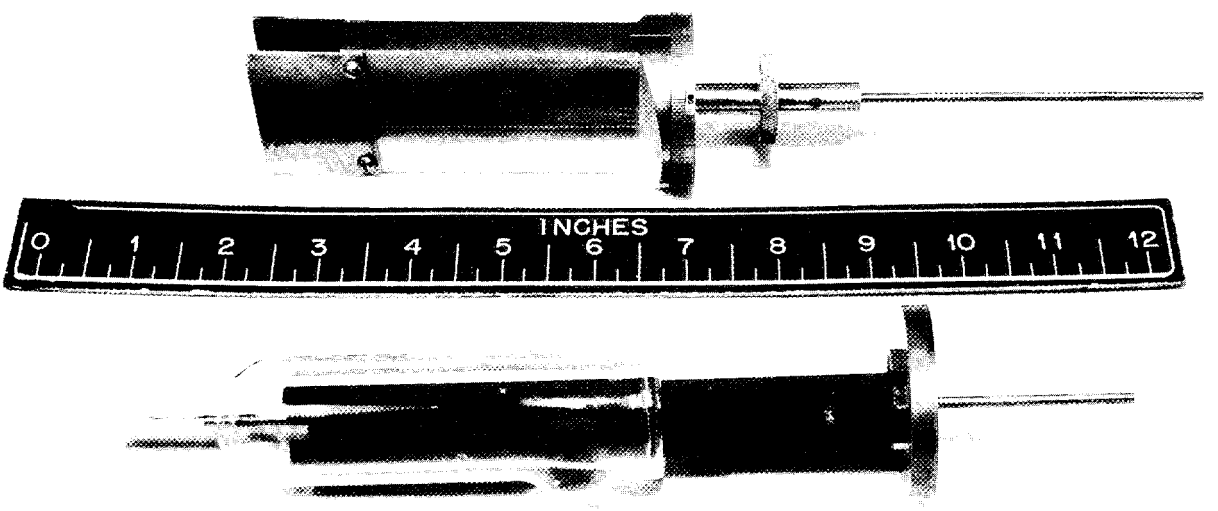

Fig. 38. Specimen Support for Orienting Specimens and Orientation Apparatus in Dewar Flask for Low-Temperature Measurements.

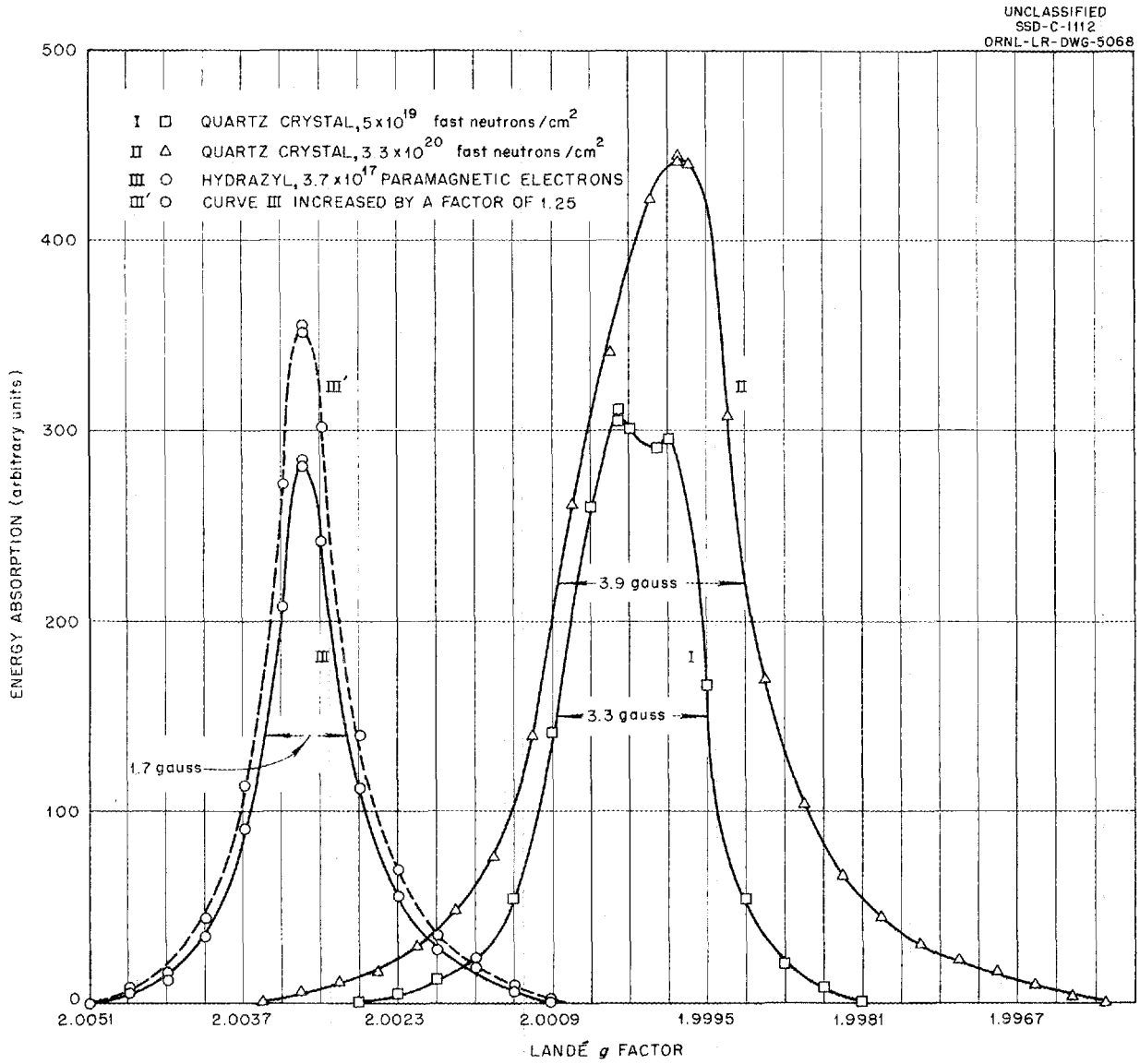

Fig. 39. Paramagnetic Resonance in Irradiated Piezo Quartz.

irregular in shape and were not of an optimum shape for the cavity. Because of their size, approximately 0.4-cm cubes, the crystals interacted with the r-f electric field in the cavity and caused some energy loss. The energy loss was made up by an increase in the detector-crystal direct current. The paramagnetic electrons in the different samples should then experience the same r-f magnetic field.

The small changes in the klystron frequency, required to tune the cavity to resonance for each sample, change by a negligible amount the voltage standing-wave ratio of the wave-guide components preceding the cavity.

The fundamental of the modulation component of the rf that results from the paramagnetic resonance is proportional to the power absorbed by the paramagnetic electrons. For amplitudes of the magnetic-field modulation that are small compared with the half-width of the resonance, this assumption is reasonable. The hydrazyl half-width in these measurements was 1.7 gauss, and the amplitude of the magnetic-field modulation component was 0.35 gauss. For the quartz the half-

widths of the resonance were 3.3 and 3.9 gauss, and the modulation amplitude was 0.46 gauss.

The molecular weight of the hydrazyl is 400, and there is 1 paramagnetic electron per molecule. In 250 μg there are 3.76×10^{17} paramagnetic electrons. The area under the hydrazyl curve gives a number proportional to this number of electrons. Upon this basis the number of paramagnetic electrons in the two quartz samples can be found. The numbers of electrons calculated by this method are shown in Table 8. The densities of the two samples were measured by M. C. Wittels and F. A. Sherrill in their study of density changes in quartz as a function of irradiation.[22] For quartz with an exposure of 5×10^{19} fast neutrons/cm^2, there is a 2% decrease in density, and for 3.3×10^{20} neutrons/cm^2, there is a 12.6% decrease.

The number of paramagnetic electrons measured by this method is in considerable disagreement with the number determined by the magnetic-susceptibility measurement.[21] The greatest disagreement is that the paramagnetic-resonance measurement shows an increase in the number of electrons with increasing irradiation, whereas the magnetic-susceptibility measurement shows a decrease. In the quartz specimen exposed to 5×10^{19} fast neutrons/cm^2, the paramagnetic-resonance measurement of the concentration of magnetic centers is an order of magnitude less than that obtained from susceptibility measurements, whereas the value obtained by resonance measurements on a specimen exposed to 3.3×10^{20} neutrons/cm^2 is less by a factor of only approximately 3. There are several possible reasons for this disagreement. One is that the purity of the hydrazyl is not known. The hydrazyl was obtained from R. Livingston, and he is of the opinion that it is reasonable pure. However, if a large amount of impurity were present, it could account for part of the difference between the two measurements on sample II but would not account for very much of the difference on sample I. In addition, only one weighed sample of the hydrazyl was used. Two samples of hydrazyl which bracket the number of paramagnetic electrons in the quartz would furnish much greater assurance as to the accuracy of the values found.

The quartz samples were not of an optimum size for the resonant cavity. From the observed shift in the resonant frequency of the cavity, it is evident that the r-f electric field interacted with the samples. This also indicates that the intensity of the r-f magnetic field was decreasing at the edge of the samples. Obviously, the paramagnetic electrons on two sides of the sample were being affected by the r-f magnetic field less than those at the center of the specimen. This effect is greater in sample I, which weighs approximately 1.5 times as much as sample II and which showed the greater disagreement with the magnetic-susceptibility measurements. In addition, this discrepancy may have been considerably increased by not centering the samples in the cavity. The irregular shape of the crystals made this rather difficult. Crystals to be used in future measurements will be of uniform shape.

In addition to the difficulties of calibration and sample shape, there is a possibility that some of

[22] M. C. Wittels and F. A. Sherrill, *Solid State Semiann. Prog. Rep. Aug. 31, 1953*, ORNL-1606, p 98–100.

TABLE 8. COMPARISON ON PARAMAGNETIC-ELECTRON CONCENTRATION OBTAINED BY RESONANCE METHOD WITH THAT OBTAINED BY THE MAGNETIC-SUSCEPTIBILITY METHOD

Sample	Exposure (fast neutrons/cm^2)	Weight	Area Under Curve (planimeter units)	Paramagnetic-Electron Concentration (paramagnetic electrons/cm^3)	
				Resonance	Magnetic Susceptibility*
Hydrazyl		250 μg	816	3.76×10^{17}	
Quartz (I)	5×10^{19}	0.292 g	1028	4.24×10^{18}	7.6×10^{19}
Quartz (II)	3.3×10^{20}	0.215 g	2053	1.02×10^{19}	3.3×10^{19}

*D. K. Stevens, H. C. Schweinler, and M. C. Wittels, *Solid State Semiann. Prog. Rep. Aug. 30, 1954*, ORNL-1762, p 89.

the paramagnetic centers were thermally or optically bleached. It has been shown that optical bleaching of some of the optical absorption bands in fused silica takes place.[23] Since it appears reasonable to assume that the paramagnetic centers are those trapped electrons which give rise to the optical absorption bands, bleaching would also be expected to reduce paramagnetic absorption.

Experiments have indicated that there is a relation between F centers and paramagnetic centers in ionic crystals.[24] The relation between color centers and paramagnetic centers in fused and crystalline quartz is being investigated.

There are two other sources for the discrepancy between the magnetic-susceptibility measurements and the resonance measurements. It is possible that there is a very broad resonance present. It is also possible that there are resonances with g factors greater than those observed. A preliminary search has been made up to a g factor of 4, but nothing was observed. The search will be repeated.

It is evident from curve I in Fig. 39 that there are two peaks with almost the same g value. The g value of the composite line is 2.000 ± 0.001. With increasing bombardment one of the peaks increases more rapidly than the other, as shown by curve II. The weaker peak in curve II produces the asymmetry that can be seen on the curve. In some preliminary measurements on the effect of crystal orientation relative to the strong magnetic field, the g value of one, or both, of the peaks was found to change with rotation of the crystal. Since neither crystal has yet been oriented with respect to its crystal axes, it is not yet possible to identify the peaks.

Some preliminary measurements on a quartz crystal that had been exposed to 10^{18} fast neutrons/cm^2 have been made. These measurements indicate a much greater complexity of the resonances than is present in either of the two crystals mentioned above. There are apparently several lines whose g values are almost the same. The crystal orientation is important. Two measurements were made with the crystal rotated 90 deg between each measurement. In one position the lines were spread out over a wider range, and their complexity was more readily observed. In the other position the lines apparently have almost the same g value, and the resonances are apparently not so complex.

In Fig. 39 the half-widths of the composite lines are given for curves I and II as 3.3 and 3.9 gauss, respectively. The lines observed in the sample exposed to 10^{18} neutrons/cm^2 were very narrow. However, until the two lines in curves I and II are resolved, no adequate comparison of line widths in the three samples can be made.

OPERATION OF THE SHIELDED X-RAY DIFFRACTOMETER

G. E. Klein

The shielded x-ray diffractometer (Fig. 40) has been placed in regular operation, and routine examination is being made of irradiated specimens.

Both solid and powdered specimens are used, but certain modifications in mounting techniques must necessarily be observed. Solid samples are mounted directly in $\frac{1}{8}$-in.-thick plastic-sheet sample holders cut into 2×2 in. squares, in which the plastic has been removed from the center section. Sample holders with circular center openings varying from $\frac{1}{2}$ to $1\frac{1}{2}$ in. are available. Flat specimens up to $2\frac{1}{2} \times 3$ in. can be mounted directly without the use of the sample holder.

Powdered materials are sprinkled on a single layer of Scotch tape and covered with another layer of tape to form a sandwich. The Scotch-tape sandwich is then mounted in the sample holder in an identical manner with that used for the solid specimens.

Samples with an intensity up to 11 r/hr at 1 cm, of which 7 r/hr is due to gamma radiation, have been examined and diffraction patterns obtained therefrom. Figure 41 shows the diffractometer traces obtained from a pressed ZrO_2 disk before and after irradiation. The irradiated specimen measured 10.4 r/hr at 1 cm. There has been no appreciable increase in pattern background caused by radiation from the sample itself.

[23] G. Mayer and J. Guèron, *J. chim. phys.* 49, 204–212 (1952).

[24] A. M. Portis, *Phys. Rev.* 91, 1071 (1953).

UNCLASSIFIED
PHOTO 12757A

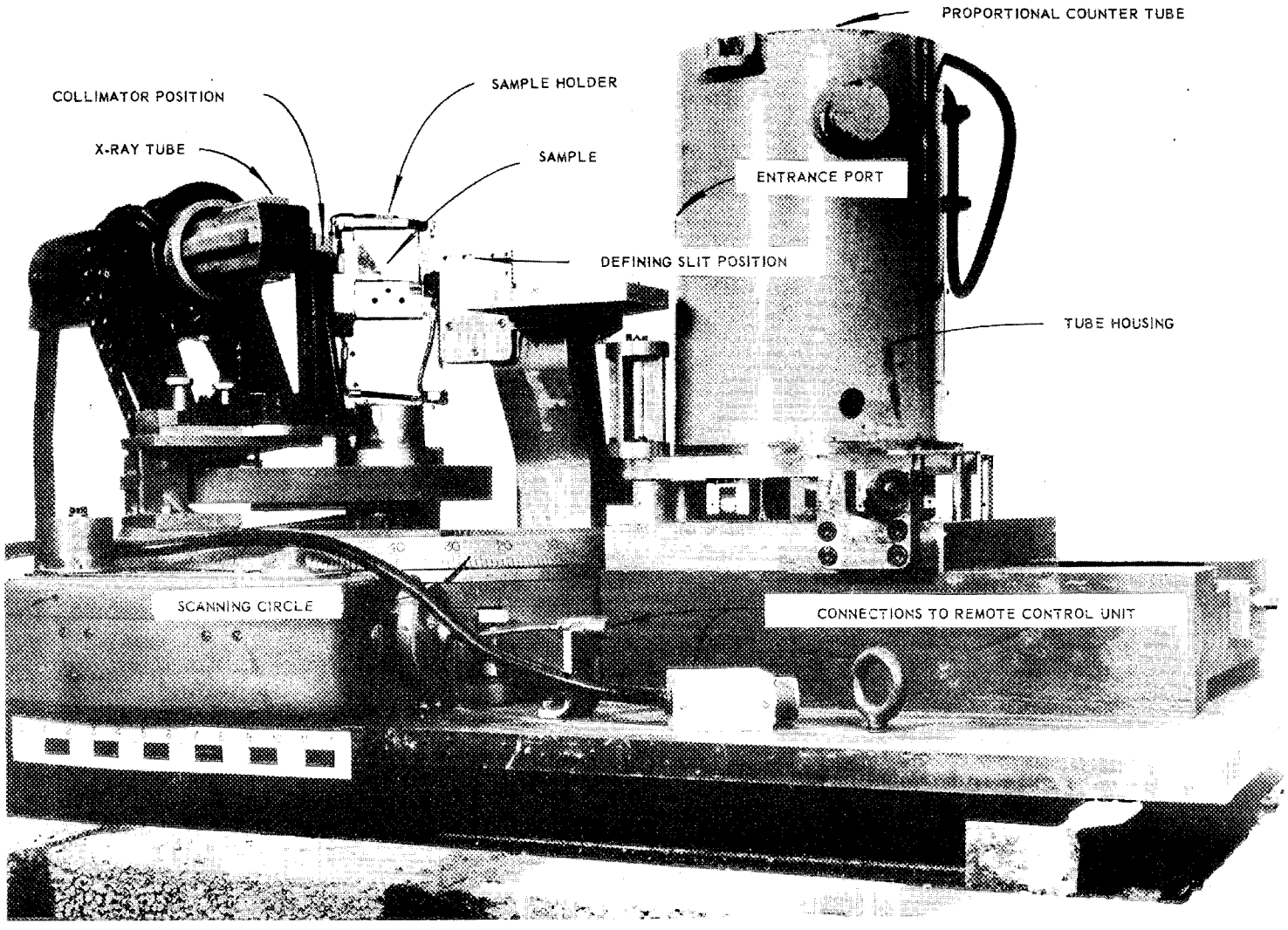

Fig. 40. Shielded X-Ray Diffractometer.

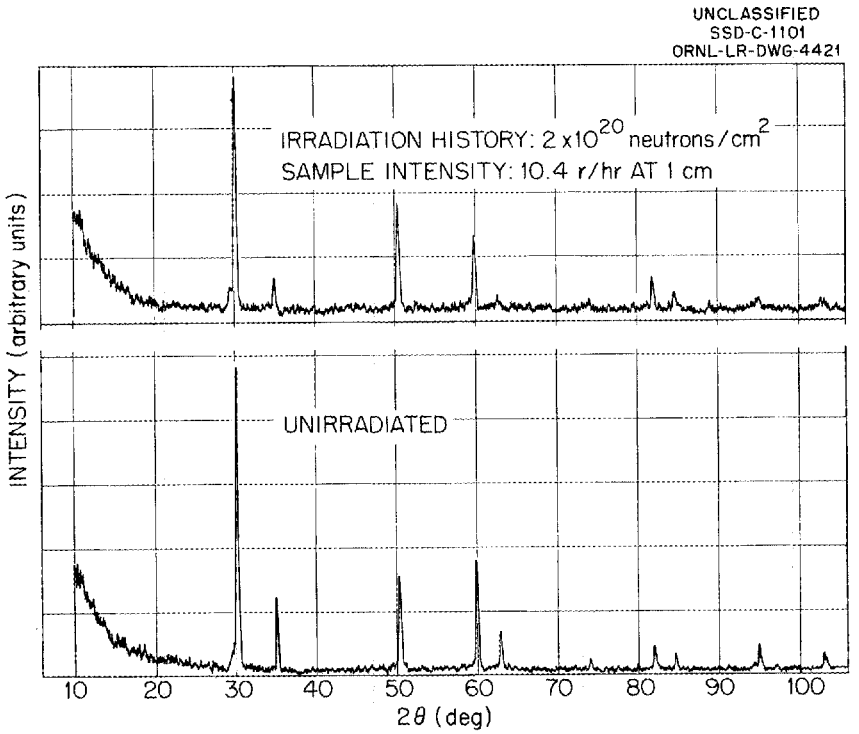

Fig. 41. Diffractometer Patterns of Irradiated and Unirradiated ZrO_2.